2012

STRUCTURAL, THERMOCHRONOLOGICAL, AND STRATIGRAPHIC CONSTRAINTS ON THE EVOLUTION OF THE CLEARWATER METAMORPHIC CORE COMPLEX, IDAHO

Victor Guevara
The University of Montana

STRUCTURAL, THERMOCHRONOLOGICAL, AND STRATIGRAPHIC CONSTRAINTS ON THE EVOLUTION OF THE CLEARWATER METAMORPHIC CORE COMPLEX, IDAHO

By

Victor Emmanuel Guevara

B.A. Geology, Middlebury College, Middlebury, VT, 2010

Thesis

presented in partial fulfillment
of the requirements for the degree of

Master of Science
in Geosciences

The University of Montana
Missoula, MT

July 2012

Approved by:

Sandy Ross, Associate Dean of The Graduate School
Graduate School

Dr. Julia Baldwin, Chair
Geosciences

Dr. Rebecca Bendick
Geosciences

Dr. Nigel Priestley
Chemistry

Dr. Johnnie Moore, Department Chair
Geosciences

Guevara, Victor, M.S., Summer 2012 Major Geosciences

Abstract

Chairperson: Julia Baldwin

The Clearwater metamorphic core complex (CMCC) in northern Idaho is one of several core complexes in the northern Rocky Mountains that were exhumed in the early Eocene and is located in the middle of the dextral Lewis and Clark fault zone (LCFZ). The CMCC has been divided into two lithologically distinct zones: an internal zone that consists of Paleoproterozoic anorthosite and basement schist, and an external zone that consists of Archean to Paleoproterozoic intrusive bodies, basement metasediments, and metasediments of the Mesoproterozoic Belt Supergroup. This thesis is focused on constraining the stratigraphy and structural geology of the eastern external zone, the architecture of Precambrian basement provinces in northern Idaho, and the exhumation history of the CMCC.

LA-ICPMS U-Pb detrital and igneous zircon geochronology in this study has confirmed the presence of pre-Belt quartzite, as well as 1870 ± 9 Ma basement orthogneiss in the CMCC. Detrital zircons in the quartzites show a dominant peak near ~1800 Ma, with smaller Neo- and Mesoarchean peaks, and suggest correlation with the pre-Belt Neihart Quartzite. The quartzites lie stratigraphically above basement metasediments that were intruded by the 1870 Ma orthogneiss. Zircon Hf isotopic analyses of the orthogneiss yield intital ε_{Hf} values between -5.23 and +5.46, suggesting that magma genesis for this body involved both a mantle source and a juvenile crustal source. Hf crustal model ages suggest that this crustal source is Paleoproterozoic to Neoarchean in age. The location of the CMCC in the LCFZ suggests that this structure represents a boundary between two distinct basement terranes along which ~1.87-1.86 Ga magmatism occurred and may be the western extension of the Great Falls tectonic zone.

A set of previously unknown east-verging normal faults called the Surveyors Ridge fault zone (SRFZ) was mapped. These faults yield footwall $^{40}Ar/^{39}Ar$ mica cooling ages of 44 Ma; the easternmost of these faults, the Surveyors fault, yields a hanging wall muscovite cooling age of 78 Ma, and thus delineates the eastern boundary of the CMCC. Faults of the SRFZ were crosscut after 44 Ma by the Collins Creek fault. The Clearwater complex can be divided into at least four zones, each with a distinct structural evolution during exhumation. The internal, western external, and eastern external zones were exhumed between 48-41 Ma along east- and west-verging brittle-ductile normal faults. A fourth zone, the Crescendo Peak block (CPB), which lies between the internal and external zones, yields $^{40}Ar/^{39}Ar$ cooling ages between 58-54 Ma. The low metamorphic grade of this zone suggests that it was not buried as deeply as the other two zones during Sevier orogenesis. The CPB may represent the remnants of a strike-slip duplex that formed during the initial stages of dextral movement in the LCFZ. The complicated exhumation history of the Clearwater complex may be due to inheritance of pre-existing structural complexity from this structure.

Acknowledgments

A large number of people deserve recognition for their roles in helping me complete this project. First and foremost, I would like to give thanks to my advisor, Julie Baldwin, for all of her guidance, always having an open office door, and answering all of my questions, regardless of how ignorant they may have sounded at the time. Also, she bought me ice cream in Avery, which was awesome. I would also like to thank Rebecca Bendick for always being willing to talk about the big picture and opening my mind about tectonics, and, more broadly, science. Reed Lewis of the Idaho Geological Survey deserves a great amount of recognition for providing vital expertise and having many productive conversations about Idaho geology, as well as housing and feeding a poor, lonely graduate student in Moscow, Idaho. Thanks go to Jim Crowley of Boise State University and David Foster of University of Florida for helping with/performing U-Pb and $^{40}Ar/^{39}Ar$ and Hf isotopic analyses, respectively. Don Winston deserves mention for always being interested in my discoveries throughout this project, endowing me with his knowledge of the Belt, his profound influence on my development and career as a geologist, and, by God, proving that one can be as excited about geology and life as ever after 81 years of existence. Department Chair Johnnie Moore also deserves recognition for supporting me throughout my time in the department and providing advice when I needed it.

Chelsea Ward-Waller helped me in the field and put up with my freight train snoring for 34 days in a tent, and the patience and thoughtfulness she demonstrated in the field are a marvel to look back upon. Especially on those days when she brought an extra bag of FTM in her pack. Erin King also helped in the field on the first cold and rainy trip I ever made to Surveyors Ridge. Thanks for bringing the soup. The owner of the fine establishment known as Scheffy's in Avery, Idaho deserves credit for lending a couple of shovels to some geologists who needed to get through the snow drifts. Matt Ruskey helped cut thin section billets, and Joel Desmoreau and Jenny Meidinger helped with rock crushing. Their company in the lab made the experience a little less mind-numbing. Thanks go to Emerald Shirley and Andrea Wolfowicz for letting me crash on their couch for four days and introducing me to the concept of a "pie party" in Boise, ID. The office staff of Christine Foster, Loreene Skeel, and Wendy Woolett can never be over-thanked for their hard work and patience. They are incredible. My external committee member, Nigel Priestley of the UM chemistry department, also deserves my gratitude for stepping in late in the game on such short notice.

Whitney Bausch deserves recognition for myriad reasons, including her willingness to listen and rally the troops when morale was low, making figures much more polished than I could ever make, getting snacks at the UC with me, and being a greater friend than I could ever ask for. I could not have been placed in a more fortuitous office situation during that first week of school. I would also like to thank my roommates and fellow geologists Neal Auchter, Jared Bean, Franklin Dekker, Spencer Paddock, and Brett Woelber for nerding out with me outside of the Clapp, whether it was at home, in the car, the trails of Pattee, or sucking wind on the skin track. Thanks also go to both departed and current UM geoscience graduate and undergraduate students, with special recognition to: Miles Anson, Tyler Dearborn, Elena Evans, Terra Hanks, Evan Hanson, Jeff Howell, Zach Hoylman, Adam Johnson, Erin Johnson, Rob Livesay, Ashley Mulholland, Thomas Palin, Dylan Schmeelk, Abe Schmidt, Matt Seaton, Amy Singer, Nick Silverman, Liane Stevens, Jenn Torres, Annika Tostengard, Zak Wall, and Margeaux Zwang. You've had a far greater impact on this project than you might think. I'm sure I forgot someone.

The faculty members and instructors I had in the Middlebury College geology department deserve thanks for fostering in me the skills, creativity, and enthusiasm to undertake this experience. This group of fine folks includes Willy Amidon, Ray Coish, Chris Koteas, Pat Manley, Tom Manley, Jeff Munroe, Pete Ryan, and Dave West. Cailey Condit, a fellow Midd geology alum and great friend, also deserves thanks for all of her encouragement.

The Geological Society of America, USGS EDMAP fund, Belt Association, Tobacco Root Geological Society, and Colorado Scientific Society helped to fund this project. Without their financial support, none of this would be possible.

Of course, this list would not be complete without mentioning Mom and Dad. I think that's it. Thank you all very, very much.

Dedication

This thesis is dedicated to S.P. Guevara, from whom I inherited an adventurous spirit and the desire to continuously follow the path cut by my curiosity.

TABLE OF CONTENTS

LIST OF FIGURES

LIST OF TABLES

Introduction

The Clearwater metamorphic core complex in northern Idaho is one of several core complexes in the northern Rocky Mountains that lie in the hinterland of the late Cretaceous Sevier orogeny. The early Eocene gravitational collapse of an overthickened crustal welt that formed during the Sevier orogeny resulted in the exhumation of the middle crust and the formation of metamorphic core complexes [*Armstrong*, 1982; *Bendick and Baldwin*, 2009]. This thesis is focused on specific aspects of the Clearwater complex and is divided into two chapters, both of which have been prepared as manuscripts to be submitted for publication. The purpose and motivation for each of the manuscripts are briefly outlined below, but are discussed in greater detail in the introduction of each manuscript. The results of each study are presented in their respective chapters.

Chapter I: *Exhumation of the middle crust within a continental-scale strike-slip fault system: constraints on the thermal and structural evolution of the Clearwater metamorphic core complex, Idaho*

The Clearwater complex lies in the middle of a releasing bend within the Lewis and Clark fault zone, a zone of northwest-southeast trending, dextral strike-slip faults that extends from northern Idaho to west-central Montana. These faults have been temporally and kinematically linked with the formation of core complexes in this region by previous workers, suggesting that the Lewis and Clark fault zone played an important role in the exhumation of the middle crust within these core complexes [*Foster et al.*, 2007]. Though published metamorphic thermobarometry, U-Pb metamorphic zircon ages, and $^{40}Ar/^{39}Ar$ cooling ages have confirmed rapid Eocene exhumation of the middle crust within the Clearwater complex, the exhumation history and structural evolution of the Clearwater complex remains uncertain due to a scarcity of

kinematic and thermochronologic data, particularly with respect to the eastern part of the complex. *Doughty et al.* [2007] invoke a complicated structural history for the Clearwater complex, which involves exhumation along both east- and west-directed normal faults. This makes the Clearwater complex unique among core complexes in the northern Rockies, which exhibit a comparatively simple structural history [*Foster et al.*, 2007]. The complex exhumational history of the Clearwater complex is likely due to its location within the Lewis and Clark fault zone.

This study presents the results of new 1:24,000 scale geologic mapping in the eastern part of the Clearwater complex, macro- and microstructural analyses of major structures within the complex, and $^{40}Ar/^{39}Ar$ mica cooling ages along an east-west transect across the complex in order to: 1) *Determine the eastern extent of Eocene mid-crustal exhumation in the Clearwater complex*, 2) *Constrain the kinematics and timing of Eocene exhumation along major structures in the complex*, and 3) *Constrain the structural dynamics of metamorphic core complex development within a continental-scale strike-slip fault zone*.

Chapter II: *U-Pb geochronology of pre-Belt Supergroup rocks of the Clearwater complex: implications for Precambrian basement provinces and stratigraphic relationships in the northern Rockies*

Hietanen [1968] was the first to map and describe the rocks that comprise the Clearwater complex, and correlated the metasedimentary units within the complex to lithologies of the Mesoproterozoic Belt Supergroup. However, recent geochronological studies have identified the presence of previously unknown Paleoproterozoic (~1.86 Ga) and Archean (~2.67 Ga) basement orthogneiss, as well as several exposures of pre-Belt quartzite in the complex [*Jansen et al.*, 2011; *Lewis et al.*, 2011; *Vervoort et al.*, 2007]. The orthogneiss bodies were previously assumed

to be Cretaceous in age, while the pre-Belt quartzite units were correlated with units of the Lower Belt Supergroup [*Hietanen*, 1968]. The orthogneiss intrudes metasedimentary rocks that were previously also correlated to the Belt Supergroup, but are only now recognized as exposures of basement upon which the Belt Supergroup was deposited, which suggests that the stratigraphic relationships in the Clearwater complex need to be reassessed.

Exposures of basement rocks in northern Idaho are rare, as they have been obscured by both Mesoproterozoic deposition of the 15-18 km thick Belt Supergroup, as well as Cretaceous intrusion of the Idaho Batholith [*Foster et al.*, 2006]. Therefore, the basement architecture in this part of western North America is poorly understood. This study utilizes 1:24,000 scale geologic mapping, U-Pb detrital and igneous zircon geochronology, as well as zircon Hf isotopic analyses in order to: 1) *Constrain the stratigraphic relationships with the eastern part of the Clearwater complex*, 2) *Map and date intrusive bodies that may represent basement exposures*, and 3) *Use zircon Hf isotopic analyses to better understand the nature of Paleoproterozoic magmatism and basement architecture in northern Idaho*.

References

Armstrong, R. L. (1982), Cordilleran Metamorphic Core Complexes - from Arizona to Southern Canada, *Annu Rev Earth Pl Sc*, *10*, 129-154.

Bendick, R., and J. Baldwin (2009), Dynamic models for metamorphic core complex formation and scaling: The role of unchannelized collapse of thickened continental crust, *Tectonophysics*, *477*(1-2), 93-101.

Doughty, P. T., K. R. Chamberlain, D. A. Foster, and G. S. Sha (2007), Structural, metamorphic, and geochronologic constraints on the origin of the Clearwater core complex, northern Idaho, *Geological Society of America Special Papers*, *433*, 211-241.

Foster, D. A., P. A. Mueller, D. W. Mogk, J. L. Wooden, and J. J. Vogl (2006), Proterozoic evolution of the western margin of the Wyoming craton: implications for the tectonic and magmatic evolution of the northern Rocky Mountains, *Can. J. Earth Sci.*, *43*(10), 1601-1619.

Foster, D. A., P. T. Doughty, T. J. Kalakay, C. M. Fanning, S. Coyner, W. C. Grice, and J. Vogl (2007), Kinematics and timing of exhumation of metamorphic core complexes along the Lewis and Clark fault zone, northern Rocky Mountains, USA, *Geological Society of America Special Papers*, *434*, 207-232.

Hietanen, A. (1968), Belt Series in the region around Snow Peak and Mallard Peak, Idaho, *USGS Professional Paper Rep. 344-E*, 1-34 pp, United States Geological Survey, Washington, D.C.

Jansen, A. C., J. D. Vervoort, and R. S. Lewis (2011), Precambrian basement rocks of the Clearwater metamorphic core complex: a new piercing point along the Western Laurentian margin, paper presented at Geological Society of America Annual Meeting, Minneapolis, MN.

Lewis, R. S., R. A. Brewer, A. C. Jansen, V. E. Guevara, J. D. Vervoort, and J. A. Baldwin (2011), Below the Belt: A Road Log of Archean and Paleoproterozoic Rocks in the Eastern Clearwater Complex, Idaho, *Northwest Geology*, *40*, 143-158.

Vervoort, J. D., N. A. Zirakparvar, R. S. Lewis, and R. F. Burmester (2007), Evidence for recurrent Paleoproterozoic and Mesoproterozoic magmatism and metamorphism in the Boehls Butte-Clarkia area, north-central Idaho, USA, paper presented at Geological Society of America Annual Meeting, Denver, CO.

Chapter I: Exhumation of the middle crust within a continental-scale strike-slip fault system: constraints on the thermal and structural evolution of the Clearwater metamorphic core complex, Idaho

Abstract

The Eocene Clearwater metamorphic core complex (CMCC) in Idaho, USA exposes some of the deepest rocks in the Cordilleran orogen. Its location in the middle of the dextral Lewis and Clark fault zone (LCFZ) suggests that it was exhumed in a releasing bend. New structural and $^{40}Ar/^{39}Ar$ thermochronological data presented in this study provide constraints on the exhumation history of the CMCC.

A set of previously unknown east-verging normal faults called the Surveyors Ridge fault zone was mapped in this study. These faults yield footwall $^{40}Ar/^{39}Ar$ cooling ages at ~44 Ma; the easternmost of these faults yields a hanging wall muscovite cooling age of 78 Ma, and thus delineates the eastern boundary of the CMCC.

The results of this study show that the Clearwater complex can be divided into at least four zones, each with a distinct structural evolution during exhumation. The internal, western external, and eastern external zones were exhumed between 48-41 Ma along east- and west-verging brittle-ductile normal faults. A fourth zone, the Crescendo Peak block (CPB), which lies between the internal and external zones, yields $^{40}Ar/^{39}Ar$ mica cooling ages between 58-54 Ma. The low metamorphic grade of this zone suggests that it was not buried as deeply as other parts of the complex. The CPB may represent the remnants of a strike-slip duplex that formed during the initial stages of dextral movement in the LCFZ. The complicated exhumation history of the Clearwater complex may be due to inheritance of pre-existing structural complexity from this structure.

1. Introduction

Metamorphic core complexes are ubiquitous features in orogenic belts worldwide. They have been classically defined as isolated domal structures that expose regionally metamorphosed mid- to lower crustal rocks in the footwall of a brittle-ductile, low-angle detachment fault that records large-magnitude crustal extension through ductile deformation of footwall rocks [*Coney*, 1980]. More recently, metamorphic core complexes have been classified to encompass all isolated domal structures in which mid- to lower-crustal rocks have been rapidly exhumed along normal faults during syn- or post-orogenic extension [*Doughty and Price*, 1999; *Doughty et al.*, 2007; *O'Neill et al.*, 2004].

The study of metamorphic core complexes allows for the most direct observation of mid-crustal processes, thus giving valuable insight to the transfer of mass and heat, as well as coupling between the ductile middle crust and brittle upper crust. Metamorphic core complexes have been described and studied in orogenic belts around the world, and many workers agree that the formation of core complexes is an important, if not fundamental, aspect of orogenesis [*Chen et al.*, 1990; *Coney and Harms*, 1984; *Dalziel and Brown*, 1989; *Whitney et al.*, 2004]. Thus, the study of metamorphic core complexes in the context of the orogenic cycle can provide insight into the rheological characteristics and behavior of the middle crust in orogenic belts.

Several metamorphic core complexes exist in the northern Rocky Mountains, forming a north-south trending belt that is inboard of and roughly follows the contour of the $^{87}Sr/^{86}Sr_{initial}$ = 0.706 line. These core complexes are geographically associated with major Cretaceous and Eocene plutonic bodies (Figure 1) [*Coney*, 1980]. The belt of northern Cordilleran core complexes stretches from southern Canada to southern Idaho and includes the Shuswap, Monshee, Valhalla, Okanogan, Kettle, Priest River, Clearwater, Bitterroot, Anaconda,

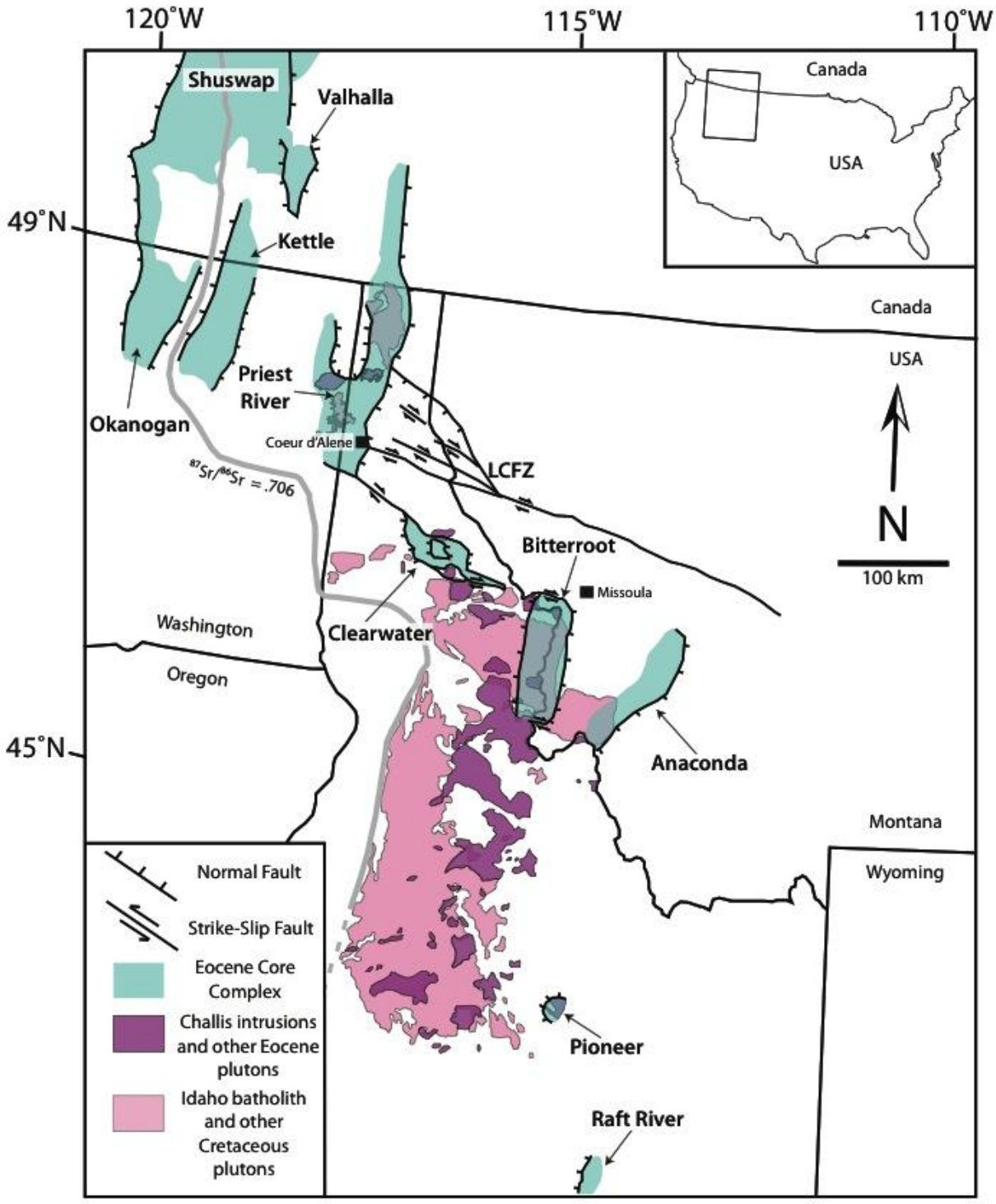

Figure 1: Map of the northwestern U.S. and southern Canada, showing Eocene metamorphic core complexes, the $^{87}Sr/^{86}Sr$ = .706 line, and Cretaceous to Eocene plutons near the Anaconda, Bitterroot, Clearwater, Pioneer, and Priest River complexes. LCFZ = Lewis and Clark fault zone. Modified after *Foster et al.* [2007], *Gaschnig et al.* [2010], and *Lewis et al.* [2010].

Pioneer, and Albion-Raft River-Grouse Creek core complexes (Figure 1) [*Coney*, 1980; *Foster et al.*, 2007].

The formation of metamorphic core complexes in the northern Rockies marks the end of a complex history that began in the early Cretaceous. Subduction of the Farallon plate under the western margin of North America during this time led to widespread contractional deformation and magmatism in a north-south trending belt from Canada to Northern Mexico culminating in the Sevier orogeny, which produced a 50 to 60 km-thick crustal welt in the hinterland of the Cordilleran fold and thrust belt [*Armstrong*, 1982; *Coney*, 1980; *Coney and Harms*, 1984; *Foster et al.*, 2001; *Jones et al.*, 2011]. The crust was at maximum thickness between 89 and 55 Ma, as inferred from the U-Pb monazite and zircon dates of peak metamorphism experienced by high-grade footwall rocks within Cordilleran core complexes [*Doughty et al.*, 1998, 2007; *Foster et al.*, 2001; *Gordon et al.*, 2008]. The Lewis and Clark fault zone (Figure 1) accommodated shortening during this time through sinistral strike-slip motion [*Sears and Hendrix*, 2004].

Widespread extension in the region occurred between 59 and 39 Ma, which manifested in the formation of metamorphic core complexes, as well as another pulse of large-volume silicic magmatism [*Foster et al.*, 2010; *Foster et al.*, 2001; *Foster et al.*, 2007]. The location of metamorphic core complexes in the northern Rockies coincides with zones of inferred maximum crustal thickness, leading many workers to suggest that Eocene extension was caused by gravitational collapse of the orogen, possibly aided by thermal weakening due to the large-volume magmatism that occurred between 65 and 54 Ma concurrent with changes in plate boundary conditions on the western margin of North America [*Bendick and Baldwin*, 2009; *Coney and Harms*, 1984; *Depine et al.*, 2008; *Foster et al.*, 2001; *Hodges and Walker*, 1992; *Jones et al.*,

2011; *Liu*, 2001; *Wells and Hoisch*, 2008]. The development of the Priest River, Clearwater, Bitterroot, and Anaconda core complexes has been kinematically and temporally linked to the change from Cretaceous sinistral to Eocene dextral movement in the Lewis and Clark fault zone [*Foster et al.*, 2007]. The Clearwater core complex (Figure 1) in northern Idaho is unique from other core complexes in the northern Rockies, as it has been exhumed in the middle of a releasing bend within the Lewis and Clark fault zone [*Foster et al.*, 2007]. The Clearwater complex thus represents a rare opportunity to study mid-crustal exhumation processes in continental-scale strike-slip fault zones [*Campani et al.*, 2010; *Martínez-Martínez*, 2006; *Searle et al.*, 2010], for which brittle faulting in the upper crust and the development of flower structures in strike-slip duplexes is well understood [e.g., *Mcclay and Dooley*, 1995; *Woodcock and Fischer*, 1986]. This study focuses on constraining the timing and structural evolution of the Clearwater complex during Eocene exhumation and presents new results of 1:24,000-scale geologic mapping, microstructural analyses, and $^{40}Ar/^{39}Ar$ thermochronological analyses along an east to west transect across the complex.

2. Geology of the Clearwater complex

2.1. Lithologic Relationships

The Clearwater metamorphic core complex is located in northern Idaho and lies approximately 100 km southwest of Coeur D'Alene (Figure 1). Two distinct zones have been characterized by previous workers within the Clearwater complex, based on lithology and stratigraphic relationships (Figure 2): 1) an internal zone that consists primarily of Paleoproterozoic pelites, anorthosite, and amphibolite collectively known as the Boehls Butte Formation, as well as metasediments that post-date the anorthosite intrusion, and 2) an external

zone that is dominantly comprised of amphibolite-facies quartzites and metapelites of the Prichard, Burke, Revett, St. Regis, and Wallace Formations, all of which are part of the lower and middle parts of the Belt Supergroup, a 15 to18 km-thick package of supracrustal rocks that was deposited in an intracratonic rift basin during Mesoproterozoic time [*Doughty and Chamberlain*, 2007; *Doughty et al.*, 2007; *Hietanen*, 1968; *Winston and Link*, 1993]. Slivers of Belt Supergroup metasediments are also present in the internal zone[*Doughty and Chamberlain*, 2007]. Both the internal and external zones are bound by sets of conjugate normal faults, which are discussed in more detail below (Figure 2). A third lithologically distinct zone that separates the internal and external zones is recognized in this study as the Crescendo Peak block and consists of biotite to garnet grade quartzite, schist, and siltite of the Prichard Formation [*Doughty et al.*, 2007; *Duke and Lewis*, 2010]. The nature of the contact between this block and the high-grade rocks of the external zone is uncertain (R. Lewis, personal communication, 2012). Several previously unknown exposures of pre-Belt quartzite, as well as Archean (~2.6 Ga) and Paleoproterozoic (1.86 Ga) granitic basement have been recently mapped and dated in parts of the external zone (Figure 2), which has led to a reassessment of original stratigraphic interpretations of the area [*Guevara et al.*, 2012; *Jansen et al.*, 2011; *Lewis et al.*, 2007a, 2007b, 2010]. Eocene plutons, dikes, and sills intrude rocks of both the internal and external zones (Figure 2) [*Doughty et al.*, 2007; *Gaschnig et al.*, 2010; *Lewis et al.*, 1999, 2000, 2005, 2007b; *Marvin et al.*, 1984].

2.2 Structures

The Clearwater complex is demarcated on the north and south respectively by the St. Joe fault and the Benton Creek, Canyon, and Kelly Forks faults, which are right-lateral strike-slip faults associated with the Lewis and Clark fault zone (Figure 2) [*Foster et al.*, 2007]. The entire

complex has been bound by previous workers on the west and east by the west-directed White Rock and east-directed Collins Creek faults respectively (Figure 2), both of which are interpreted to be normal faults that juxtapose high-grade metamorphic rocks on the footwall against less metamorphosed rocks of the Middle Belt Supergroup on the hanging wall, but have not been studied in detail prior to this paper [*Doughty et al.*, 2007].

To the north, the White Rock fault bends west and joins the St. Joe fault (Figure 2), which exists as a zone of dextral strike-slip faults north of the Clearwater complex that have mylonitized the 52 Ma Roundtop pluton [*Marvin et al.*, 1984]. To the south, the White Rock fault bends east and turns into the dextral Benton Creek fault, which is part of a 8 km wide zone of east-west trending dextral strike slip faults that delineates the southern boundary of the Clearwater complex, extending as far east as the Kelly Forks fault (Figure 2). These faults were active during early Eocene time, based on the 46 Ma crystallization ages of the syntectonic Beaver Creek and Bungalow plutons, which have been mylonitized and brecciated by dextral movement along faults within this zone [*Burmester et al.*, 2004; *Childs*, 1982; *Gaschnig et al.*, 2010; *Lewis et al.*, 2002].

The internal zone is broken up into two distinct blocks of basement anorthosite and schist, separated by rocks of the external zone (Figure 2). The northern block of the internal zone is bound by the Orphan Point fault on the west and the Jug Rock fault on the east. The east-dipping Jug Rock fault separates mylonitized basement schist and anorthosite of the ~500 m thick Jug Rock shear zone from biotite-grade quartzite of the Prichard Formation and amphibolite-facies rocks of the external zone to the east. The Orphan Point fault has been interpreted by *Doughty et al.* [2007] to be a west-dipping normal fault, and also separates mylonitized basement schist and anorthosite on the footwall from rocks of the external zone to the west (Figure 2). This block of

the internal zone is bound on the north by a dextral strike-slip fault, and on the south by a sinistral strike-slip fault (Figure 2) [*Doughty et al.*, 2007; *Sha*, 2004].

The southern body of anorthosite and basement schist is bound on the south by the dextral Canyon fault and on the north by another dextral strike-slip fault that juxtaposes Paleoproterozoic tonalite gneiss and surrounding metasediments on the north against the anothosite and schist on the south [*Doughty et al.*, 2007]. Based on kinematic indicators in mylonitic fabrics, the eastern boundary of this block has been interpreted to be a brittle-ductile, east-verging normal fault [*Doughty et al.*, 2007].

A third lithologically-distinct block lies adjacent to the northern block of the internal zone, which is comprised of relatively undeformed, biotite to garnet grade quartzite, schist, and siltite of the Prichard Formation and is herein referred to as the Crescendo Peak block [*Doughty et al.*, 2007; *Duke and Lewis*, 2010]. This block lies between kyanite- and sillimanite-grade rocks of the internal and external zones. The high-grade rocks of the external zone have been interpreted to be thrust over this block of low-strain, low-grade rocks along a west-directed thrust fault on the east, and an east-directed thrust fault on the west (Figure 2) [*Lewis et al.*, 2007b]. However, there is no kinematic or structural data to support this, and these faults may instead be normal faults (R. Lewis, personal communication, 2012). These faults connect to the dextral Clugs Jumpoff fault, which separates the Crescendo Peak block from external zone rocks to the south [*Doughty et al.*, 2007; *Lewis et al.*, 2007b].

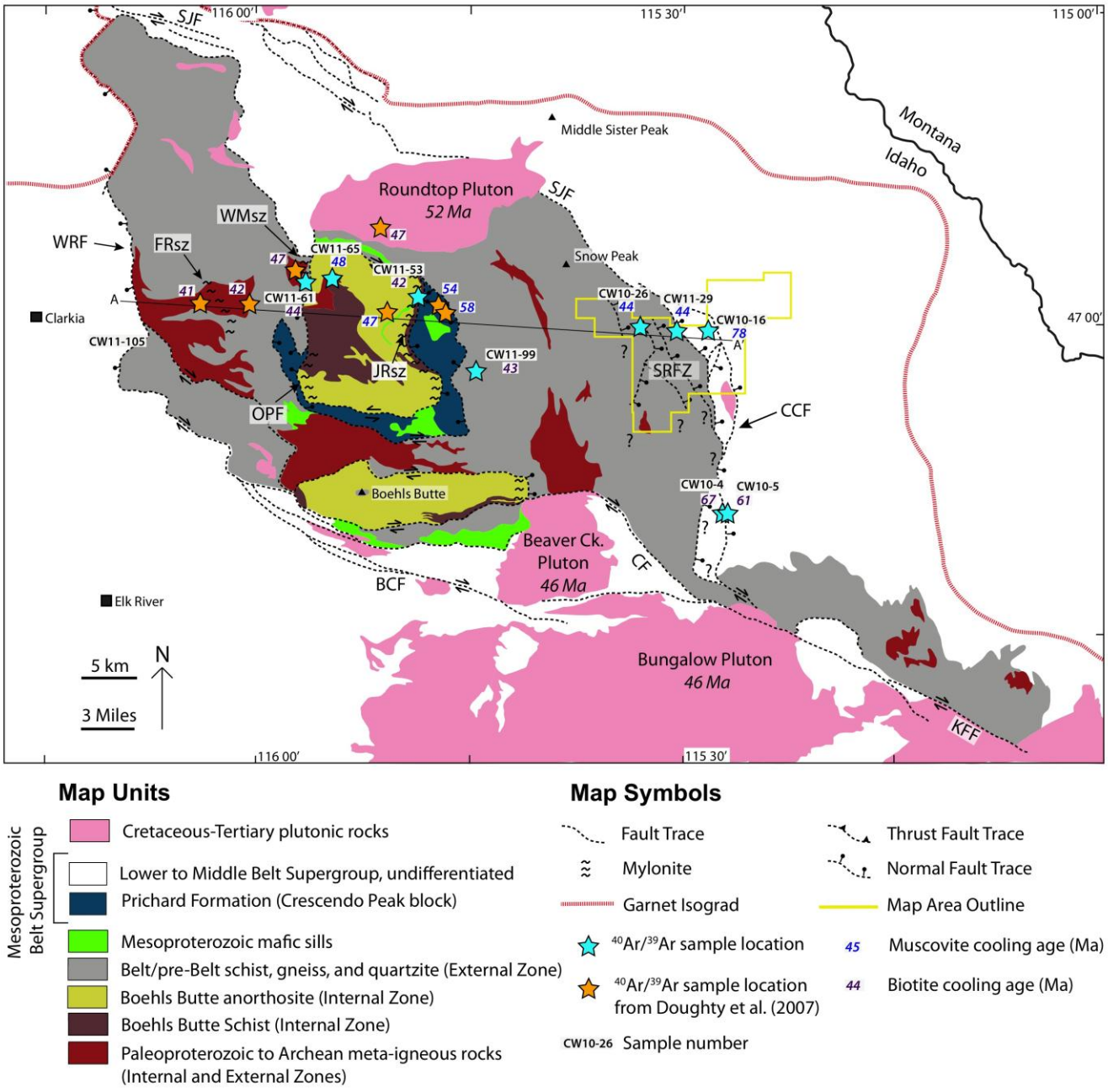

Figure 2: Simplified geologic map of the Clearwater complex, showing major structures, shear zones, and intrusive bodies. The area outlined in yellow was mapped at the 1:24,000 scale for this study, and is shown in more detail in Plate 1. BCF = Benton Creek fault, CF = Canyon fault, CCF = Collins Creek fault, FRsz = Freezeout Ridge shear zone, KFF = Kelly Forks fault, JRsz = Jug Rock shear zone, OPF = Orphan Point fault, SJF = St. Joe fault, SRFZ = Surveyors Ridge fault zone, WMsz = Widow Mountain shear zone, WRF = White Rock fault. Modified after *Nesheim et al.* [2012].

2.3 Structural and metamorphic evolution: previous work

The existence of the Clearwater metamorphic core complex was first recognized by *Seyfert* [1984] and has recently been confirmed by *Doughty et al.* [2007] based on thermobarometric data, structural data, and late Cretaceous to early Eocene $^{40}Ar/^{39}Ar$ cooling ages, all of which confirm the rapid exhumation of regionally metamorphosed mid-crustal rocks within the complex during the Eocene. Previous petrologic work on rocks of the Clearwater complex identified two distinct prograde metamorphic episodes, both of which were followed by a retrograde metamorphic event [*Lang and Rice,* 1985]. The earliest event was thought to have occurred during the Cretaceous by some workers [*Grover et al.*, 1992; *Lang and Rice*, 1985], but a biotite K-Ar age of 1780 ± 53 Ma in the Snow Peak area in the external zone caused others to assign it a Proterozoic age [*Hietanen,* 1969]. *Hietanen* [1963, 1968] was the first to map and describe the anomalously high-grade metamorphic rocks that comprise the Clearwater complex, and found that regional metamorphic isograds are roughly concentric with the northern outline of the Idaho batholith. Metamorphic textures in the Snow Peak area show post-kinematic kyanite and staurolite porphyroblasts that crosscut the foliation of the first prograde metamorphic event [*Hietanen*, 1963, 1968; *Lang and Rice*, 1985]. The second event was thus initially interpreted to be the result of contact metamorphism from late Cretaceous emplacement of the Idaho Batholith. The retrograde event is evident in the Snow Peak area by the pseudomorphic replacement of staurolite and kyanite by muscovite and andalusite [*Lang and Rice,* 1985].

More recent thermobarometric and geochronologic data have identified five distinct metamorphic events recorded by the rocks within the Clearwater complex. Rocks from the internal zone of the complex contain metamorphic zircon and sphene that yield $^{207}Pb/^{206}Pb$ ages between 1434 and 1349 Ma (M1), as well as garnet porphyroblasts that yield Lu-Hf ages of 1463

Ma and ~1.1 Ga (M1 and M2, respectively) [*Doughty and Chamberlain*, 2007; *Sha*, 2004; *Zirakparvar et al.*, 2010]. Lu-Hf garnet geochronology and U-Th-Pb EMPA monazite chemical dating of rocks from the the external zone near Snow Peak and the region surrounding the complex has confirmed the occurrence of two distinct Proterozoic metamorphic events that occurred at ~1.3 Ga (M1) and ~1.1 Ga (M2), which have been correlated to the 1.3 Ga East Kootenay orogeny and a 1.1 Ga Grenville-aged orogenic event, respectively [*Flagg et al.*, 2010; *Lang et al.*, 2010; *Nesheim et al.*, 2012; *Zirakparvar et al.*, 2010]. The spatial extent and nature of these metamorphic events are unknown.

Peak metamorphism in the complex, which has been inferred to be the result of the Late Cretaceous Sevier and Laramide orogenies (M3), records maximum temperatures and pressures of 650-750°C and 8-11 kbar in the internal zone, and may have occurred from 66 to 64 Ma, based on $^{206}Pb/^{238}U$ ages of metamorphic zircon rims [*Baldwin and Guevara*, 2012; *Carey et al.*, 1992; *Doughty et al.*, 2007; *Grover et al.*, 1992; *Zirakparvar et al.*, 2010]. Peak metamorphism in the external zone is believed to have occurred at 565-650°C and 6-7 kbar, but the timing of this metamorphism is yet unknown [*Baldwin and Guevara*, 2012; *Lang and Rice*, 1985]. $^{206}Pb/^{238}U$ ages of metamorphic zircon rims in the external zone yield ages in three distinct pulses: 82-80 Ma, 72-70 Ma, and 65 Ma [*Doughty et al.*, 2007; *Lewis et al.*, 2011]. The most recent metamorphic event was retrograde and occurred between 64 and 59 Ma at 570°C and 3-4 kbar in the internal zone, and has been interpreted to reflect isothermal decompression due to footwall exhumation during Eocene core complex formation [*Baldwin and Guevara*, 2012; *Doughty et al.*, 2007].

$^{40}Ar/^{39}Ar$ mica cooling ages and microstructural analyses presented by *Doughty et al.* [2007] suggest that the Clearwater complex was exhumed between 54 and 41 Ma, with a complex

structural evolution. The distribution of $^{40}Ar/^{39}Ar$ mica cooling ages and ages of fractured metamorphic zircon rims, presumably associated with footwall hydration due to movement along the Jug Rock fault, indicates that exhumation began on the east side of the complex at 59 Ma along the Jug Rock fault and continued until 47 Ma, when extension was accommodated on the west side of the complex by the White Rock fault. Exhumation was likely related to Eocene dextral movement along the St. Joe and Kelly Forks faults in the middle of a releasing bend in the Lewis and Clark fault zone (Figure 2), as evidenced in mylonitic fabrics of the 52-46 Ma Beaver Creek, Bungalow, and Roundtop Plutons on the northern and southern margins of the complex [*Burmester et al.*, 2004; *Doughty and Sheriff*, 1992; *Gaschnig et al., 2010*; *Foster et al.*, 2007].

The results of previous workers described above outlines the complex structural evolution of the Clearwater complex, which differs markedly from the comparatively straightforward structural geometry of the Priest River, Bitterroot, and Anaconda core complexes [*Foster et al.*, 2007]. The structural complexity of the Clearwater complex may be due to its location in a releasing bend within the Lewis and Clark fault zone, and therefore provides a rare opportunity to study how the middle crust is exhumed within a continental-scale strike-slip fault system [*Campani et al.*, 2010; *Martínez-Martínez*, 2006; *Searle et al.*, 2010].

Despite the previous work outlined above, the evolution of the Clearwater complex remains uncertain, specifically with respect to rocks of the external zone, as there is a scarcity of structural and geochronologic data in this area. In particular, there are no thermochronologic data for rocks east of the Jug Rock shear zone, nor are there any kinematic data for the Collins Creek fault, which has been postulated by *Doughty et al.* [2007] to be the east-bounding normal fault of the external zone and therefore the eastern extent of Eocene exhumation. This study seeks to

elucidate the thermal and structural evolution of the Clearwater complex by presenting the results of new geologic mapping, microstructural analyses, and $^{40}Ar/^{39}Ar$ thermochronology.

3. Structural Analyses

3.1. Sample collection

Rock samples for microstructural analyses were selected from the following major structures and shear zones: the White Rock fault, Widow Mountain shear zone, Orphan Point fault, Jug Rock shear zone, and Collins Creek fault, as well as faults and shear zones indentified by this study: the Freezeout Ridge shear zone, Saddle fault, Lookout fault, Collins Peak fault, and Surveyors fault, the latter four of which form a series of conjugate northwest trending, northeast-verging normal faults in the northeastern part of the external zone, collectively known as the Surveyors Ridge fault zone (Figure 2; Plate 1). Structural and petrographic observations discussed below suggest that these structures may have played a significant role in the exhumation of the Clearwater complex.

3.2 White Rock fault

The White Rock fault was postulated by *Doughty et al.* [2007] to be the western boundary of the Clearwater complex and has been described as a brecciated, high-angle, top to the west normal fault that juxtaposes schist and quartzite of the Wallace formation in the hanging wall against Paleoproterozoic orthogneiss and Belt/pre-Belt schist and gneiss in the footwall (Figure 2) [*Doughty et al.*, 2007; *Lewis et al.*, 2000; 2011; 2005]. Shallow west-plunging mineral lineations on the footwall may represent an early period of ductile deformation that has been truncated by more recent high-angle brittle faulting and chloritic brecciation. If this is the case, then the White Rock fault post-dates formation of the core complex, and the fault responsible for the formation

of west-vergining ductile fabrics and exhumation of the core complex has disappeared due to erosion or translation along the White Rock fault. However, these fabrics have not been studied in any detail, and could represent an older shearing event that occurred in either the Cretaceous or Proterozoic (R. Lewis, personal communication, 2012). Alternatively, the White Rock fault may owe its steep dip to progressive doming of the core complex during exhumation. In the absence of better structural constraints, we prefer to interpret the White Rock fault as a steep, west-verging normal fault that has crosscut and translated an older, west-verging brittle-ductile detachment, which is herein referred to as the White Rock detachment.

3.3. Freezeout Ridge shear zone

The Freezeout Ridge shear zone is a zone of high strain rocks approximately 8 km east of the White Rock fault and is described for the first time in this study. The rocks within the shear zone typically consist of coarse-grained schist containing garnet, kyanite, and staurolite, intruded by sills of garnet amphibolite. The ages of these these rocks are uncertain, and they may be older than the Belt Supergroup [*Lewis et al.*, 2005]. Mineral lineations that plunge shallowly (5-35°) to the east are abundant, with well-developed S-C fabrics showing top-to-the-east shear sense (Figure 3A). The spatial extent of the Freezeout Ridge shear zone is unknown due to a lack of mapping and microstructural analyses, and was inferred for this study primarily from structural data and mapping by *Lewis et al.* [2000; 2005]. Though it is referred to here as a distinct shear zone within the Clearwater complex, it is possible that it is continuous with the Widow Mountain shear zone to the east.

3.4 Orphan Point fault and Widow Mountain shear zone

The Orphan Point fault separates anorthosite and schist of the Boehls Butte Formation of the internal zone from metasediments and orthogneiss of the external zone (Figure 2). *Doughty et al.* [2007] interpret this structure to be a west-verging brittle-ductile detachment fault. Mylonitic footwall rocks east of the fault display both east- and west-directed shear sense, some of which are antithetic to the trend and plunge of downdip mineral lineations. *Doughty et al.* [2007] observed that in some cases, the east-directed fabrics are younger than west-directed fabrics, while in other cases the opposite is true. They interpreted the west-dipping, east-directed shear fabrics to be a part of the Jug Rock shear zone that was arched and back rotated during exhumation. They suggested that both fabrics are Eocene in age and represent an overlap between top-to-the-east and top-to-the-west shearing resulting from coeval movement along the west-verging White Rock and east-verging Jug Rock faults. However, these opposing shear fabrics may also differ significantly in age and thus may represent Eocene reactivation of an older shear zone.

The Widow Mountain shear zone (Figure 2) is a zone of mylonitic orthogneiss and metasedimentary rocks in the external zone, west of the Orphan Point fault [*Doughty et al.*, 2007]. Mylonites in this zone exhibit east-directed shear fabrics that are crosscut by west-directed shear fabrics (Figure 3D). The west-verging fabrics display a sense of shear that is antithetic to the trend and plunge of east-dipping mineral lineations. However, some samples only display an east-verging fabric (Figure 3B-C).

All samples collected from the Widow Mountain shear zone in this study display down-dip stretching lineations that plunge gently to the east between 23° and 14° (Figure 4A). Some of

samples display east-directed kinematic indicators, while others display the younger west-directed kinematic indicators that crosscut the east-directed fabrics.

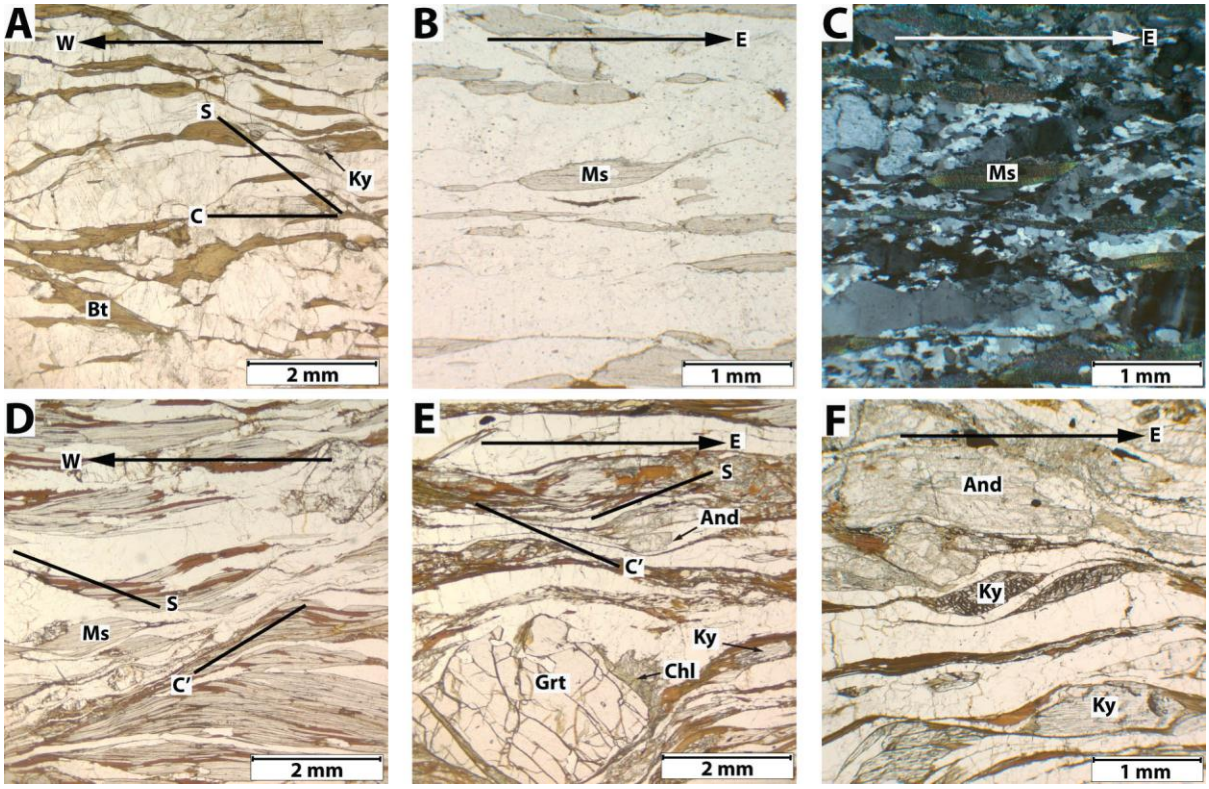

Figure 3: Photomicrographs of A): mylonite from the Freezeout Ridge shear zone with a well-developed S-C fabric showing top-to-the-east shear sense. PPL. B) and C): muscovite fish from the Widow Mountain shear zone showing top-to-the-east shear sense in PPL (B) and XPL (C). D): S-C' fabric in the Widow Mountain shear zone with top-to-the-west shear sense. Muscovite fish with top-to-the-east shear sense on the left side of the photograph are crosscut by the younger west-verging S-C' fabric. PPL. E): S-C' fabric in the Jug Rock shear zone, showing top-to-the-east shear sense. PPL. F): Kyanite fish in the Jug Rock shear zone show top-to-the-east shear sense. PPL. Index of mineral abbreviations: And = andalusite, Bt = biotite, Ky = Kyanite, Ms = Muscovite.

3.5 Jug Rock shear zone

The Jug Rock shear zone is a ~500 m thick, north-south trending, ductile shear zone with east-dipping, top to the east mylonitic fabrics on the footwall of the Jug Rock fault. Well-developed top-to-the-east S-C and S-C' fabrics, mica fish and asymmetric porphyroclasts of kyanite and andalusite showing top-to-the-east shear sense, and retrograde metamorphic reaction textures indicative of isothermal decompression are ubiquitous within the Jug Rock shear zone,

which have been well-documented by previous workers [*Carey et al.*, 1992; *Doughty et al.*, 2007; *Grover et al.*, 1992; *Sha*, 2004] and are further confirmed in this study (Figure 3E-F). Stretching lineations measured in this study plunge ~30° to the east (Figure 4B). The greatest strain in the Jug Rock shear zone is found in the schist, while only protomylonitic fabrics are evident in the anorthosite; this distribution of strain is likely controlled by the relative strength contrast between the anorthosite and schist [*Sha*, 2004].

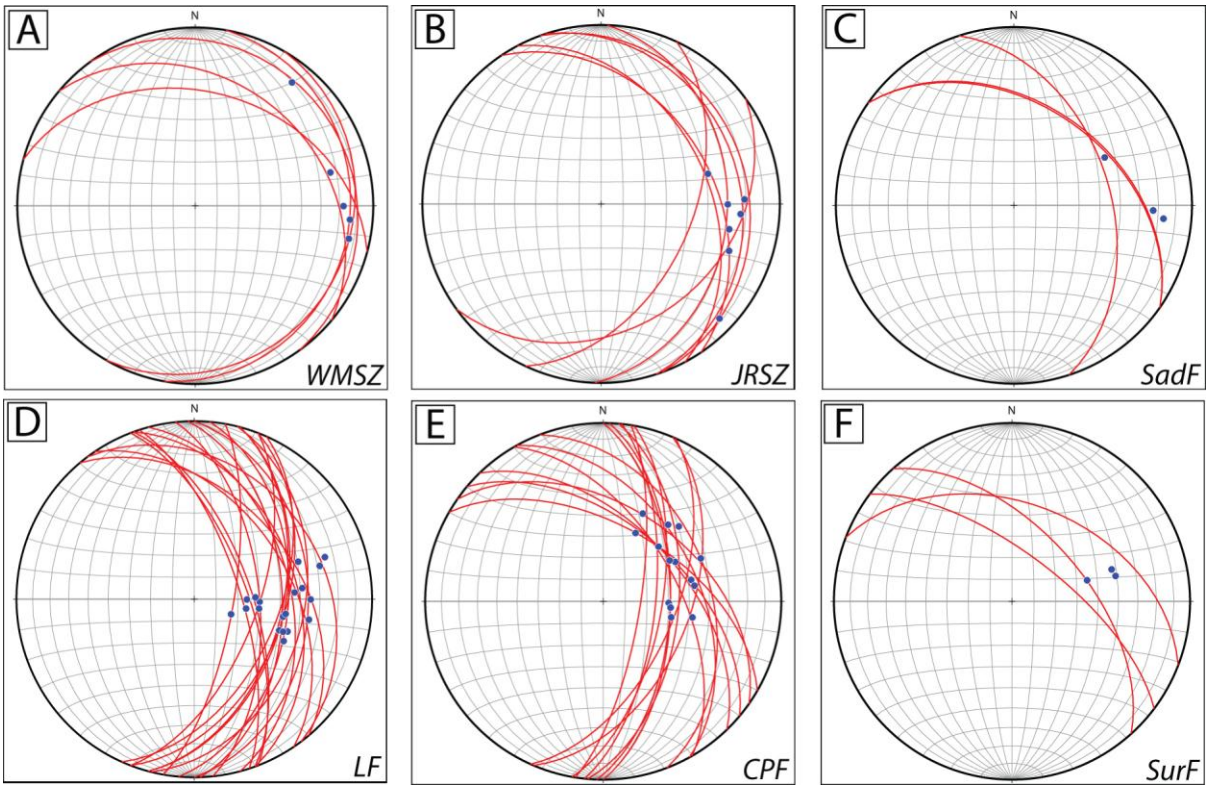

Figure 4: Equal area stereonet projections of foliation planes (red great circles) and mineral stretching lineations (blue points) from: A) Widow Mountain shear zone (WMSZ), B) Jug Rock shear zone (JRSZ), C) Saddle fault (SadF), D) Lookout fault (LF), E) Collins Peak fault (CPF), and F) Surveyors fault (SurF).

3.6 Saddle fault

The Saddle fault is a top-to-the-east normal fault in the Surveyors Ridge fault zone that separates basement schist and gneiss and pre-Belt quartzite in the footwall against low-grade, low-strain quartzite of the Ravalli Group (Middle Belt Supergroup) in the hanging wall (Plate 1).

Hietanen [1968] mapped the quartzite on the footwall as part of the Revett Formation, but detrital zircon U-Pb geochronological data from *Guevara et al.* [2012] suggest that this quartzite predates the Belt Supergroup. This unit is herein referred to as the Fawn Lake quartzite. Downdip stretching lineations plunge to the east between 17° and 42° (Figure 4C). Mica fish and synthetic microfaults in muscovite on the footwall indicate top to the east shear sense (Figure 5A-B). Elongate subgrains and deformation lamellae in quartz are abundant.

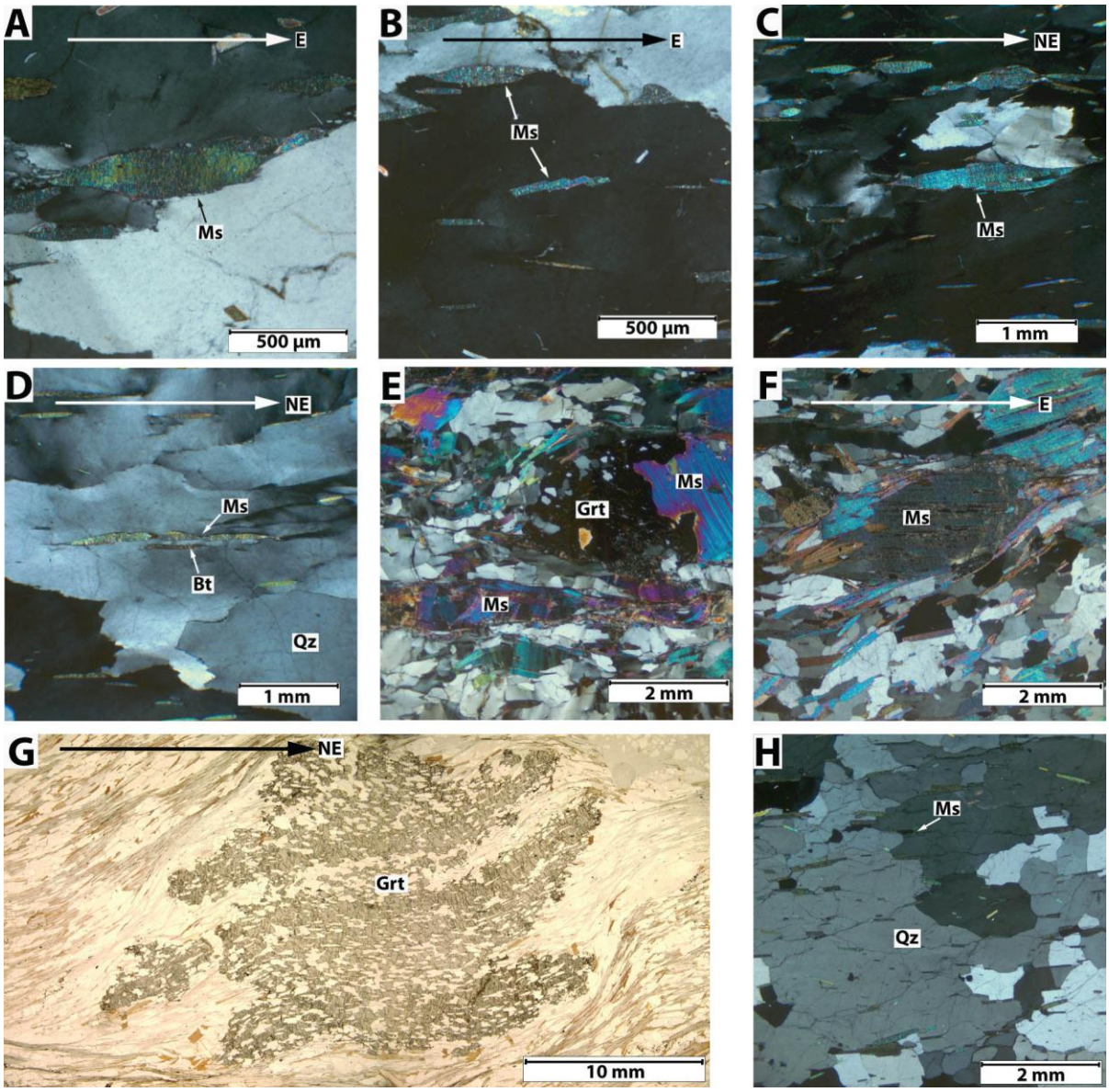

Figure 5: Photomicrographs of footwall microstructures from faults in the Surveyors Ridge fault zone. A) and B): Muscovite fish and faulted muscovite from the Saddle Fault show top-to-the-east shear sense. XPL. C) and D): Mica fish

and boudinaged muscovite from the Lookout fault show top-to-the-northeast shear sense. XPL. E) Kinked muscovite grains and post-kinematic muscovite replacing garnet from the Collins Peak fault. XPL. F): Muscovite fish from the Collins Peak fault shows top-to-the-east shear sense. G): Syn-kinematic garnet porphyroblast with asymmetric strain shadows records top-to-the-northeast shear sense. H): Quartzite from the footwall of the Surveyors fault, showing relatively simple deformational textures and a lack of kinematic indicators. Index of mineral abbreviations: Bt = biotite, Grt = garnet, Ms = muscovite, Qz = quartz.

3.7 Lookout fault

The Lookout fault is another top-to-the-east normal fault in the Surveyors Ridge fault zone that juxtaposes the pre-Belt Fawn Lake quartzite in the footwall against schist of the Prichard Formation in the hanging wall and lies ~2 km east of the Saddle fault. Downdip stretching lineations have an average plunge of 48° to the east (Figure 4D). Mica fish show top-to-the-northeast shear sense, and microboudins of muscovite suggest that deformation occurred during extension (Figure 5C-D). Elongate subgrains and deformation lamellae in quartz grains are common (Figure 5C-D).

3.8 Collins Peak fault

The Collins Peak fault is a top-to-the-east normal fault that lies ~1 km east of the Lookout fault in the Surveyors Ridge fault zone and separates garnet-staurolite-kyanite schist of the Prichard Formation in the footwall from low-grade, low-strain quartzite of the Ravalli Group in the hanging wall. Downdip stretching lineations plunge 40° to 59° to the northeast (Figure 4E). Kink banding is evident in some mica grains and mica fish record top-to-the-east shear sense (Figure 5E-F). Syn-kinematic garnet porphyroblasts with asymmetric strain shadows record top-to-the-northeast shear (Figure 5G).

3.9 Surveyors fault

The Surveyors fault is a northwest-southeast-trending, top-to-the-northeast normal fault that lies ~1.5 km east of the Collins Peak fault in the Surveyors Ridge fault zone and juxtaposes Fawn Lake quartzite in the footwall against schist of the Prichard Formation in the hanging wall. Stretching lineations formed by mica grains on the footwall have an average plunge of 38° to the east (Figure 4F). Quartz grains in these rocks exhibit undulatory extinction and micas are flattened in the plane of foliation, however, no kinematic indicators in these rocks are present (Figure 5H).

3.10 Collins Creek fault

The Collins Creek fault was first mapped by *Hietanen* [1968] as a top-to-the-east normal fault. It has been postulated by *Doughty et al.* [2007] to be the eastern boundary of the Clearwater complex. The southern part of the fault juxtaposes garnet-sillimanite schist in the footwall against low-grade quartzite of the Wallace formation in the hanging wall, and thus delineates a significant break in metamorphic grade. To the north, however, the metamorphic break across the fault is not as sharp, and the fault separates low-strain quartzite of the Ravalli group in the footwall from calc-silicate gneiss and garnet-kyanite schist of the Wallace formation in the hanging wall.

4. $^{40}Ar/^{39}Ar$ Thermochronological analyses

4.1 Sample selection and Methods

Samples for $^{40}Ar/^{39}Ar$ analyses were chosen from the footwall and hanging wall of major structures described in the previous section in order to elucidate their roles in exhumation of the Clearwater complex. Sample selection was also based on existing thermochronological data from

previous workers, abundance and degree of alteration of micas, and spatial distribution of thermochronological data across an east west transect of the complex. Muscovite separates from all 4 samples and biotite separates from 4 samples were analyzed in this study. Micas were separated by standard heavy liquid and magnetic separation techniques. 10 mg of pure separate were picked hand-picked. Mineral separates were irradiated at the Radiation Center at Oregon State University and underwent $^{40}Ar/^{39}Ar$ analyses at the University of Florida following analytical procedures described by *Foster et al.* [2009]. These methods are described in more detail in Appendix 1. The locations and cooling ages of these samples, as well as those of samples analyzed by *Doughty et al.* [2007] are shown in Figure 2.

A table summary of sample information and cooling ages is shown in Table 1, which includes: geographical coordinates (decimal degrees), sample location, lithology, metamorphic grade (using index minerals in a Barrovian style sequence), and muscovite and biotite $^{40}Ar/^{39}Ar$ cooling ages.

Table 1. Summary of $^{40}Ar/^{39}Ar$ Thermochronology Results

Sample Number	**Latitude, Longtitude**	**Sample Location**	**Lithology**	**Metamorphic grade**	**Muscovite $^{40}Ar/^{39}Ar$ cooling age, Ma**	**Biotite $^{40}Ar/^{39}Ar$ cooling age, Ma**
CW11-61	47.02219, -115.56467	Orphan Point, Widow Mountain shear zone	garnet schist	garnet		44.6 ± 5.1
CW11-65	47.02330, -115.54830	Between Goat Mountain and Orphan Point, middle of internal zone	garnet- sillimanite-staurolite-andalusite schist	sillimanite	48.0 ± 2.1	
CW11-53	47.01383, -115.48468	South Butte, Jug Rock shear zone	garnet-kyanite-staurolite-andalusite schist	kyanite/ staurolite		42.2 ± 4.4
CW11-99	46.57514, -115.43782	Indian Dip, footwall of Saddle fault	garnet schist	garnet		43.0 ± 4.3
CW10-26	46.59695, -115.32599	Sawtooth Saddle, footwall of Lookout fault, hanging wall of	quartzite	garnet	44.1 ± 3.4	

		Saddle fault				
CW11-29	46.59574, -115.29730	Surveyors Ridge, footwall of Surveyors fault, hanging wall of Collins Peak fault.	quartzite	biotite	44.2 ± 4.8	
CW10-16	46.59277, -115.27956	Surveyors Ridge, footwall of Collins Creek fault, hanging wall of Surveyors fault.	garnet schist	garnet	78.1 ± 4.0	
CW10-4	46.50696, -115.27000	Skull Creek, footwall of Collins Creek fault	garnet-sillimanite schist	sillimanite		67.7 ± 2.6
CW10-5	46.50690, -115.26909	Skull Creek, hanging wall of Collins Creek fault	quartzite	biotite		61.4 ± 2.1

4.2 Results

Widow Mountain shear zone (CW11-61)

Sample CW11-61 is a mylonitized garnet schist collected from the Widow Mountain shear zone (Figure 2). This unit was originally mapped by *Hietanen* [1968] as part of the Prichard Formation, but is currently mapped as Belt/pre-Belt schist due to uncertainties in those interpretations [*Lewis et al.*, 2007b]. Biotite from this sample yields a total fusion age of 44.6 ± 5.1 Ma.

Internal Zone (CW11-65)

Sample CW11-65 is a highly strained garnet-sillimanite-staurolite-andalusite schist of the Boehls Butte Formation from the middle of the northern block of the internal zone (Figure 2). Muscovite from this sample yields a total fusion age of 48.0 ± 2.1 Ma.

Jug Rock shear zone (CW11-53)

Sample CW11-53 is a mylonitized garnet-kyanite-staurolite-andalusite schist of the Boehls Butte Formation from the footwall of the Jug Rock shear zone. Biotite from this sample yields a total fusion age of 42.2 ± 4.4 Ma.

Saddle fault (CW11-99)

Sample CW11-99 is a crenulated garnet schist collected east of the Cresscendo Peak block on the footwall of the Saddle fault, approximately 13 km west of the fault (Figure 2; Plate 1). It was mapped as part of the Prichard formation by *Hietanen* [1963], but may predate the Belt Supergroup [*Lewis et al.*, 2007b]. Biotite from this sample yields a total fusion age of 43.0 ± 4.3 Ma.

Lookout fault (CW10-26)

Sample CW10-26 is a highly strained pre-Belt biotite quartzite from the footwall of the Lookout fault (Figure 2). Muscovite from this sample yields a total fusion age of 44.1 ± 3.4 Ma.

Surveyors fault (CW11-29, CW10-16)

Sample CW11-29 is a biotite quartzite from the footwall of the Surveyors fault (Figure 2). Muscovite from this sample yields a total fusion age of 44.2 ± 4.8 Ma. Sample CW10-16 is a garnet biotite schist from the hanging wall of the Surveyors fault and footwall of the Collins Creek fault. It was originally mapped by *Hietanen* [1968] as part of the St. Regis Formation, but this study has mapped it as part of the Prichard Formation, due to its stratigraphic location (Plate 1; Figure 2). Muscovite from this sample yields a total fusion age of 78.1 ± 4.0 Ma.

Collins Creek fault (CW10-4, CW10-5)

The nature of the Collins Creek fault changes significantly from south to north. In the southern part of the fault, the Collins Creek fault juxtaposes garnet-sillimanite schist of the Prichard Formation on the footwall against biotite-grade quartzite of the Wallace Formation in which primary sedimentary structures are present [*Lewis et al.*, 2011]. In the north, the fault juxtaposes quartzite of the Ravalli Group on the footwall and calc-silicate gneiss and garnet-kyanite schist of the Wallace Formation on the hanging wall, with no distinct break in metamorphic or deformational grade (Plate 1). The southern part, consisting of sample CW10-4 (garnet-sillimanite schist) on the footwall and sample CW10-5 on the hanging wall (biotite quartzite) was analyzed for this study (Figure 2).

Step heating analyses of biotite grains from CW10-4 yield a plateau age of 67.7 ± 2.6 Ma for 87% of gas released. The inverse isochron for this sample yields an age of 65.5 ± 5.4 Ma and an intial $^{40}Ar/^{36}Ar$ ratio within error of atmospheric composition. The step heating age of CW10-4 is considered to be the more robust age because of its lower error. Three grains of biotite from CW10-5 yield a plateau age of 61.4 ± 2.1 Ma for 85.7% of gas released (Figure 11; Table 1).

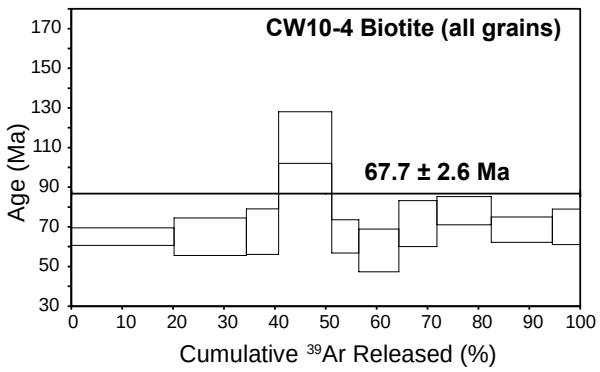

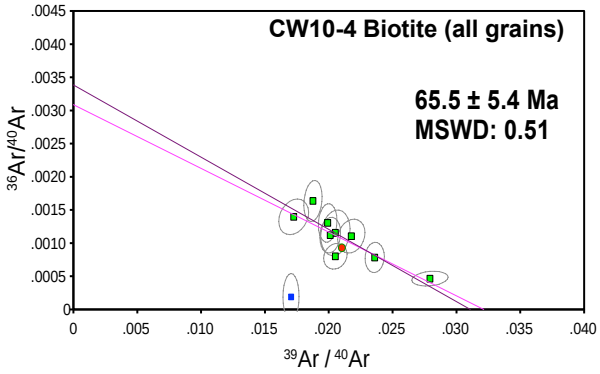

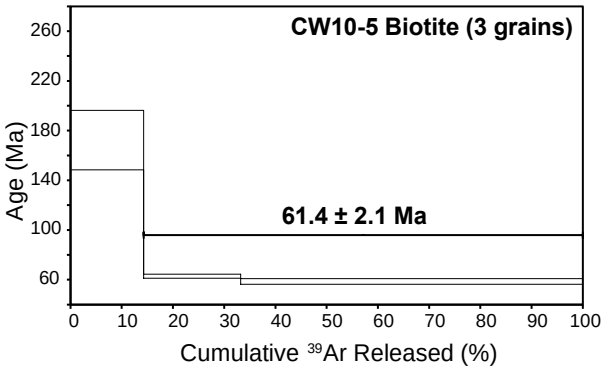

Figure 6: ^{40}Ar/^{39}Ar age spectra and isochron diagrams for samples from the Collins Creek fault (CW10-4, CW10-5).

5. Discussion

5.1 Eastern boundary of the Clearwater complex

The Cretaceous ages of samples CW10-4 and CW10-5 from the Collins Creek fault suggest that these rocks were not exhumed to upper crustal levels during Eocene time and are thus not part of the footwall of the core complex. The difference in cooling ages between the footwall (CW10-4) and hanging wall (CW10-5) of the fault is considered to be insignificant, as these ages have errors greater than 2 Ma and when taken into account, yield a minimum age difference of 1.6 Ma. Regardless, these ages suggest that the Collins Creek fault did not play a role in the exhumation of the Clearwater complex.

Instead, the sharp discontinuity in cooling ages across the footwall (44.2 ± 4.8 Ma) and the hanging wall (78.1 ± 4.0 Ma) of the Surveyors fault indicates that this is the east-bounding fault

of the Clearwater complex. The 44.1 ± 3.4 Ma cooling age of sample CW10-26 from the footwall of the Lookout fault to the west confirms that rocks within the Surveyors Ridge fault zone were exhumed at ~44 Ma. The Surveyors fault is crosscut by the Collins Creek fault, which suggests that the Collins Creek fault is younger and was active after exhumation of the core complex. The extent of faults in the Surveyors Ridge fault zone is unknown; these faults may also be truncated by the Collins Creek fault, or merge with each other and the dextral Kelly Forks fault to the south. The northwest-southeast strike of faults in the Surveyors Ridge fault zone indicates that they likely merge with the dextral St. Joe fault to the north.

5.2 Exhumation History

The structural and thermochronological data presented here provide important constraints on the exhumation history of the Clearwater complex. Rocks within the Crescendo Peak block cooled below the muscovite closure temperature by 54 Ma before rocks of the internal or external zones, and their relatively low metamorphic grade suggests that they did not reach deep crustal levels during Sevier orogenesis [*Duke and Lewis*, 2010]. The eastern and western boundaries of this block have been interpreted by *Lewis et al.* [2007b] to be west- and east-directed thrust faults, respectively. However, if this were true, the cooling ages of the external zone would be older than those of the Cresendo Peak block. Instead, the distribution of cooling ages between the two zones are more consistent with the eastern and western boundaries of the Crescendo Peak block being west- and east-dipping normal faults, respectively. In the absence of better structural contraints, this is our preferred interpretation (Figure 7). These normal faults likely originated as brittle faults that were coeval with early Eocene dextral movement in the Lewis and Clark fault zone. This is consistent with several classical models for metamorphic core complex development, which

suggest that inward-dipping brittle normal faults develop in the upper crust prior to core complex exhumation and doming [e.g., *Lister and Davis*, 1989; *Wernicke and Axen*, 1988].

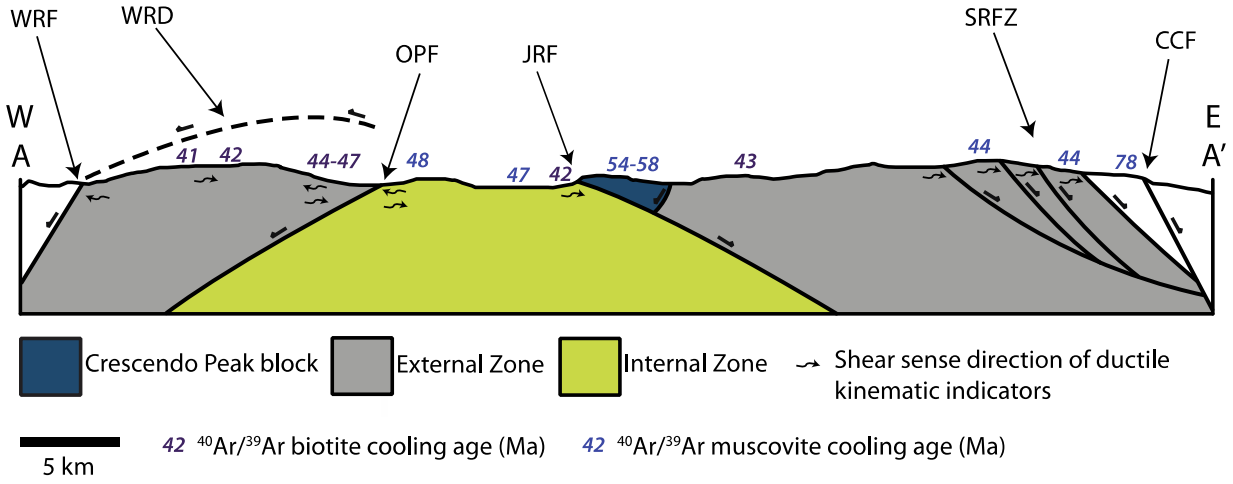

Figure 7: Simplified cross section across line A-A' in Figure 2. $^{40}Ar/^{39}Ar$ ages are from samples along the line, as well as north or south of the line. Index of abbreviations: CCF = Collins Creek fault, JRF = Jug Rock fault, OPF = Orphan Point fault, SRFZ = Surveyors Ridge fault zone, WRD = White Rock Detachment, WRF = White Rock fault.

The Jug Rock shear zone was likely active during this period as a deep-seated shear zone in the middle crust, based on fractured zircons with euhedral metamorphic overgrowths that yield ages from 59-55 Ma reported by *Doughty et al.*, [2007]. Isothermal decompression and exhumation of rocks in the internal zone was probably initiated at this time. The inward-dipping normal faults that bound the Crescendo Peak block were likely crosscut by the brittle-ductile Jug Rock fault by ~48-47 Ma, when rocks of the internal zone started to cool below the muscovite closure temperature. Exhumation along the Jug Rock fault continued until 42 Ma. The distribution of cooling ages (Figure 2) in the internal zone shows a younging trend from west to east, with the youngest age (42 Ma, biotite, CW11-53) coming from within the Jug Rock shear zone. This can be interpreted as a reflection of progressive exhumation along the Jug Rock fault from 48-42 Ma. Alternatively, the 48 Ma muscovite cooling age from sample CW11-65 may represent exhumation due to movement along the Orphan Point fault. If this is the case, then the Orphan

Point fault and Jug Rock fault were coeval at ~48-47 Ma, but exhumation ceased along the Orphan Point fault at some point after this time. The opposing shear sense indicators observed by *Doughty et al.* [2007] on the footwall of the Orphan Point fault may represent an overlap between top-to-the-east motion along the Jug Rock fault and top-to-the-west motion along the Orphan Point fault. *Doughty et al.* [2007] report variable crosscutting relationships between the two fabrics, as in some cases the east-verging fabric is older while in others the opposite is observed. Thus, we interpret both the Orphan Point and Jug Rock faults to have been active at ~48 Ma. At some point after this, exhumation of the internal zone was solely accommodated by the Jug Rock fault. A similar relationship between conjugate detachment faults with opposite vergence has been observed between the Newport and Purcell-Trench faults in the Priest River complex to the north [*Doughty and Price*, 1999; *Foster et al.*, 2007].

Rocks of the external zone record a similar cooling history to rocks of the internal zone, and yield cooling ages (47-41 Ma) that are coeval with those of the internal zone, suggesting that both the Surveyors Ridge fault zone and the White Rock detachment were active during this time. Rocks in the western external zone cooled below the biotite closure temperature from 47 to 41 Ma. The distribution of cooling ages in the western external zone shows a westward younging trend, with the oldest ages (47 and 44 Ma) produced from rocks within the Widow Mountain shear zone. As previously discussed, the older east-directed fabrics in the Widow Mountain shear zone may be representative of a shearing event that occurred prior to Eocene time. However, they may instead represent an early, short-lived period of ductile deformation in the footwall of the east-directed normal fault that bounds the Crescendo Peak block, similar to what we propose here for exhumation of the internal zone along the Orphan Point and Jug Rock faults. Because of this, we prefer the latter scenario, in which east-directed extension stopped some time prior to ~47 Ma,

at which point west-directed extension along the White Rock detachment occurred. This scenario may also explain the origin of east-directed fabrics in the Freezeout Ridge shear zone. This east-directed fault was then either translated along the White Rock detachment or eroded away, and thus no longer exists in the area of the Widow Mountain shear zone.

The eastern external zone cooled below the muscovite closure temperature at ~44-43 Ma. Unlike the internal and western external zones, there is no apparent distributional pattern in cooling ages across the eastern external zone. The similar cooling ages from all samples of the eastern external zone suggest that these rocks were exhumed simultaneously, and thus the east-directed faults of the Surveyors Ridge fault zone were probably active concurrently.

The east-directed ductile kinematic indicators of faults in the Surveyors Ridge fault zone differ markedly from the mylonitic fabrics that are ubiquitous in rocks of the other shear zones of the Clearwater complex, as there are no mylonites in the Surveyors Ridge fault zone (Figure 5). This is also markedly different from footwall rocks of other Cordilleran core complexes, all of which exhibit strong mylonitic fabrics [*Foster et al.*, 2007]. One explanation for the lack of mylonites is that footwall rocks of the Surveyors Ridge fault zone are dominantly quartzites, and the simple rheological contrast between these quartzites and schist of the internal zone may be responsible for this difference. However, the footwall of the Collins Peak fault consists of schist and also does not contain any mylonites. Instead, the lack of mylonitization may simply be due to a difference in metamorphic history between the internal and external zones.

Based on previous thermobarometric work, rocks of the internal zone were subjected to higher temperatures and pressures (~650-750 °C and 8-11 kbar) than those of the eastern external zone (565-650°C and 6-7 kbar) [*Baldwin and Guevara*, 2012; *Grover et al.*, 1992; *Lang and Rice*, 1985]. Additionally, metamorphic reaction textures indicative of isothermal decompression, such

as pseudomorphic replacement of kyanite by andalusite and garnets rimmed by cordierite that are ubiquitous in rocks of the internal zone, are not observed in the external zone (Figure 2). Though the age of peak metamorphism in the internal zone is unknown, it is most likely related to Cretaceous crustal thickening, as the decompression textures probably formed during Eocene exhumation. The age of peak metamorphism in the eastern external zone is also unknown, but it is possible that it is Proterozoic, based on 1.3-1.1 Lu-Hf garnet ages found by *Nesheim et al*. [2012]. If so, rocks of the eastern external zone were at a structurally higher level of the crust than rocks of the internal zone during the Cretaceous immediately prior to core complex exhumation, and were thus not as thermally weakened and did not record as much ductile strain. Subsequently, the amount of displacement along faults of the Surveyors Ridge fault zone would not be as large as that on the Jug Rock fault or White Rock detachment, therefore explaining a decrease in strain in rocks of the Surveyors Ridge fault zone. This scenario is also consistent with rocks of the Surveyors Ridge fault zone being less mylonitized than those of other Cordilleran core complexes, as footwall rocks from both the Priest River and Bitterroot complexes experienced suprasolidus temperatures during the late Cretaceous to early Eocene, and were thus much more ductile during exhumation [*Foster et al.*, 2007].

The above discussion suggests that rocks of the eastern external zone, western external zone, and internal zone experienced different exhumation histories. Additionally, *Doughty et al*. [2007] propose the southern block of anorthosite around Boehls Butte to have its own distinct exhumation history, but there are no thermochronological constraints. For these reasons, we agree with *Doughty et al*. [2007] that the Clearwater complex is not a singular metamorphic core complex in the classical sense, but a composite body of distinct, isolated blocks, or culminations, of mid-crustal rocks that were exhumed synchonously. This structural complexity is probably due

to the location of the Clearwater complex in the middle of a releasing bend in the Lewis and Clark fault zone, where a negative flower structure may have formed at the onset of Eocene dextral motion. The bounding normal faults of the Crescendo Peak block may have been part of this early flower structure, though there is little evidence to support this. The structural complexity of the Clearwater complex might therefore be explained by inheritance of pre-existing structural complexity from this initial flower structure.

5.3 Sequence of events

Given the data presented in this paper in synthesis with data from previous workers, we invoke the following sequence of events to explain the exhumation history of the Clearwater complex, which is outlined in a schematic diagram in Figure 8.

Rocks of the Crescendo Peak block never experienced deep burial during Sevier orogenesis and cooled below the muscovite closure temperature by 54 Ma. Dextral movement in the Lewis and Clark fault zone began in the early Eocene, and the inward-dipping normal faults that bound the Crescendo Peak block began to form in a negative flower structure in a releasing bend in the Lewis and Clark fault zone. The Jug Rock shear zone was active as a deep-seated shear zone in the middle crust as early as 59 Ma. The Roundtop Pluton intruded at 52 Ma, and was mylonitized by dextral movement along the St. Joe fault. Progressive extension and crustal thinning lead to the exhumation of mid-crustal rocks by 48 Ma along the Orphan Point and Jug Rock faults in the internal zone. Exhumation of rocks in the western external zone also began during this early stage through east-directed motion along the west-bounding fault of the Crescendo Peak block. At some point after 48 Ma, the Orphan Point fault was abandoned and exhumation of internal zone rocks was due solely to movement along the Jug Rock fault. West-

verging motion along the White Rock detachment also began at this time, and movement along the west-bounding fault of the Crescendo Peak block ceased shortly after, resulting in both east- and west-directed kinematic indicators in rocks of the Widow Mountain shear zone. The southern block of anorthosite around Boehls Butte was also likely exhumed near 46 Ma in a releasing bend along an east-directed normal fault (Figure 2) based on the 46 Ma crystallization age of the mylonitized Beaver Creek pluton, though there are no thermochronological constraints to support this.

Exhumation in the eastern external zone may have begun slightly later than in the internal or western external zones. East-directed motion along faults in the Surveyors Ridge fault zone exhumed rocks of the eastern external zone by 44 Ma. Exhumation in both the internal zone and western external zone was also active at this time, accommodated by east-directed motion along the Jug Rock fault and west-directed motion along the White Rock detachment. Exhumation of mid-crustal rocks in the complex ended at approximately 41 Ma. The White Rock and Collins Creek faults likely formed soon after, truncating the White Rock detachment and the Surveyors fault, respectively.

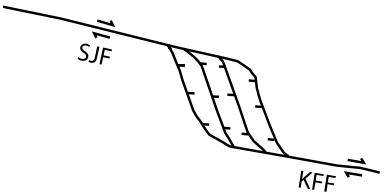

>59-54 Ma

• Flower structure with inward-dipping normal faults formed in releasing bend between KFF and SJF. Crescendo Peak block cooled below muscovite closure temperature

• JRF active as deep-seated shear zone in middle crust

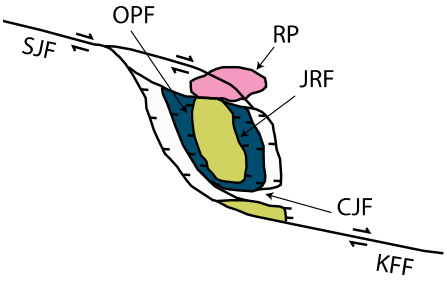

53-48 Ma

• Exhumation of internal zone begins along OPF and JRF.

• RP intrudes SJF at 52 Ma.

• Southern block of internal zone possibly being exhumed

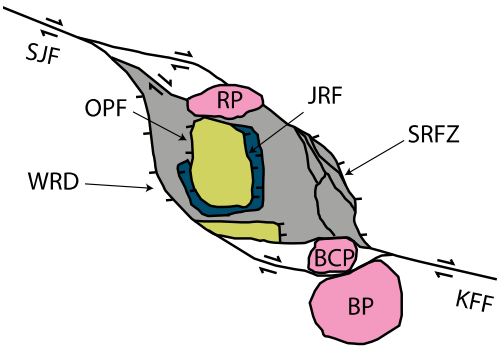

47-44 Ma

• Exhumation of western and eastern external zones begins along WRD and SRFZ.

• Movement along OPF ceases, continued exhumation of internal zone along JRF.

• BCP and BP intrude KFF.

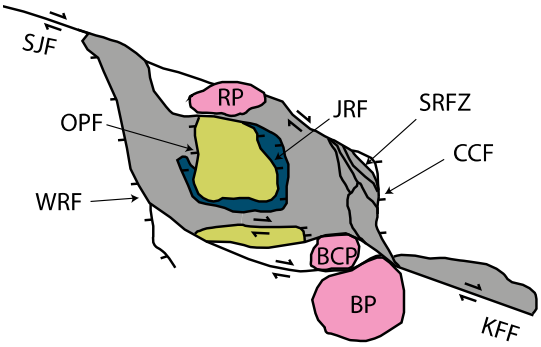

44-40 Ma

• Continued exhumation of internal zone and western external zone along JRF and WRD, respectively

• Exhumation of eastern external zone ceases by 44 Ma.

• CCF and WRF active after 41 Ma, truncating SRFZ and WRD

Figure 8: Schematic cartoon showing exhumation history of the Clearwater complex. Colors are the same as in Figure 7. Index of abbreviations: BP = Bungalow Pluton, BCP = Beaver Creek Pluton, CCF = Collins Creek fault, CJF = CLugs Jumpoff fault, JRF = Jug Rock fault, KFF = Kelly Forks fault, OPF = Orphan Point fault, RP = Roundtop Pluton, SJF = St. Joe fault, SRFZ = Surveyors Ridge fault zone, WRD = White Rock detachment, WRF = White Rock fault.

6. Conclusions

The new structural and $^{40}Ar/^{39}Ar$ thermochronological data presented in this study provide important constraints on the exhumation history of the Clearwater complex. The eastern boundary of the Clearwater complex is demarcated by the Surveyors fault, which is part of the Surveyors Ridge fault zone, a series of northwest trending, east-verging normal faults that were unknown prior to this study and exhumed rocks of the eastern external zone by ~44 Ma. The Collins Creek fault, which was previously thought to be the east-bounding fault of the complex, did not play a role in core complex exhumation and is a younger brittle normal fault that truncated the Surveyors fault.

The distribution of $^{40}Ar/^{39}Ar$ cooling ages with respect to major structures support the idea that the Clearwater complex is not a simple, singular entity as the traditional definitition of a metamorphic core complex suggests. Rather, it should be recognized as a collage of distinct blocks of mid-crustal rocks that were exhumed at approximately the same time, from 48-41 Ma. Despite the similarities in thermal evolution, these blocks experienced distinct structural histories. The complex exhumation history of the Clearwater complex may be due to its location in a releasing bend in the Lewis and Clark fault zone, where it may have inherited the structural complexity of a pre-existing flower structure.

7. References

Armstrong, R. L. (1982), Cordilleran Metamorphic Core Complexes - from Arizona to Southern Canada, *Annu Rev Earth Pl Sc*, *10*, 129-154.

Baldwin, J. A., and V. E. Guevara (2012), Reconstruction of P-T paths in polymetamorphic rocks of the Clearwater core complex, northern Idaho, paper presented at 47th V.M. Goldschmidt Conference, Montreal, QC.

Bendick, R., and J. Baldwin (2009), Dynamic models for metamorphic core complex formation and scaling: The role of unchannelized collapse of thickened continental crust, *Tectonophysics*, *477*(1-2), 93-101.

Burmester, R., W. C. McClelland, and R. S. Lewis (2004), U-Pb dating of plutons along the transfer zone between the Bitterroot and Priest River metamorphic core complexes, in *Geological Society of America Rocky Mountain and Cordilleran Joint Meeting*, edited, p. 72, Boise, ID.

Campani, M., N. Mancktelow, D. Seward, Y. Rolland, W. MÔøΩller, and I. Guerra (2010), Geochronological evidence for continuous exhumation through the ductile-brittle transition along a crustal-scale low-angle normal fault: Simplon Fault Zone, central Alps, *Tectonics*, *29*(3), TC3002-TC3002.

Carey, J. W., J. M. Rice, and T. W. Grover (1992), Petrology of Aluminous Schist in the Boehls Butte Region of Northern Idaho - Geologic History and Aluminum-Silicate Phase-Relations, *Am J Sci*, *292*(7), 455-473.

Chen, Z., Y. Liu, K. V. Hodges, B. C. Burchfiel, L. H. Royden, and C. Deng (1990), The Kangmar Dome - a Metamorphic Core Complex in Southern Xizang (Tibet), *Science*, *250*(4987), 1552-1556.

Childs, J. F. (1982), Geology of the Precambrian Belt Supergroup and the Northern Margin of the Idaho Batholith, Clearwater County, Idaho, 491 pp, University of California, Santa Cruz, Santa Cruz, CA.

Coney, P. J. (1980), Cordilleran metamorphic core complexes: An overview, *Geological Society of America Memoir*, *153*, 24.

Coney, P. J., and T. A. Harms (1984), Cordilleran Metamorphic Core Complexes - Cenozoic Extensional Relics of Mesozoic Compression, *Geology*, *12*(9), 550-554.

Dalziel, I. W. D., and R. L. Brown (1989), Tectonic Denudation of the Darwin Metamorphic Core Complex in the Andes of Tierra-Del-Fuego, Southernmost Chile - Implications for Cordilleran Orogenesis, *Geology*, *17*(8), 699-703.

Depine, G. V., C. L. Andronicos, and J. Phipps-Morgan (2008), Near-isothermal conditions in the middle and lower crust induced by melt migration, *Nature*, *452*(7183), 80-83.

Doughty, P. T., and S. D. Sheriff (1992), Paleomagnetic Evidence for En Echelon Crustal Extension and Crustal Rotations in Western Montana and Idaho, *Tectonics*, *11*(3), 663-671.

Doughty, P. T., and R. A. Price (1999), Tectonic evolution of the Priest River complex, northern Idaho and Washington: A reappraisal of the Newport fault with new insights on metamorphic core complex formation, *Tectonics*, *18*(3), 375-393.

Doughty, P. T., and K. R. Chamberlain (2007), Age of Paleoproterozoic basement and related rocks in the Clearwater Complex, Northern Idaho, U.S.A., in *Proterozoic Geology of Western North America and Siberia*, edited by P. K. Link and R. S. Lewis, pp. 9-35, SEPM Special Publication, Tulsa, OK.

Doughty, P. T., R. A. Price, and R. R. Parrish (1998), Geology and U-Pb geochronology of Archean basement and Proterozoic cover in the Priest River complex, northwestern United States, and their implications for Cordilleran structure and Precambrian continent reconstructions, *Can J Earth Sci*, *35*(1), 39-54.

Doughty, P. T., K. R. Chamberlain, D. A. Foster, and G. S. Sha (2007), Structural, metamorphic, and geochronologic constraints on the origin of the Clearwater core complex, northern Idaho, *Geological Society of America Special Papers*, *433*, 211-241.

Duke, E. F., and R. S. Lewis (2010), Near infrared spectra of white mica in the Belt Supergroup and implications for metamorphism, *American Mineralogist*, *95*(7), 908-920.

Flagg, E. M., W. C. McClelland, J. A. Gilotti, H. M. Lang, K. J. Largent, and J. D. Vervoort (2010), U-Th-Pb Monazite Evidence of Proterozoic metamorphism in the Belt-Purcell Supergroup of Northern Idaho, paper presented at Geological Society of America Annual Meeting, Denver, CO.

Foster, D. A., and C. Mark Fanning (1997), Geochronology of the northern Idaho batholith and the Bitterroot metamorphic core complex: Magmatism preceding and contemporaneous with extension, *Geological Society of America Bulletin*, *109*(4), 379-394.

Foster, D. A., B. D. Goscombe, and D. R. Gray (2009), Rapid exhumation of deep crust in an obliquely convergent orogen: The Kaoko Belt of the Damara Orogen, *Tectonics*, *28*(4), TC4002-TC4002.

Foster, D. A., W. C. Grice, and T. J. Kalakay (2010), Extension of the Anaconda metamorphic core complex: 40Ar/39Ar thermochronology and implications for Eocene tectonics of the northern Rocky Mountains and the Boulder batholith, *Lithosphere*, *2*(4), 232-246.

Foster, D. A., C. Schafer, C. M. Fanning, and D. W. Hyndman (2001), Relationships between crustal partial melting, plutonism, orogeny, and exhumation: Idaho Bitterroot batholith, *Tectonophysics*, *342*(3-4), 313-350.

Foster, D. A., P. T. Doughty, T. J. Kalakay, C. M. Fanning, S. Coyner, W. C. Grice, and J. Vogl (2007), Kinematics and timing of exhumation of metamorphic core complexes along the Lewis and Clark fault zone, northern Rocky Mountains, USA, *Geological Society of America Special Papers*, *434*, 207-232.

Gaschnig, R. M., J. D. Vervoort, R. S. Lewis, and W. C. McClelland (2010), Migrating magmatism in the northern US Cordillera: in situ U-Pb geochronology of the Idaho batholith, *Contributions to Mineralogy and Petrology*, *159*, 863-883.

Gordon, S. M., D. L. Whitney, C. Teyssier, M. Grove, and W. J. Dunlap (2008), Timescales of migmatization, melt crystallization, and cooling in a Cordilleran gneiss dome: Valhalla complex, southeastern British Columbia, *Tectonics*, *27*(4), TC4010-TC4010.

Grover, T. W., J. M. Rice, and J. W. Carey (1992), Petrology of Aluminous Schist in the Boehls Butte Region of Northern Idaho - Phase-Equilibria and P-T Evolution, *Am J Sci*, *292*(7), 474-507.

Guevara, V. E., J. A. Baldwin, J. L. Crowley, R. S. Lewis, and D. A. Foster (2012), U-Pb geochronology of pre-Belt Supergroup rocks in the Clearwater complex, Idaho: implications for Precambrian basement provinces and stratigraphy of the northern Rockies, paper presented at Geological Society of America Rocky Mountain Section Meeting, Albuquerque, NM.

Hietanen, A. (1956), Kyanite, andalusite, and sillimanite in the schist in Boehls Butte quadrangle, Idaho, *American Mineralogist*, *41*, 1-27.

Hietanen, A. (1963), Anorthosite and Associated Rocks in the Boehls Butte Quadrangle and Vicinity, Idaho, *USGS Professional Paper Rep. 344-B*, 1-78 pp, United States Geological Survey, Washington, D.C.

Hietanen, A. (1968), Belt Series in the region around Snow Peak and Mallard Peak, Idaho, *USGS Professional Paper Rep. 344-E*, 1-34 pp, United States Geological Survey, Washington, D.C.

Hietanen, A. (1969), Distribution of Fe and Mg between garnet, staurolite, and biotite in aluminum-rich schist in various metamorphic zones north of the Idaho Batholith, *Am J Sci*, *267*(3), 422-456.

Hodges, K. V., and J. D. Walker (1992), Extension in the Cretaceous Sevier orogen, North American Cordillera, *Geological Society of America Bulletin*, *104*(5), 560-569.

Jones, C. H., G. L. Farmer, B. Sageman, and S. Zhong (2011), Hydrodynamic mechanism for the Laramide orogeny, *Geosphere*, *7*(1), 183-201.

Lang, H. M., and J. M. Rice (1985), Geothermometry, Geobarometry and T-X(Fe-Mg) Relations in Metapelites, Snow Peak, Northern Idaho, *Journal of Petrology*, *26*(4), 889-924.

Lang, H. M., K. J. Largent, T. O. Nesheim, W. C. McClelland, J. D. Vervoort, E. M. Flagg, and J. A. Gilotti (2010), Garnet Zoning as a Record of Proterozoic polymetamorphism in Belt-Purcell Supergroup metapelites, Western Laurentia, paper presented at Geological Society of America Annual Meeting, Denver, CO.

Lewis, R. S., R. F. Burmester, J. D. Kauffman, and T. P. Frost (2000), Geologic Map of the St. Maries 30x60 Minute Quadrangle, Idaho, Idaho Geoogical Survey, Moscow, ID.

Lewis, R. S., R. F. Burmester, T. P. Frost, and W. C. McClelland (2002), Newly mapped Eocene strike-slip faults south of the Boehls Butte Anorthosite, Northern Idaho, paper presented at Geological Society of America Cordilleran Section Meeting, Corvallis, OR.

Lewis, R. S., J. D. Vervoort, R. F. Burmester, and P. J. Oswald (2007a), Geochronological constraints on Mesoproterozoic and Neoproterozoic high-grade metasedimentary rocks of north-central Idaho, U.S.A, in *Proterozoic Geology of Western North America and Siberia*, edited by P. K. Link and R. S. Lewis, pp. 37-53, SEPM, Tulsa, OK.

Lewis, R. S., J. D. Vervoort, R. F. Burmester, and P. J. Oswald (2010), Detrital zircon analysis of Mesoproterozoic and Neoproterozoic metasedimentary rocks of north-central Idaho: implications for development of the Belt-Purcell basin, *Can. J. Earth Sci.*, *47*(11), 1383-1404.

Lewis, R. S., R. F. Burmester, M. D. McFaddan, P. D. Derkey, and J. R. Oblad (1999), Digital Geologic Map of the Wallace 1:100,000 quadrangle, Idaho, Idaho Geological Survey, Moscow, Idaho.

Lewis, R. S., R. A. Brewer, A. C. Jansen, V. E. Guevara, J. D. Vervoort, and J. A. Baldwin (2011), Below the Belt: A Road Log of Archean and Paleoproterozoic Rocks in the Eastern Clearwater Complex, Idaho, *Northwest Geology*, *40*, 143-158.

Lewis, R. S., J. H. Bush, R. F. Burmester, J. D. Kauffman, D. L. Garwood, P. E. Myers, and K. L. Othberg (2005), Geologic Map of the Potlatch 30 x 60 Minute Quadrangle, Idaho., Idaho Geological Survey, Moscow, ID.

Lewis, R. S., R. F. Burmester, M. D. McFaddan, J. D. Kauffman, P. T. Doughty, W. L. Oakley, and T. P. Frost (2007b), Geologic Map of the Headquarters 30 x 60 Minute Quadrangle, Idaho, Idaho Geological Survey, Moscow, ID.

Lister, G. S., and G. A. Davis (1989), The origin of metamorphic core complexes and detachment faults formed during tertiary continental extension in the northern Colorado River region, USA, *Journal of Structural Geology*, *11*(1-2), 65-94.

Liu, M. (2001), Cenozoic extension and magmatism in the North American Cordillera: the role of gravitational collapse, *Tectonophysics*, *342*(3-4), 407-433.

Martinez-Martinez, J. M. (2006), Lateral interaction between metamorphic core complexes and less-extended, tilt-block domains: the Alpujarras strike-slip transfer fault zone (Betics, SE Spain), *Journal of Structural Geology*, *28*(4), 602-620.

Marvin, R. F., R. E. Zartman, J. D. Obradovich, and J. E. Harrison (1984), Geochronometric and Lead Isotope Data on Samples from the Wallace 1° x 2° Quadrangle, Montana and Idaho, United States Geological Survey, Denver, CO.

Mcclay, K., and T. Dooley (1995), Analog Models of Pull-Apart Basins, *Geology*, *23*(8), 711-714.

Nesheim, T. O., J. D. Vervoort, W. C. McClelland, J. A. Gilotti, and H. M. Lang (2012), Mesoproterozoic syntectonic garnet within Belt Supergroup metamorphic tectonites: Evidence of Grenville-age metamorphism and deformation along northwest Laurentia, *Lithos*, *134*(0), 91-107.

O'Neill, J. M., J. D. Lonn, D. R. Lageson, and M. J. Kunk (2004), Early Tertiary Anaconda Metamorphic Core Complex, southwestern Montana, *Can. J. Earth Sci.*, *41*(1), 63-72.

Searle, M. P., M.-W. Yeh, T.-H. Lin, and S.-L. Chung (2010), Structural constraints on the timing of left-lateral shear along the Red River shear zone in the Ailao Shan and Diancang Shan Ranges, Yunnan, SW China, *Geosphere*, *6*(4), 316-338.

Sears, J. W., and M. S. Hendrix (2004), Lewis and Clark line and the rotational origin of the Alberta and Helena salients, North American Cordillera, *Geological Society of America Special Papers*, *383*, 173-186.

Seyfert, C. K. (1984), The Clearwater core complex, a new Cordilleran metamorphic core complex and its relation to a major continental transform fault, paper presented at Geological Society of America Annual Meeting.

Sha, G. S. (2004), Tectonic evolution of the eastern and southern boundaries of the Boehls Butte-Clearwater core complex, north-central Idaho. , 141 pp, Washington State University, Pullman, WA.

Vervoort, J. D., N. A. Zirakparvar, R. S. Lewis, and R. F. Burmester (2007), Evidence for recurrent Paleoproterozoic and Mesoproterozoic magmatism and metamorphism in the Boehls Butte-Clarkia area, north-central Idaho, USA, paper presented at Geological Society of America Annual Meeting, Denver, CO.

Vogl, J. J., D. A. Foster, C. M. Fanning, K. A. Kent, D. W. Rodgers, and T. Diedesch (2012), Timing of extension in the Pioneer metamorphic core complex with implications for the spatial-temporal pattern of Cenozoic extension and exhumation in the northern U.S. Cordillera, *Tectonics*, *31*(1), TC1008-TC1008.

Wells, M. L., and T. D. Hoisch (2008), The role of mantle delamination in widespread Late Cretaceous extension and magmatism in the Cordilleran orogen, western United States, *Geological Society of America Bulletin*, *120*(5-6), 515-530.

Wernicke, B., and G. J. Axen (1988), On the role of isostasy in the evolution of normal fault systems, *Geology*, *16*(9), 848-851.

Whitney, D. L., C. Teyssier, and O. Vanderhaeghe (2004), Gneiss domes and crustal flow, *Geological Society of America Special Papers*, *380*, 15-33.

Winston, D., and P. K. Link (1993), Middle Proterozoic rocks of Montana, Idaho, and Eastern Washington: The Belt Supergroup, in *Precambrian: Conterminous U.S.*, edited by J. C. Reed, M. E. Bickford, R. S. Houston, P. K. Link, D. W. Rankin, P. K. Sims and W. R. Van Schmus, pp. 487-517, Geological Society of America, Boulder, CO.

Woodcock, N. H., and M. Fischer (1986), Strike-Slip Duplexes, *Journal of Structural Geology*, *8*(7), 725-735.

Zirakparvar, N. A., J. D. Vervoort, W. McClelland, and R. S. Lewis (2010), Insights into the metamorphic evolution of the Belt-Purcell basin; evidence from Lu-Hf garnet geochronology, *Can. J. Earth Sci.*, *47*(2), 161-179.

Chapter II: U-Pb geochronology of pre-Belt Supergroup rocks of the Clearwater complex: implications for Precambrian basement provinces and stratigraphic relationships in the northern Rockies

Abstract

The Clearwater metamorphic core complex in northern Idaho is comprised of polymetamorphosed Precambrian rocks. While the presence of basement intrusive rocks in the Clearwater complex has long been known, only recent geochronological data has confirmed their ages and spatial extent. However, the ages of metasedimentary rocks in the Clearwater complex remain cryptic, as direct correlation with ~1450 Ma Belt Supergroup lithologies is nearly impossible due to the obliteration of sedimentary structures through multiple metamorphic events.

This study presents the results of new 1:24,000-scale mapping, LA-ICPMS U-Pb detrital and igneous zircon geochronology, and LA-MC-ICP-MS zircon Hf isotopic analyses of rocks within the Clearwater complex. This study has identified the presence of pre-Belt quartzite, as well as 1870 ± 9 Ma orthogneiss in the Clearwater complex. Detrital zircon populations of the quartzites show a dominant zircon population near ~1800 Ma, with smaller Neo- and Mesoarchean peaks, and suggest correlation with the pre-Belt Neihart Quartzite. The quartzites lie stratigraphically above schist and gneiss that were intruded by the 1870 Ma orthogneiss. The contact between the quartzite and the underlying metasediments therefore represents the boundary between basement and an overlying sedimentary package.

Zircon Hf isotopic analyses of the orthogneiss yield intital ε_{Hf} values between -5.23 and +5.46, suggesting that magma genesis for this body involved both a mantle source and a juvenile crustal source. Hf crustal model ages suggest that this crustal source is Paleoproterozoic to Mesoarchean in age. The ages of ~1.86 Ga intrusive bodies in the Clearwater complex are similar to those of the Great Falls tectonic zone, suggesting that the same pulse of magmatism is present in northern Idaho. The location of the Clearwater complex in the Lewis and Clark fault zone suggests that this structure may delineate a tectonic boundary between two distinct basement terranes along which ~1.86 Ga magmatism occurred.

1. Introduction

The study of basement rocks in the northern Rocky Mountains has been paramount to understanding Precambrian tectonics, supercontinent reconstructions, and the assembly of North America. While exposures of basement rocks are abundant in Montana and Wyoming, they are rare in northern Idaho, where deposition of the Mesoproterozoic Belt Supergroup and intrusion of the Cretaceous Idaho batholith has obscured their presence. Basement rocks in northern Idaho are located adjacent to the $^{87}Sr/^{86}Sr_{initial} = 0.706$ line, which is inferred to be western margin of North American cratonic crust, and thus provide rare opportunites to study the basement architecture of the western edge of Laurentia. The only locations in northern Idaho where basement rocks have been documented are the Priest River and Clearwater metamorphic core complexes (Figure 1), which expose polymetamorphosed Precambrian rocks that were rapidly exhumed from mid-crustal depths during Eocene time [*Brewer et al.*, 2008; *Doughty and Chamberlain*, 2007, 2008; *Doughty et al.*, 1998; *Jansen et al.*, 2011]. These core complexes are comprised of both Archean and Paleoproterozoic basement intrusive rocks, as well as metasediments of the overlying Mesoproterozoic Belt Supergroup [*Doughty and Chamberlain*, 2007, 2008]. This study focuses on characterizing the age and isotopic geochemistry of previously unknown basement orthogneiss, as well as the signatures of detrital zircon populations of the overlying quartzite to this basement in the northeastern part of the Clearwater complex in order to 1) define stratigraphic relationships in the Clearwater complex, and 2) provide further constraints on the nature of ~1.86 Ga magmatism and basement architecture of northern Idaho.

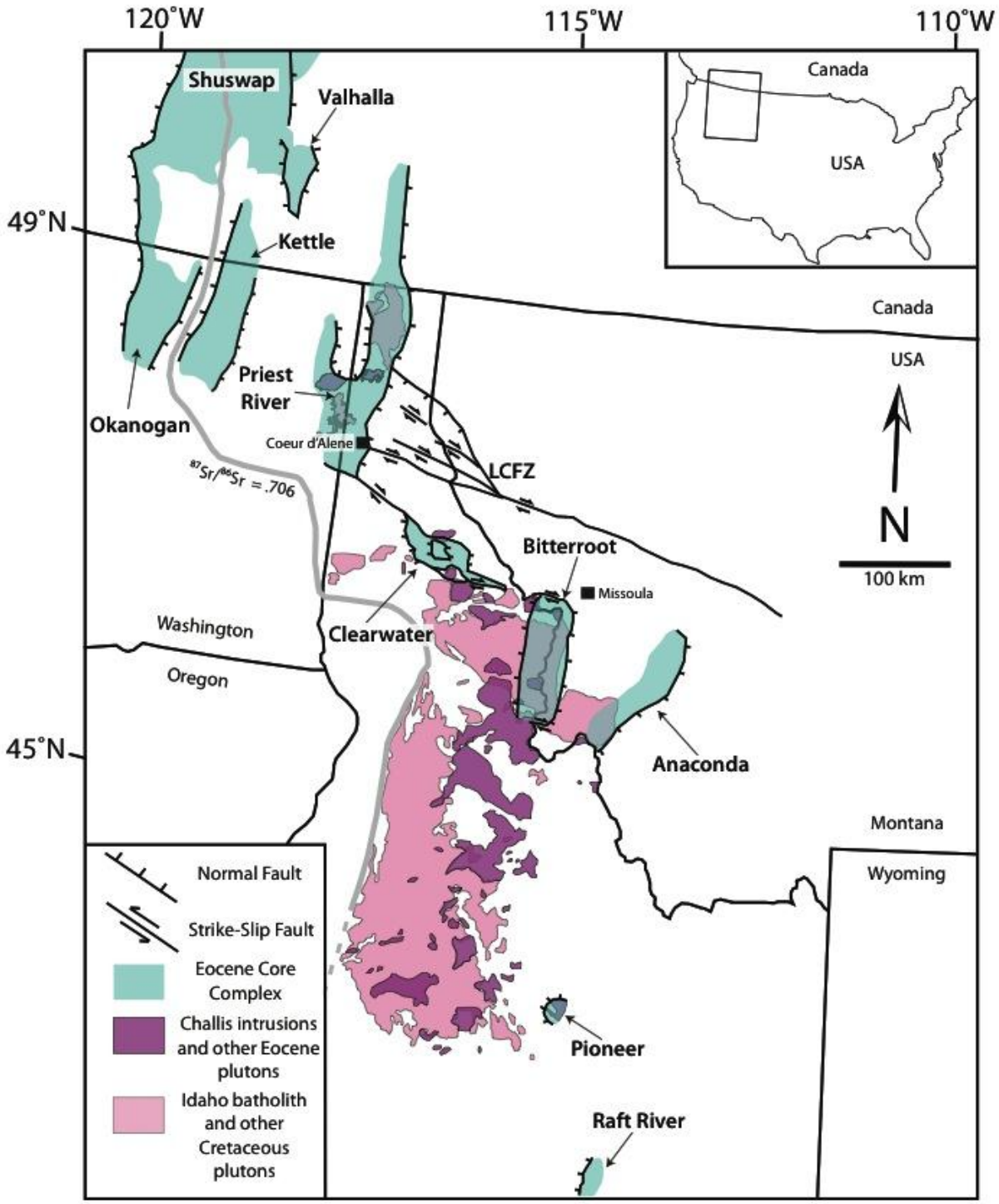

Figure 1: Map of the northwestern U.S. and southern Canada, showing Eocene metamorphic core complexes, the $^{87}Sr/^{86}Sr$ = .706 line, and Cretaceous to Eocene plutons in and around northern Idaho. LCFZ = Lewis and Clark fault zone. Modified after *Foster et al.* [2007], *Gaschnig et al.* [2010], and *Lewis et al.* [2010].

2. Geologic Background

2.1 Precambrian basement provinces of the northern Rockies

The northern Rocky Mountains of the U.S. and southernmost Canada are underlain by at least three Archean to Paleoproterozoic cratonic provinces, based on distinct geophysical, geochemical, and geochronological characteristics: the Medicine Hat Block, Wyoming Province, and Grouse Creek Block (Figure 2) [*Foster et al.*, 2006; *Foster et al.*, 2012; *Whitmeyer and Karlstrom*, 2007]. A fourth basement province, the Selway terrane, has been proposed by *Foster et al.* [2006], but its existence is poorly defined due to the scarcity of basement exposures in this region (Figure 2). The Medicine Hat block, Wyoming Province, and Selway Terrane are discussed in the following section.

2.1.1 Medicine Hat block

The 3.3 to 2.6 Ga Medicine Hat block is the northernmost of the documented basement provinces in this region, extending from south-central Alberta to as far south as north-central Montana (Figure 2) [*Lemieux et al.*, 2000; *Ross et al.*, 1991]. Because of poor exposure, the geologic significance and spatial extent of the Medicine Hat block is unclear. Some workers consider it to be a southern extension of the Hearne Province [*Hoffman*, 1988]; others have placed it with the Wyoming Province to the south, based on seismic data [*Henstock et al.*, 1998]. The western boundary is also unknown; it is possible that the Medicine Hat block extends as far west as the Priest River complex, where 2.6 to 1.5 Ga rocks are exposed, as inferred by isotopic data from xenocrystic zircons [*Doughty et al.*, 1998; *Whitehouse et al.*, 1992], but *Sims et al.* [2004] suggest that the basement in this region is distinct from Medicine Hat crust based on magnetic anomalies. The southwestern border of the Medicine Hat block may be the Lewis and

Clark fault zone, a zone of northwest-trending right-lateral strike-slip faults that have experienced several episodes of activity from Proterozoic to Eocene time [*Foster et al.*, 2006; *Sears and Hendrix*, 2004].

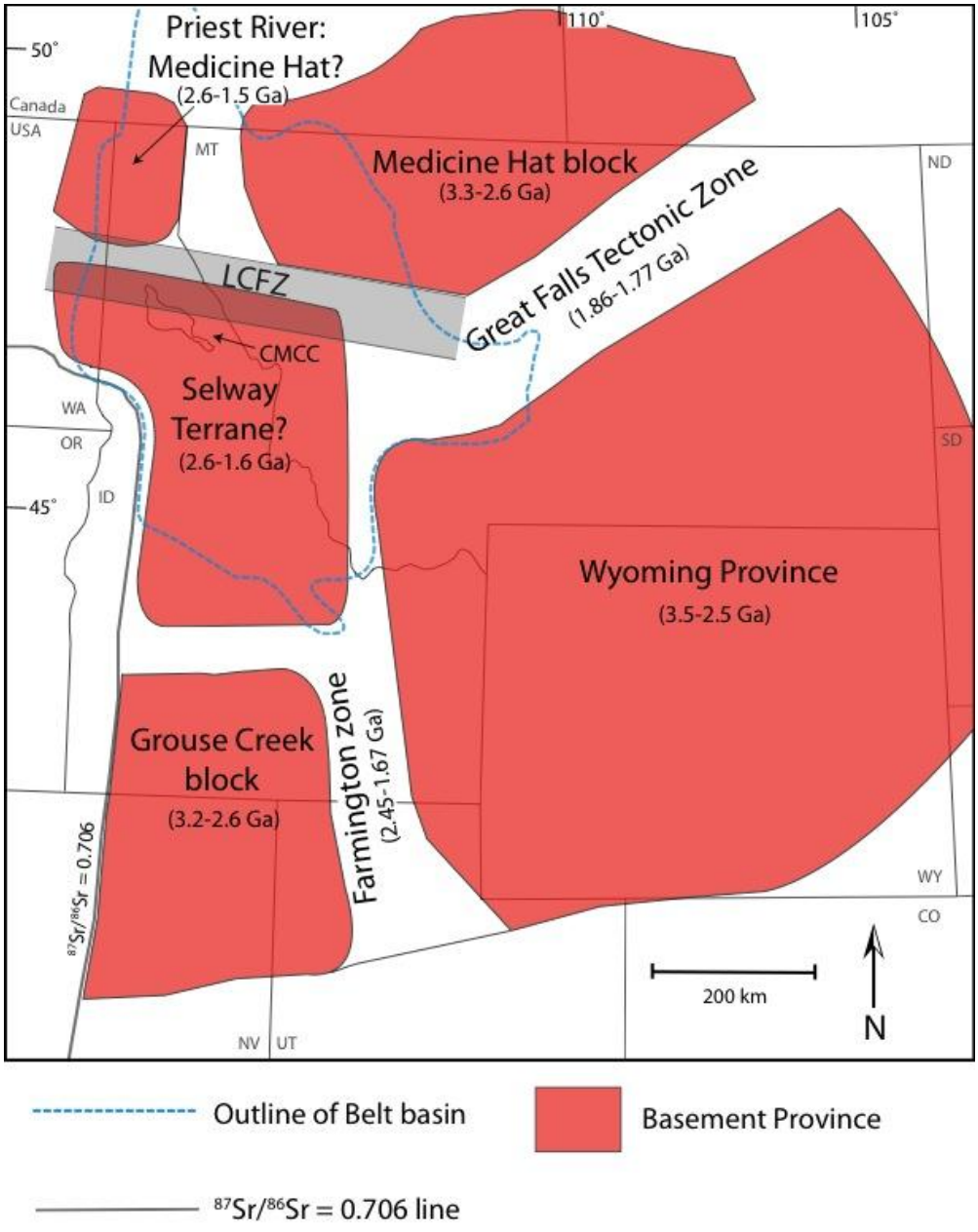

Figure 2: Map of basement provinces in the northwestern U.S. and southern Canada. The Belt basin is outlined by the blue dashed line. LCFZ = Lewis and Clark fault zone, CMCC = Clearwater metamorphic core complex. Modified after *Foster et al.* [2006].

2.1.2 Wyoming Province

The Wyoming Province lies south of the Medicine Hat block in Montana, Wyoming, and eastern Idaho (Figure 2). Rocks of the Wyoming Province are well exposed and range in age from 3.5 Ga gneisses in the northwestern part of the block in the Tobacco Root Mountains, to 2.5 Ga greenstones in the southwestern part of the craton [*Chamberlain et al.*, 2003; *Mueller et al.*, 2004b]. The lithosphere of the Wyoming Province is anomalously thick and strong, as inferred from a seismic velocity structure that is distinct from that of younger adjacent lithospheric blocks [*Henstock et al.*, 1998]. The spatial distribution of recent U-Pb ages and Hf isotopic compositions of xenocrystic zircons from the Pioneer batholith in southwestern Montana indicate that it is underlain by a distinct boundary between crust of the Wyoming craton to the east and crust of the Great Falls tectonic zone to the west [*Foster et al.*, 2012].

2.1.3 Great Falls tectonic zone

The boundary of the Medicine Hat block and Wyoming Province is the Great Falls tectonic zone (Figure 2), which is considered to be the Paleoproterozoic suture between the two basement blocks that formed during the closure of an ocean basin between these two provinces from 1.86 to 1.77 Ga [*Mueller et al.*, 2002]. Zircons from calc-alkaline meta-plutonic rocks in the Little Belt Mountains of central Montana yield U-Pb crystallization ages ranging from 1870 to 1790 Ma [*Vogl et al.*, 2004]. These rocks exhibit trace element and Nd isotopic signatures that suggest subduction of oceanic crust between the Medicine Hat block and Wyoming Province, forming a volcanic arc between the two terranes during this time [*Mueller et al.*, 2002; *Vogl et al.*, 2004]. Other workers suggest the Great Falls tectonic zone is not a suture between Archean provinces, but rather a reactivated intracontinental shear zone within the Wyoming Province,

based on the lack of strong electromagnetic anomalies [*Boerner et al.*, 1998]. The collision between the Wyoming Province and the Medicine Hat Block occurred at approximately 1.77 Ga [*Cheney et al.*, 2004].

2.1.4 Selway terrane

The Selway terrane has been postulated by *Foster et al.* [2006] to be the westernmost of the cratonic blocks underlying the northwestern U.S., north of the Grouse Creek block and south of the Lewis and Clark fault zone (Figure 2). They describe the Selway Terrane as a collage of accreted juvenile Paleoproterozoic terranes characterized by ca.1.8 Ga U-Pb zircon ages and primitive Sr, Nd, and Pb isotopic compositions. The Selway Terrane includes the basement rocks exposed in the Clearwater complex, as well as those exposed in the Pioneer Range, Highland Range, Beaverhead Range, and Bitterroot Range. Magnetic anomaly data suggests the presence of a significant basement boundary along the western edge of the Sevier fold and thrust belt, which has been interpreted to delineate the boundary between the Wyoming craton and a distinct basement terrane to the west [*Sims et al.*, 2004]. However, because the Selway Terrane is overlain by sediments of the Mesoproterozoic Belt Supergroup and has been intruded by the Cretaceous Idaho Batholith, its geographic extent, geochemical nature, and existence have remained poorly constrained.

Recent geochronological data has revealed the presence of Archean (~2.67 Ga) and Paleoproterozoic (~1.86 Ga) basement intrusive rocks within the Clearwater complex [*Jansen et al.*, 2011; *Lewis et al.*, 2011]. Additionally, major and trace element data, whole-rock Sr, Nd, Pb, and Hf isotopic analyses, and zircon Hf isotopic analyses of the Idaho batholith suggest it is underlain by these Paleoproterozoic and Neoarchean orthogneisses [*Gaschnig et al.*, 2011].

Though the Clearwater complex lies within the proposed Selway Terrane, it is also possible that the basement within the complex belongs to a different basement terrane, such as the Medicine Hat block or Wyoming Craton. The basement rocks within the Clearwater complex thus provide rare windows to investigate whether northern Idaho is underlain by one contiguous cratonic block or by a mélange of Archean to Paleoproterozoic juvenile terranes.

2.2 The Belt Supergroup

The Belt Supergroup is a 15-18 km-thick package of sedimentary rocks (Figure 2-3) that were deposited in an intracratonic rift basin on the western margin of Laurentia in the present-day locations of western Montana, Idaho, and eastern Washington during Mesoproterozoic time [*Sears et al.*, 1998; *Winston and Link*, 1993]. The timing of deposition of the Belt Supergroup has been constrained by the intrusion of 1.47-1.46 Ga gabbroic sills and dikes in the Prichard Formation, as well as 1.44-1.40 Ga rhyolitic tuff layers that occur within the middle and upper Belt Supergroup [*Evans et al.*, 2000; *Sears et al.*, 1998]. A stratigraphic column for the Belt Supergroup in the Coeur D'Alene mining district in northern Idaho is shown in Figure 4. The Belt Supergroup units that are relevant to this study include the Prichard, Burke, Revett, St.Regis, and Wallace Formations, as well as the underlying Neihart quartzite. A general overview of these formations is presented here.

The Neihart quartzite is a supermature quartz arenite that was deposited over a broad erosional surface and directly on crystalline basement prior to intracratonic rifting and formation of the Belt basin during Mesoproterozoic time [*Schieber*, 1989]. In Idaho and western Montana, the Neihart quartzite is overlain by the Prichard Formation (Lower Belt), which consists of interstratified argillite, siltite, and matrix-rich quartzite [*Winston and Link*, 1993]. The Ravalli

Group overlies the Prichard Formation and consists of quartzites and argillites of the Burke, Revett, and St. Regis Formations [*Winston and Link,* 1993]. A carbonate-rich layer known as the Middle Belt Carbonate lies on top of the St. Regis Formation, and is referred to as the Wallace Formation in Idaho and Western Montana. The Wallace Formation consists of m-scale to cm-scale couples and couplets of alternating quartzite and siltite layers, with abundant calcite [*Winston and Link,* 1993].

Based on paleocurrent indicators and detrital zircon populations, rocks in the eastern part of the Belt basin are thought to be sourced from the Canadian shield and Wyoming craton/Great Falls tectonic zone [*Ross and Villeneuve,* 2003]. Detrital zircon signatures of rocks in the western Belt basin are characterized by dominant populations at ~1.6 Ga, indicating sediment input from a non-North American continent, as the ages of zircons in this population fall within the North American Magmatic Gap, a period of magmatic quiescence between 1610 and 1490 Ma throughout much of North America [*Lewis et al.,* 2007; *Ross and Villeneuve,* 2003]. The west-bounding craton of the Belt basin has remained a controversial issue, and several cratons have been proposed as likely candidates, including Australia, Siberia, and Antarctica [*Goodge et al.*, 2008; *Sears and Price*, 2003]. Because the rocks of the Clearwater complex have experienced several high-grade metamorphic events, many of the sedimentary structures upon which Belt nomenclature is based have been erased from the rocks of the Clearwater complex. Therefore, many metasedimentary units in complex cannot be assigned to a particular Belt formation based solely on appearance, and can only be reasonably identified based on comparing their distinct detrital zircon populations with known detrital zircon signatures of unmetamorphosed Belt/pre-Belt units. By characterizing the stratigraphy of metasediments in the Clearwater complex in this

manner, stratigraphic relationships within the complex proposed by previous workers [*Hietanen*, 1968] can be reassessed.

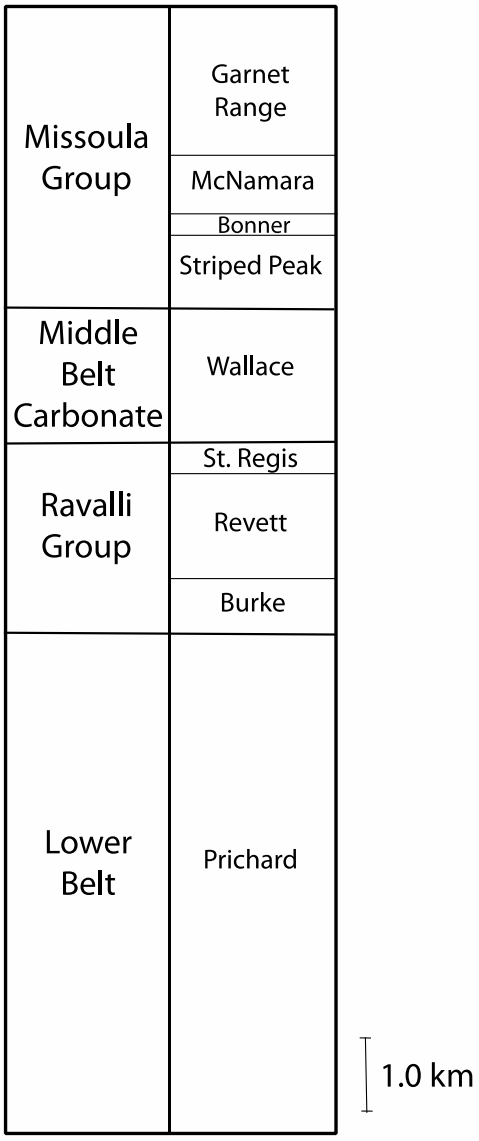

Figure 3: Simplified stratigraphic section of the Belt Supergroup in the Coeur D'Alene mining district in northern Idaho. Modified after *Ross and Villenueve* [2003].

2.3 Clearwater complex

The Clearwater metamorphic core complex is located in northern Idaho, approximately 100 km southwest of Coeur D'Alene (Figure 1). The Clearwater complex has been divided by previous workers into two distinct zones, based on lithological and structural relationships: 1) an "internal zone" that consists primarily of pelites intruded by 1787 Ma anorthosite and 1587 Ma amphibolite collectively known as the Boehls Butte Formation, as well as metasediments that post-date the anorthosite intrusion, and 2) an "external zone" that is dominantly comprised of amphibolite-facies quartzites and metapelites of the Prichard, Burke, Revett, St. Regis, and Wallace Formations (Figure 4) [*Doughty and Chamberlain*, 2007; *Doughty et al.*, 2007; *Hietanen*, 1968]. While the presence of basement rocks in the internal zone of the complex has been recognized for over 40 years, the recent discovery of ~2.67 Ga and ~1.87-1.86 Ga intrusive bodies in the external zone has revealed the spatial extent of basement rocks in the complex to be much larger than previously thought

[*Brewer et al.*, 2008; *Hietanen*, 1968; *Jansen et al.*, 2011; *Lewis et al.*, 2011; *Vervoort et al.*, 2007]. Moreover, the ages of metasedimentary rocks in the Clearwater complex remain cryptic, since direct correlation with Belt Supergroup lithologies is nearly impossible due to the obliteration of sedimentary structures through multiple episodes of high-grade metamorphism. It is thus possible that some metasedimentary rocks are exposures of pre-Belt basement. Characterizing the ages, isotopic geochemistry, and spatial extent of pre-Belt rocks in the complex has implications for interpretations of the stratigraphic and structural relationships within the complex, as well as the geologic evolution of basement provinces and their role in the Paleoproterozoic assembly of North America.

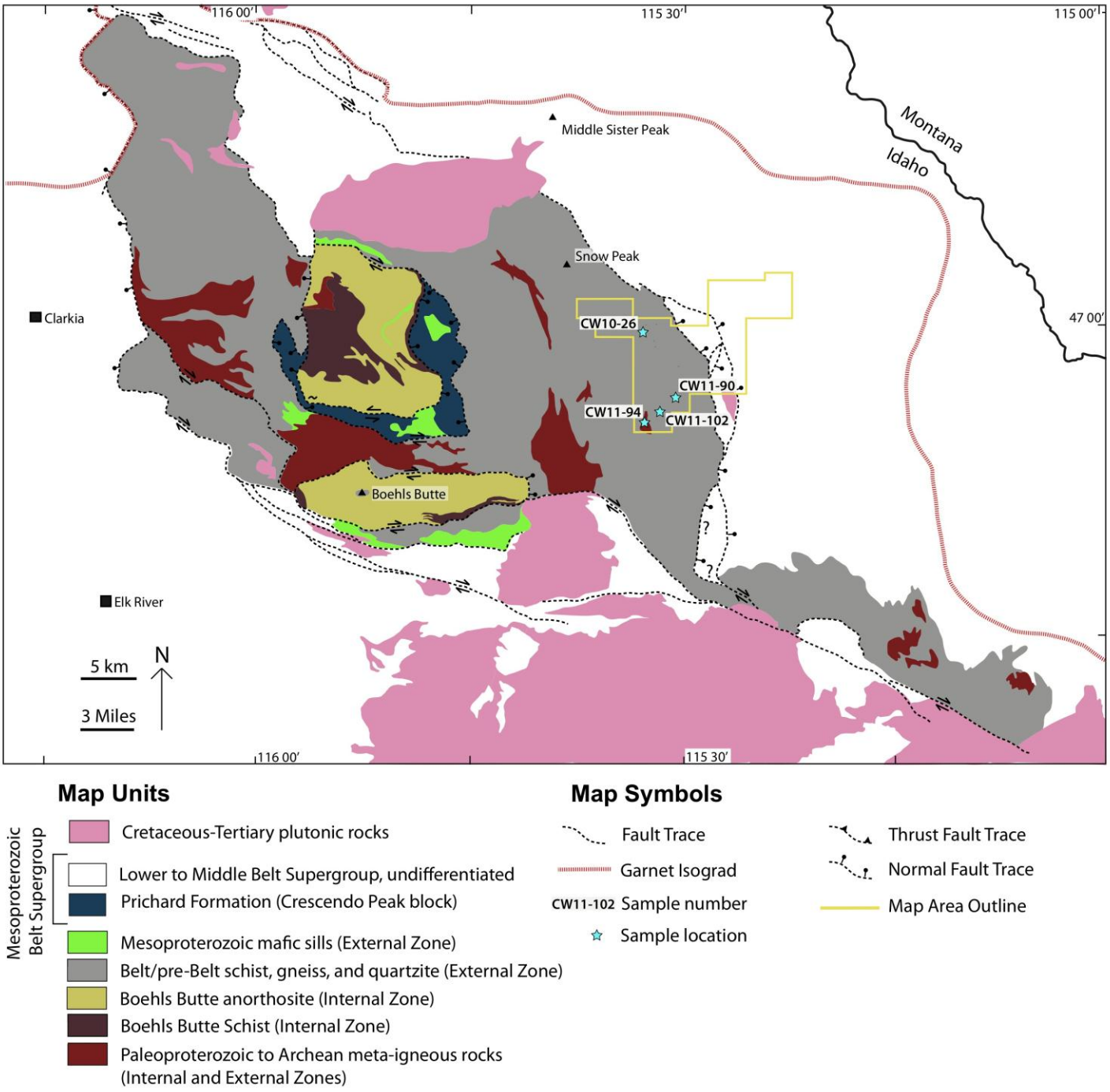

Figure 4: Simplified geologic map of the Clearwater complex. The area outlined in yellow was mapped at the 1:24,000 scale for this study, and is shown in more detail in Plate 1. Paleoproterozoic anorthosite and schist of the Boehls Butte Formation are shown in yellow stripes and brown, respectively. Recently dated Paleoproterozoic to Archean intrusive bodies in the external zone are shown in red. Modified after *Nesheim et al.* [2012].

Geologic mapping at the 1:24,000 scale, LA-ICP-MS U-Pb detrital and igneous zircon geochronology, and LA-MC-ICP-MS Hf isotopic analyses of zircon were employed in this study. An area of 45 mi^2 in the northeastern part of the Clearwater complex was mapped at the 1:24,000 scale (Plate 1). Recent geochronological studies have identified 2.67 Ga and 1.86 Ga basement overlain by pre-Belt quartzite, calling for further detailed mapping to the north [*Lewis et al.,* 2011] (Figure 4). Additionally, an orthogneiss body in the southern part of the map area in this study was postulated to be Cretaceous by *Hietanen* [1968], but no geochronological data exist to support such an assignment. Therefore, geochronological and geochemical analyses of these rocks have the potential to unravel the stratigraphic and structural intricacies of the complex as well as extend our understanding of Precambrian tectonism in the northern Rocky Mountains.

3. Methods

3.1. Geologic Map

The area mapped in this study consists of approximately 45 mi^2 in the St. Joe and Clearwater National forests in northern Idaho, ~130 km SW of Coeur D'Alene. The mapped area lies in portions of the Bathtub Mountain, Mallard Peak, Peggy Peak, Pole Mountain, and Red Ives Peak USGS 7.5 minute quadrangles. It is bound approximately by Surveyors Ridge and Copper Ridge to the north, Collins Peak and Mallard Peak to the south, Canyon Peak to the west, and Copper Point and Pole Mountain to the east (Plate 1).

3.2. LA-ICP-MS U-Pb zircon geochronology

LA-ICP-MS U-Pb detrital and igneous zircon geochronology were employed in order to identify the detrital zircon populations of several quartztite units and the age of an orthogneiss

body in the map area. Zircon grains were separated from rocks using standard density and magnetic mineral separation techniques and mounted in epoxy and polished until the centers of the grains were exposed. For detrital zircon analyses, ~130-150 zircon grains were randomly picked from sample separates. Of these grains, ~100 grains were randomly selected for LA-ICP-MS analysis. For magmatic zircon analyses, 34 of the cleanest, most euhedral grains were picked from the sample separate.

Cathodoluminescence (CL) images were obtained with a JEOL JSM-1300 scanning electron microscope and Gatan MiniCL at Boise State University. The images were used to guide the placement of spots during the analyses. U-Pb isotope systematics and trace element compositions were analyzed by LA-ICPMS using a ThermoElectron X-Series II quadrupole ICPMS and New Wave Research UP-213 Nd:YAG UV (213 nm) laser ablation system at Boise State University. In-house analytical protocols, standard materials, and data reduction software were used for simultaneous acquisition and real-time calibration of U-Pb dates and a suite of HFSE and REE elements using the high sensitivity and unique properties of the interface (Xs cones), extraction lens, and quadrupole analyzer of the X-Series II. Zircons were ablated with a laser diameter of 30 microns using fluence and pulse rates of 12 J/cm^2 and 5 Hz, respectively, during a 60 second analysis (15 sec gas blank, 45 sec ablation) that excavated a pit ~25 μm deep. Ablated material was carried by a 1 L/min He gas stream to the nebulizer flow of the plasma. Dwell times were 5 ms for Si and Zr; 100 ms for ^{49}Ti and ^{207}Pb, 40 ms for ^{238}U, ^{232}Th, ^{202}Hg, ^{204}Pb, ^{206}Pb and ^{208}Pb isotopes; and 10 ms all other HFSE and REE elements. Background count rates for each analyte were obtained prior to each spot analysis and subtracted from the raw count rate for each analysis. For U-Pb dates, instrumental fractionation of the background-subtracted ^{206}Pb/^{238}U and ^{207}Pb/^{206}Pb ratios was corrected, and dates were calibrated with respect

to interspersed measurements of the Plesovice zircon standard [*Slama et al.*, 2008]. Signals at mass 204 were indistinguishable from zero following subtraction of mercury backgrounds measured during the gas blank (<1000 cps ^{202}Hg), and thus dates are reported without common Pb correction. Radiogenic isotope ratio and age error propagation for each spot includes uncertainty contributions from counting statistics and background subtraction. For concentration calculations, background-subtracted count rates for each analyte were internally normalized to ^{29}Si and calibrated with respect to NIST SRM-612, USGS BCR-2, and BIR-1 glasses as the primary standards.

Errors on U-Pb dates are given at 2σ and presented as follows: weighted mean date ± x [y], where x is the internal error and y is the error including the uncertainty on the standard calibration, which are propagated in quadrature. The standard calibration uncertainties for this experiment are 0.96% and 0.78 % (2σ) for the ^{207}Pb/^{206}Pb and ^{206}Pb/^{238}U dates, respectively. Internal errors should be used when comparing weighted mean dates that were measured in the same analytical session, and the errors including the calibration uncertainties should be used when comparing against all other dates. Weighted mean calculations were performed using Isoplot 3.0 [*Ludwig*, 2003].

The FC-1 zircon standard was measured as an unknown during the experiment as a quality control standard. The 14 spots measured yield weighted mean ^{207}Pb/^{206}Pb and ^{206}Pb/^{238}U dates of 1089 ± 17 [20] and 1097 ± 11 [14], respectively. These dates agree with the chemical abrasion - isotope dilution thermal ionization mass spectrometry weighted ^{207}Pb/^{206}Pb and ^{206}Pb/^{238}U dates of 1098.3 ± 0.3 and 1095.4 ± 0.2 Ma, respectively (internal errors at 2σ**,** unpublished data, Boise State University).

3.3. LA-MC-ICP-MS Hf isotopic analyses of zircon

LA-MC-ICP-MS zircon Hf isotopic analyses were utilized in this study to understand the nature of ~1.87-1.86 Ga magmatism in the Clearwater complex, as well as the basement architecture underlying the complex. Analyses were completed at the University of Florida. Analytical methods used are outlined in *Foster et al.,* [2012] and are described in more detail in Appendix 2.

4. Results

4.1. CW10-26: Quartzite east of Sawtooth Saddle

CW10-26 is a coarse-grained, feldspar-poor, foliated quartzite collected from an outcrop adjacent to Sawtooth Saddle, approximately 0.8 km west of the lookout tower on Surveyors Ridge (46.59695°, -115.32599°) (Plate 1; Figure 4). This unit was previously mapped as part of the Revett Formation by *Hietanen* [1968]. Small, 0.5-2 mm-wide flakes of biotite and muscovite are present, but greater than 95% of the rock is comprised of quartz grains 1-10 mm in diameter with undulose extinction. No feldspar was observed in thin section. (Figure 5A).

110 zircon grains from this sample were randomly selected for analysis. Cathodoluminescence (CL) images of zircon grains are shown in Figure 6A, B, and F. Zircons from this sample are colorless to pale yellow and range in length from ~100-250 μm. Most grains are very well rounded, but some are are sub-rounded to sub-angular. Grains with lower degrees of rounding in this sample tend to exhibit less patchy CL zoning, while well-rounded grains exhibit both oscillatory zoning and patchy zoning. There is little to no correlation between shape, CL zoning, and age. The detrital zircon population of this sample shows a prominent peak at approximately 1840 Ma, with a large population of grains between 1780 and 1942 Ma (Figure 7). There is also a small Paleoproterozoic-Archean plateau, with grains ranging in age from 2359

to 2795 Ma. Two grains from this sample yielded Archean ages (Figure 7). The youngest grain with less than 10% discordance analyzed in this sample yields an age of 1696 ± 40 Ma.

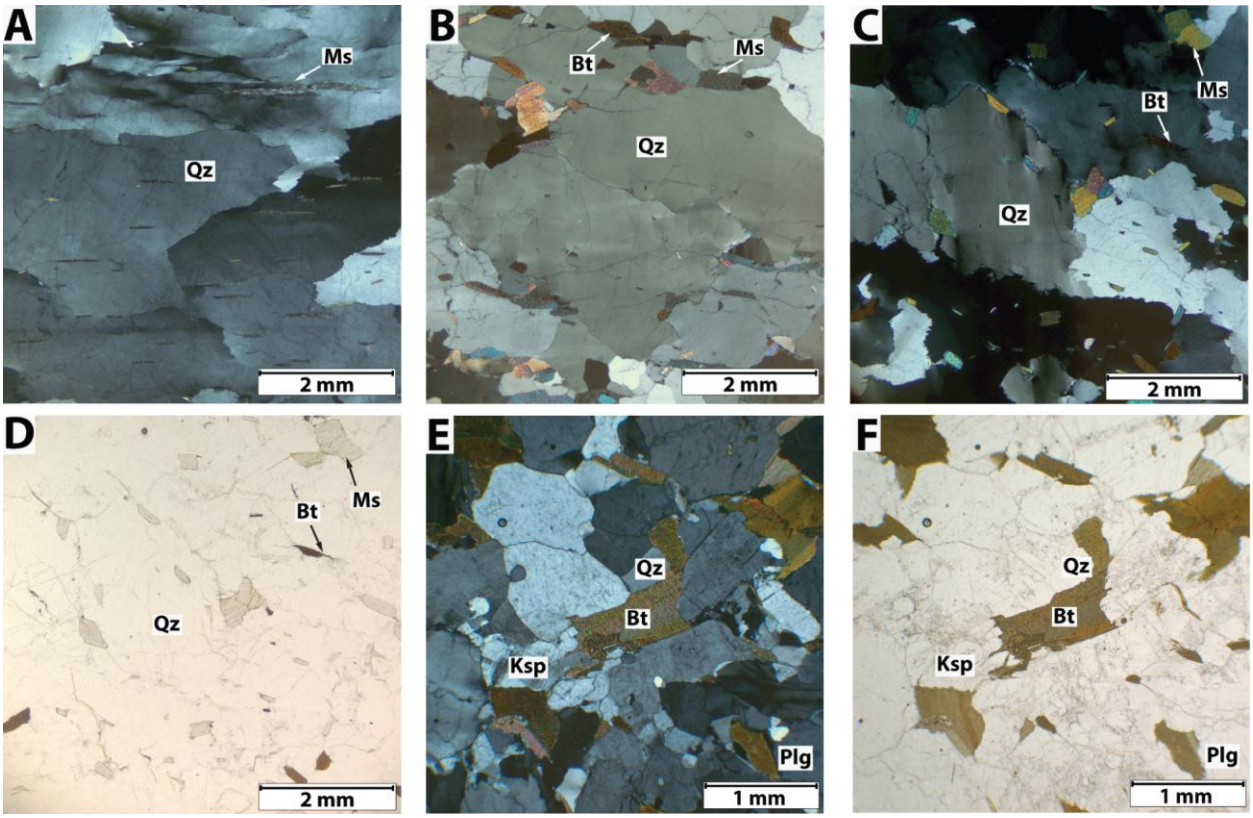

Figure 5: A-C): Photomicrographs of representative sections of samples CW10-26 (A), CW11-90 (B), and CW11-102 (C) in XPL. Quartz grains are very coarse and exhibit undulose extinction. All three quartzite samples are feldspar-poor. D): Same as C) in PPL. E-F): Photomicrographs in XPL and PPL of a representative section of sample CW11-94, showing the mineral assemblage of biotite, plagioclase feldspar, quartz, and potassium feldspar, and coarse-grained igneous texture. Index of mineral abbreviations: Bt = biotite, Ms = muscovite, Plg = plagioclase feldspar, Ksp = Potassium feldspar, Qz = quartz

4.2. CW11-90: Quartzite south of Collins Peak

CW11-90 is a coarse-grained, feldspar-poor, foliated quartzite that was collected from an outcrop approximately 1.8 km southwest of Collins Peak (Plate 1; Figure 4). This unit was also previously mapped as part of the Revett Formation [*Hietanen*, 1968]. Quartz grains range in size from 0.5-6 mm in width, exhibit undulose extinction, and comprise greater than 95% of the rock.

No feldspar was observed in thin section. Biotite and muscovite flakes 0.5-3 mm in width form very thin (<0.5 mm) laminae that separate 10-15-mm-thick zones of pure quartz (Figure 5B).

105 zircon grains from this sample were randomly selected for analysis. CL images of zircon from this sample are shown in Figure 6D and E. Zircons from this sample are colorless to pale yellow and are generally larger than grains in sample CW10-26, ranging in length from ~150-400 μm. Grains range in shape from very well rounded to angular and exhibit both patchy and oscillatory CL zoning. There is little to no correlation between shape, zoning, and age. The probability density plot of this sample shows a large population of 1765-1914 Ma grains, with a smaller Archean peak between 2387 and 2699 Ma (Figure 7). Two grains from this sample are Paleoarchean and were dated at 3383 ± 51 Ma and 3513 ± 12 Ma. The youngest grain in this sample yields an age of 1703 ± 48 Ma.

4.3. CW11-102: Quartzite south of Mallard Peak

CW 11-102 is also a very coarse-grained, feldspar-poor quartzite collected from an outcrop approximately 0.4 km south of the Mallard Peak summit (46.55990°, -115.31456°) (Plate 1). This was originally mapped as quartzite of the Burke Formation by *Hietanen* [1968]. Subhedral garnet porphyroblasts 2-10 mm in width are present but rare. Biotite and muscovite flakes 0.5-3 mm in width form thin laminae that separate thicker layers of quartz 1-4 cm thick. Quartz grains range in size from 1 to 10 mm in width (Figure 5C-D).

107 zircon grains from this sample were randomly selected for analysis. A CL image of zircon is shown in Figure 6. Zircons from this sample are colorless to pale yellow and range in length from ~150-500 μm. Grains range in shape from well rounded to sub-rounded. Grains that are more euhedral and less rounded tend to fall into the age populations near 1.8 Ga and 2.6 Ga.

The probability density plot of this sample shows a large population of 1775-1925 Ma grains, with a smaller Archean peak between 2400 and 2717 Ma (Figure 7). Five grains from this sample are Paleoarchean in age, ranging from 3243 ± 37 Ma to 3520 ± 19 Ma. The youngest grain from this sample is 1554 ± 23 Ma.

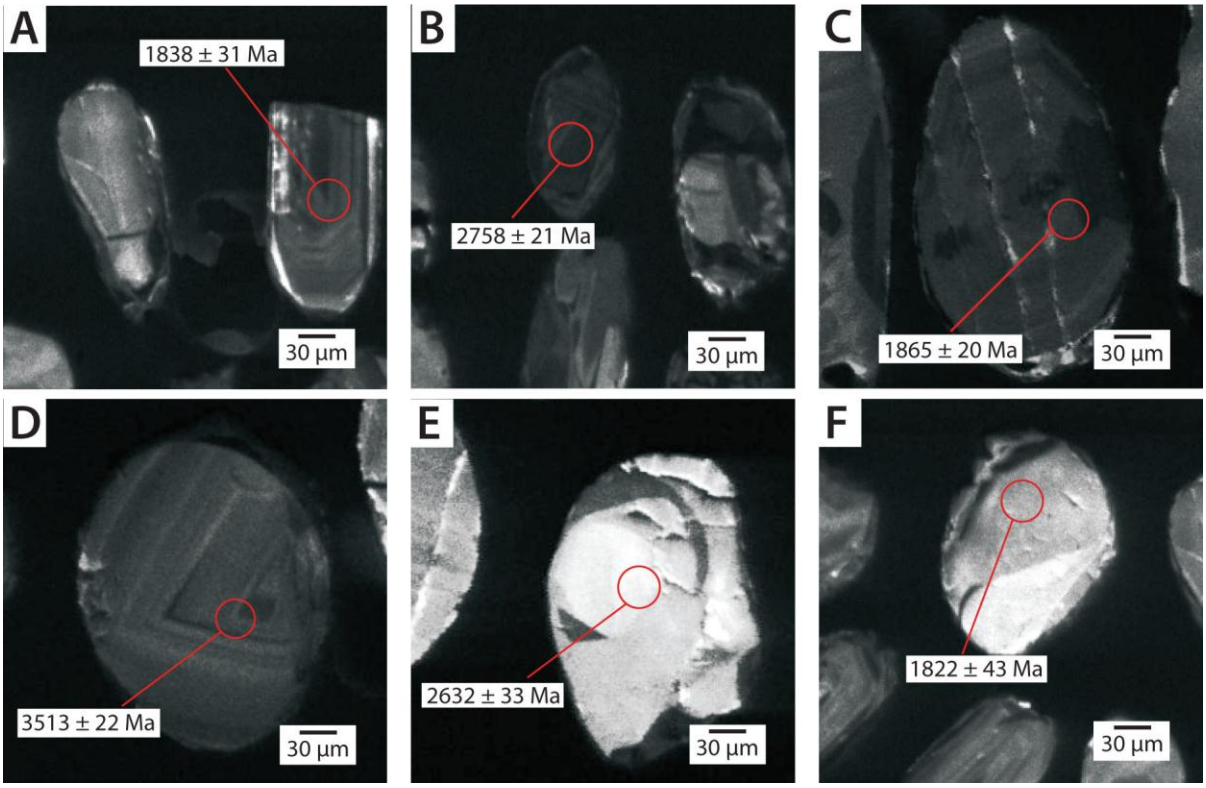

Figure 6: Cathodoluminescence (CL) images of representative detrital zircon grains from the quartzites analyzed in this study. A) through D): Rounded, anhedral zircon grains with oscillatory zoned cores. Some cores are euhedral (A, C); others are anhedral and rounded, surrounded by later overgrowths. A and B are from sample CW10-26; C and D are from CW11-102 and CW11-90, respectively. E) and F): Rounded, anhedral zircon grains with patchy zoning and embayed overgrowths. E is from sample CW11-90 and F is from sample CW10-26. Spot size is 30 µm

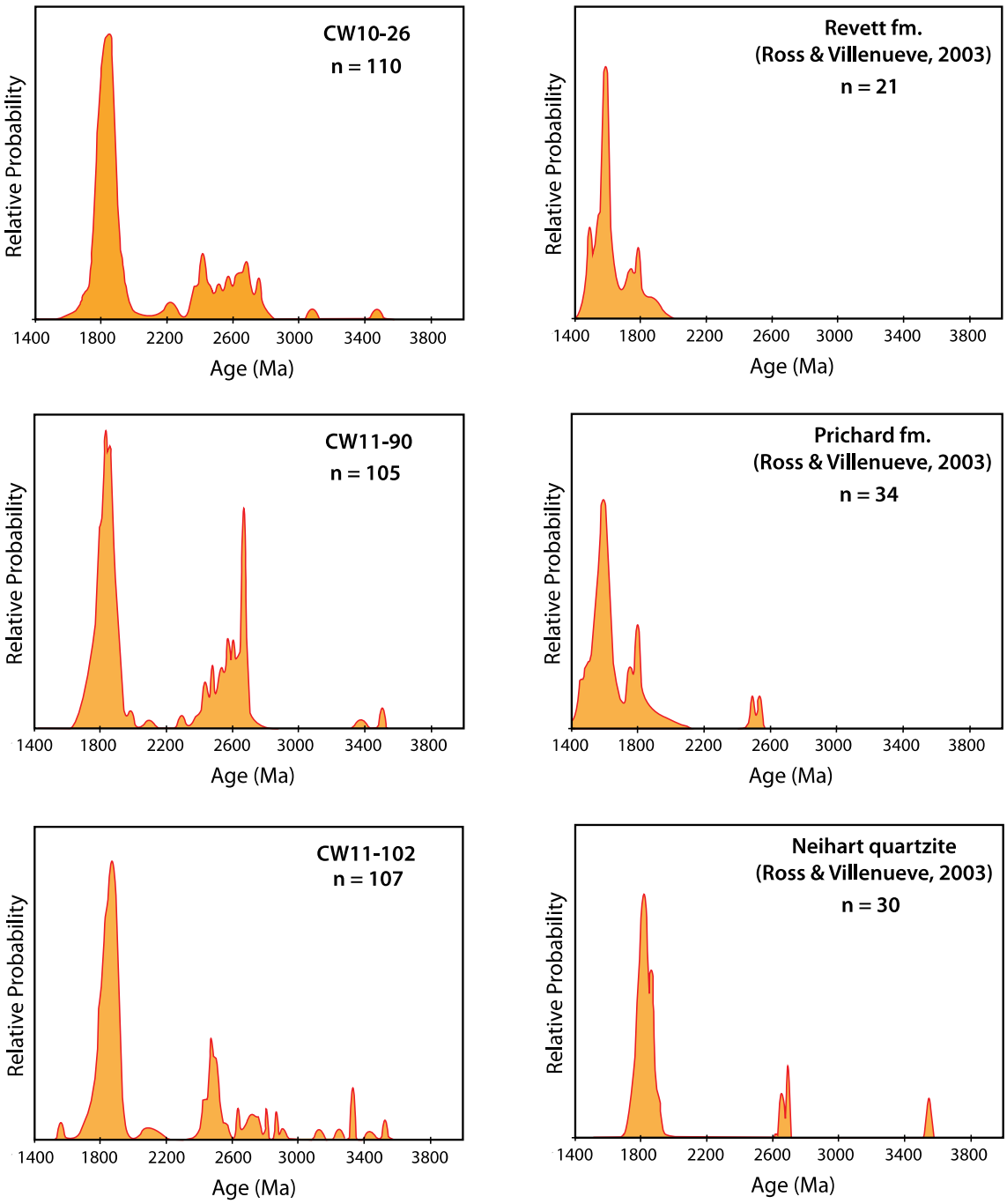

Figure 7: Detrital zircon probability density plots for quartzite samples CW10-26, CW11-90, and CW11-102, as well as the Revett and Prichard Formations of the Belt Supergroup, and the pre-Belt Neihart quartzite from *Ross and Villenueve* [2003]. The three quartzite samples in this study show dominant detrital zircon populations with ages between ~1700 and 1900 Ma, as well as smaller early Paleoproterozoic and Archean populations, which is most similar to the detrital zircon population of the Neihart quartzite. The Revett and Prichard Formations both have a dominant population of ~1.6 Ga grains, indicating provenance from a non-North American source. The Neihart quartzite has a dominant population of ~1.8 Ga grains, and has a detrital zircon signature most similar to the quartzites analyzed in this study.

4.4. CW11-94: Orthogneiss southwest of Mallard Peak

CW11-94 is a medium-grained, foliated biotite granodiorite from a pluton that comprises much of a north-south-trending ridge approximately 1.3 km southwest of the summit of Mallard Peak (46.55873°, -115.32376°) (Plate 1). This body intrudes the surrounding metasediments and was originally mapped as Cretaceous quartz diorite by *Hietanen* [1968]. Photomicrographs of this sample, showing the phaneritic texture and mineral assemblage of quartz, biotite, plagioclase, and potassium feldspar are shown in Figure 5E-F. Zircon grains from this sample are elongate in shape, pale yellow in color, and range in length from 100-300 µm. Grains exhibit oscillatory zoning with dark overgrowths that yield ages with errors that overlap with those from the cores, which are euhedral to anhedral (Figure 8). 17 cores and 15 rims from 29 grains were analyzed.

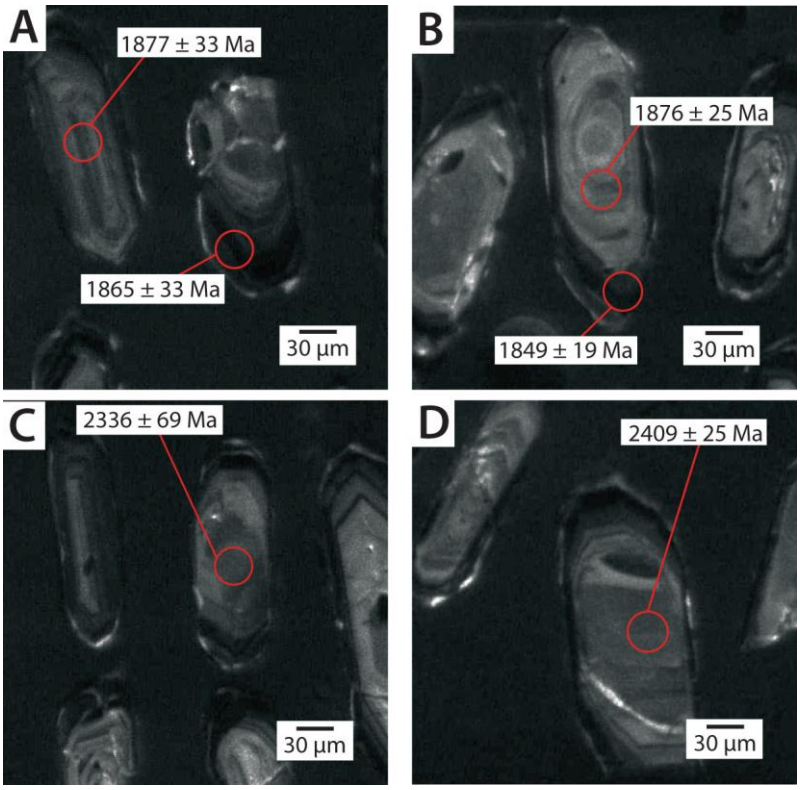

Figure 8: CL images of oscillatory-zoned magmatic zircon from sample CW11-94. A) and B): Euhedral magmatic cores and magmatic rims yield ages near 1.87 Ga. C) and D): Zircons with rounded, anhedral xenocrystic cores, which yield ages near 2.4 Ga. Spot diameter is 30 µm.

4.4.1. U-Pb geochronology

23 laser spots from 22 grains (16 cores and 6 rims) from this sample produced a $^{207}Pb/^{206}Pb$ weighted mean age of 1870 ± 9 Ma with a mean square weighted deviation (MSWD) of 1.6, and a concordia intercept age of 1874 ± 12 Ma with a MSWD of 2.3 (Figure 9). The $^{207}Pb/^{206}Pb$ weighted mean age of 1870 ± 9 Ma is interpreted to be the more accurate age determination, as both the error and MSWD are lower than those for the intercept age on the concordia diagram. Two xenocrysts were analyzed in this sample, yielding ages of 2409 ± 25 and 2336 ± 69 Ma (Figure 8C-D).

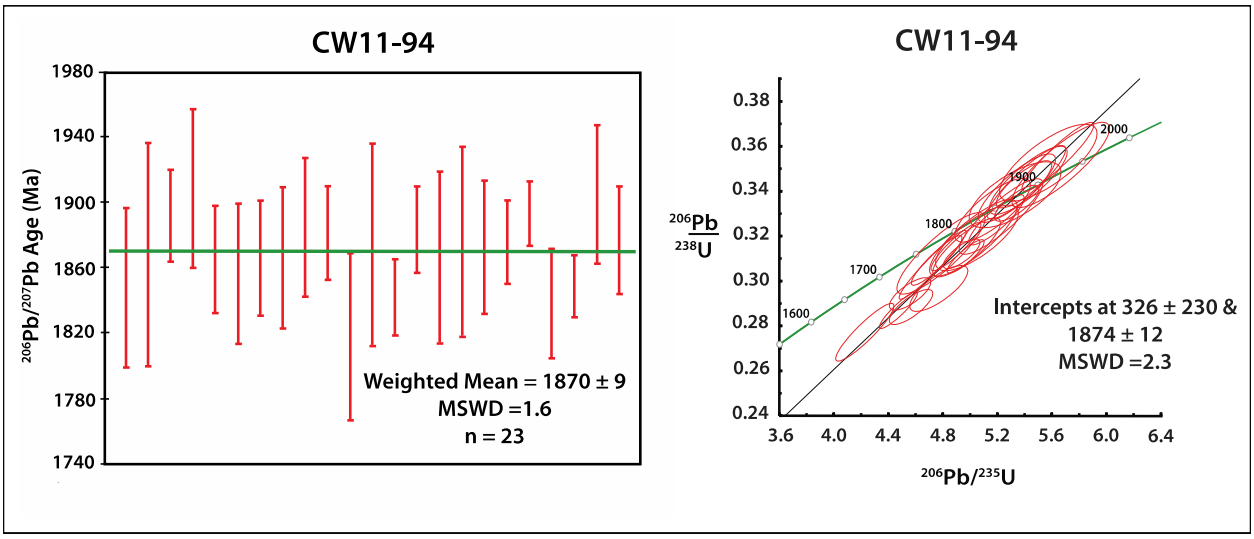

Figure 9: Weighted mean plot and Concordia diagram of 23 zircon laser spots from sample CW11-94. The weighted mean age is 1870 ± 9 Ma, which has a lower error and MSWD than the Concordia intercept age, and is thus interpreted to be the best age for this sample.

4.4.2. Hf isotopic analyses in zircon

LA-MC-ICP-MS Hf isotopic analyses of the same zircon grains used for U-Pb geochronology yield a narrow range of ε_{Hf} values, varying from -5.23 to +5.45 (Figure 10). Calculated bulk crustal Hf model ages for spots with negative initial ε_{Hf} values, based on the $^{176}Lu/^{177}Hf$ value of bulk crust (0.0115) from *Rudnick and Gao* [2003], span from 2.34 to 2.59

Ga, with an average value of 2.43 Ga and median value of 2.37 Ga. Calculated lower crustal Hf model ages for spots with negative initial ε_{Hf} values, based on the $^{176}Lu/^{177}Hf$ value of mafic lower crust (0.0187) from *Rudnick and Gao* [2003], range from 2.51 to 2.85 Ga, with average and median values of 2.6 and 2.5 Ga, respectively. One xenocryst was included in this analysis ($^{207}Pb/^{206}Pb$ age of 2409 ± 25 Ma), which yielded an initial ε_{Hf} value of -1.75 and a bulk crust model age of 2.84 Ga and mafic lower crust model age of 2.99 Ga.

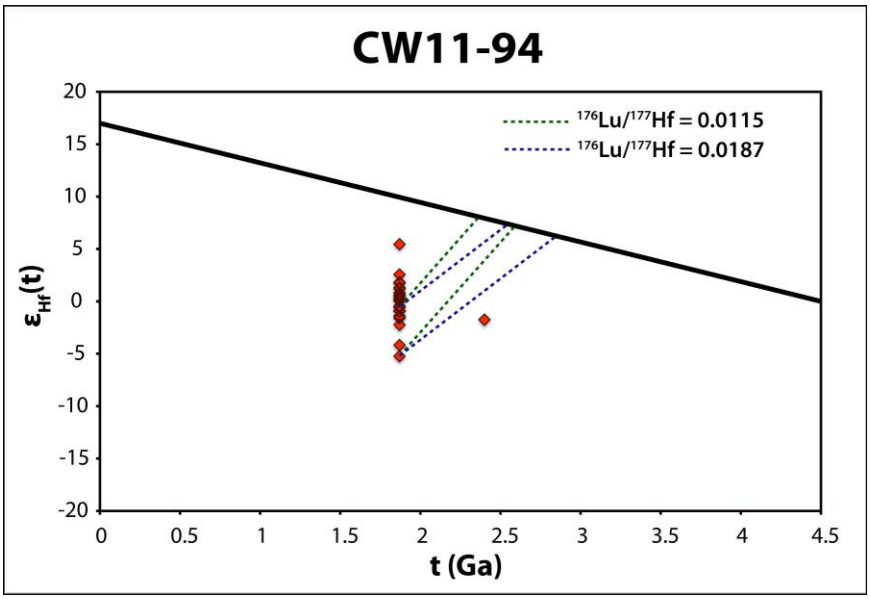

Figure 10: Plot of zircon initial ε_{Hf} vs. U-Pb age showing model Hf isotopic evolution lines with respect to the depleted mantle for ε_{Hf} values of -0.94 and -5.23. The dashed green lines represent Hf isotopic evolution lines assuming $^{176}Lu/^{177}Hf$ = 0.0115 (bulk crust); the blue dashed lines represent Hf isotopic evolution lines assuming $^{176}Lu/^{177}Hf$ = 0.0187 (mafic lower crust) from *Rudnick and Gao* [2003].

5. Discussion

5.1. Detrital zircons

The three quartzite units analyzed in this study have detrital zircon populations that display a prominent peak near 1800 Ma, smaller Paleoproterozoic to Neo-Archean peaks, and few grains that are Mesoarchean to Paleoarchean in age (Figure 7). These detrital zircon signatures are significantly different from those exhibited by rocks of the Belt Supergroup in the

western part of the Belt basin, which characteristically display a pronounced peak near 1600 Ma (Figure 7) [*Lewis et al.*, 2010; *Ross and Villeneuve*, 2003]. The youngest grains in the samples analyzed are between 1703 ± 48 Ma and 1554 ± 23 Ma and are significantly older than the youngest grains in the detrital zircon populations of Belt Supergroup units in the western part of the Belt basin, which typically contain syn-depositional zircon grains with ages between 1400 and 1500 Ma [*Lewis et al.*, 2010; *Ross and Villeneuve*, 2003]. Instead, the detrital zircon signatures of these samples are most similar to the detrital zircon population of the Neihart quartzite in western Montana determined by *Ross and Villenueve* [2003], who reported a dominant Paleoproterozoic zircon population between 1766 and 1912 Ma, with a small number of Archean grains that range in age from 2663 Ma to 3612 Ma (Figure 7).

Other quartzite units in the Clearwater complex also have detrital zircon populations characterized by pronounced peaks at ~1.8 Ga and smaller Paleoproterozoic to Archean fractions. Previously analyzed quartzites with this detrital zircon signature include the quartzites of O'Donnell Creek and Monumental Buttes in the internal zone of the complex, and a quartzite in the external zone of the complex near Skull Creek [*Doughty and Chamberlain*, 2007; *Lewis et al.*, 2007]. The youngest zircon grains found in the quartzites of O'Donnell Creek and Monumental Buttes yield ages of 1649 ± 11 Ma and 1763 ± 25 Ma, which are similar to the youngest grains found in the samples analyzed in this study [*Doughty and Chamberlain*, 2007].

The Gold Cup Quartzite in the Priest River complex, which lies to the northeast of the Clearwater complex, also exhibits a detrital zircon population similar to the units analyzed in this study, and its protolith has been interpreted to be either the Neihart quartzite or the Fort Steele Formation, a correlative unit to the Neihart quartzite in the northern part of the Belt basin [*Doughty and Chamberlain*, 2008; *Ross and Villeneuve*, 2003]. The detrital zircon signature of

the Fort Steele Formation also shows a strong peak near 1800 Ma [*Ross and Villenueve*, 2003]. However, the Fort Steele Formation shows an even larger peak between 2517 and 2794 Ma, which is unlike the detrital zircon signatures from the quartzites analyzed in this study, for which the peak near 1800 Ma is significantly larger than any Neo- or Mesoarchean peaks.

The detrital zircon populations of the quartzites in this study are also similar to those reported by *Gehrels and Ross* [1998] for the lower sandstone unit of the Cambrian Hamill Group in British Columbia, which shows a large population between 1750 and 1859 Ma, and a small fraction of Mesoarchean grains. However, it is unlikely that the quartzites analyzed in this study are correlative with the Hamill Group, as they lie directly on top of basement rocks (Plate 1), while the Hamill Group does not [*Devlin*, 1989]. Additionally, the lower sandstone unit of the Hamill Group has been described as being both feldspathic and interbedded with silty layers [*Devlin*, 1989]. The extremely low feldspar content and lack of interbedded pelitic layers in the quartzites analyzed in this study are inconsistent with these characteristics, and thus make it unlikely that these quartzites are part of the Hamill Group.

The Cambrian Gold Creek quartzite in northern Idaho also exhibits a very similar detrital zircon signature to the quartzites analyzed in this study [*Lewis et al.*, 2010]. Additionally, the Gold Creek quartzite has been described as very feldspar-poor [*Lewis et al.*, 2010]. However, the Gold Creek quartzite lies stratigraphically above the Belt Supergroup, while the quartzites analyzed in this study lie stratigraphically below Belt units and directly above basement, which suggests that they do not correlate to the Gold Creek quartzite (Plate 1).

The extremely low feldspar content of these samples suggests a feldspar-poor, mature quartz arenite as a protolith, which is consistent with the Neihart quartzite, while quartzites of the Belt Supergroup are feldspathic [*Schieber*, 1989; *Winston and Link*, 1993]. When combined with

the comparison of detrital zircon signatures to those of known lithologies, the samples analyzed in this study are thus interpreted to represent a mature, feldspar-poor quartz sandstone that was deposited directly on crystalline basement prior to Belt rifting and sedimentation, and are thus likely correlative with the Neihart quartzite.

The dominant population of ~1.8 Ga zircons in the Neihart quartzite is consistent with derivation from either the Great Falls tectonic zone or the Trans-Hudson orogen and the Black Hills, while the smaller Archean population may have been sourced from the Wyoming Province [*Ross and Villenueve*, 2003]. The dominant zircon populations (1.6-1.4 Ga) of the Belt Supergroup in the western Belt basin is consistent with derivation from a non-North American continent, as these ages fall within the North American Magmatic Gap, and Belt units in the western part of the basin contain abundant paleocurrent indicators that show east-directed flow [*Ross and Villenueve*, 2003]. However, unlike the overlying units of the Belt Supergroup, the Neihart quartzite does not contain paleocurrent indicators, so conclusions about the provenance of detrital zircon in the Neihart quartzite cannot be substantial when based solely on age populations, especially in light of recent geochronological data from the various basement terranes of the northern Rockies.

The data presented here, in synthesis with data from samples analyzed by *Lewis et al.* [2011] and *Doughty and Chamberlain* [2007], suggest that the mature quartz arenite unit between the Lower Belt Supergroup and underlying basement extends much farther to the west than was previously known. Both the Wyoming Province and the Great Falls tectonic zone are not known to extend this far to the west, though it is possible that they do. Although *Ross and Villenueve* [2003] invoke provenance for the Neihart quartzite from the Wyoming craton, these quartzites may have local input from Archean (~2.67 Ga) to Paleoproterozoic (~1.86 Ga)

intrusive bodies that have recently been discovered within the Clearwater complex, as well as 1787 Ma anorthosite and 1587 Ma amphibolite from the internal zone of the complex, which are all included in the Selway terrane [*Brewer et al.*, 2008; *Foster et al.*, 2006; *Jansen et al.*, 2011; *Lewis et al.*, 2011; *Vervoort et al.*, 2007]. This is supported by the presence of euhedral zircons with low degrees of rounding from sample CW11-102 that fall into the age populations of ~1.8 Ga and ~2.6 Ga. However, the disparity in population size between ~1.8 Ga and ~2.6 Ga zircons in the quartzites analyzed in this study suggests that local sources were not the sole contributor of sediment to these quartzites. If this were true, the populations between the 1.8 and 2.6 Ga zircons would be expected to be fairly equal. Moreover, the presence of Meso- and Paleoarchean (2.8-3.5 Ga) zircons in the quartzites suggests some input from a block that is significantly older than any rocks found within the proposed Selway terrane.

Though there could be some input from the Grouse Creek block, some of the zircons in these quartzites are older than the oldest ages from the Grouse Creek block, thus making the Wyoming craton a likely source. Any grains in these samples with ages between 2.4 and 1.8 Ga could have also been sourced from the Farmington Canyon complex [*Mueller et al.*, 2004a]. Additionally, the youngest grain analyzed in this study yields an age (1554 ± 23 Ma) that falls within the North American magmatic gap (1610-1490 Ma) and leaves open the possibility that there may have been some non-North American input as well. This grain could also have been either locally derived from 1587 Ma amphibolite within the Cleawater complex or from the Priest River complex, where basement intrusive rocks as young as 1.58 Ga have been found [*Doughty and Chamberlain*, 2007; *Doughty et al.*, 1998]. It is therefore possible that the quartzites analyzed in this study received sediment input from rocks from any combination of the following sources: the Selway terrane, Great Falls tectonic zone, Wyoming craton, Grouse Creek

block, Farmington Canyon zone, Medicine Hat block, and a non-North American continent. Hf and Nd isotopic analyses of detrital zircons in the rocks analyzed in this study would provide better constraints on the provenance of these quartzites, as they can then be compared to the unique Hf and Nd isotopic signatures of different basement terranes of the northern Rocky Mountains.

5.2. Intrusive Basement Rocks

The $^{207}Pb/^{206}Pb$ age of 1870 ± 9 Ma for the orthogneiss of CW11-94 provides a minimum age constraint for the metasediments that it intrudes. The foliation in this body strikes east and dips to the south, which is markedly different from the dominantly northwest strike and northeast dip of the foliation in the surrounding metasediments probably related to east-west Cretaceous shortening, and is thus interpreted to be a pre-Cretaceous deformational fabric.

ε_{Hf} values range from positive to negative, but do not differ greatly from that of chondrite ($\varepsilon_{Hf} = 0$). This suggests that magma genesis for this body involved two isotopically distinct sources: a depleted mantle source and a juvenile crustal source. The Hf crustal model ages and tight spread of initial ε_{Hf} values near 0 suggest that the crustal source for this magma is dominantly comprised of juvenile Paleoproterozoic to late Archean (2.35 to 2.85 Ga) lower crust. The presence of a 2409 ± 25 Ma xenocryst with a low negative ε_{Hf} value is consistent with this interpretation, as this grain may be inherited from this juvenile lower crustal source. However, the rounded, anhedral shape of the core of this grain suggests a detrital origin and it may have been inherited from the surrounding metasedimentary rocks (Figure 8).

The ε_{Hf} values are generally consistent with those of other Paleoproterozoic orthogneisses in the Clearwater complex analyzed by *Brewer et al.* [2008], which yielded internally consistent,

low negative initial ε_{Hf} values of -1 and -8, suggesting recycling of pre-existing crust. However, the sample analyzed in this study is unique from these bodies in that its initial ε_{Hf} values are not internally consistent and instead range from ~-5 to ~+5. As previously stated, this may be suggestive of this orthogneiss having two isotopically distinct magma sources, while the bodies analyzed by *Brewer et al.* [2008] may have been produced solely by melting of pre-existing juvenile crust. The ~2.67 Ga orthogneiss bodies exposed in the Clearwater complex fall within the range of model ages presented in this study, have zircon ε_{Hf} values between +2.4 and +5.2, and thus are a likely crustal source for regional magmatism at ~1.87-1.86 Ga [*Brewer et al.*, 2008]. This juvenile Paleopreoterozoic to Late Archean crust is also thought to underlie much of the Idaho batholith to the south [*Gaschnig et al.*, 2011].

The 1870 ± 9 Ma age of this sample is similar to other ~1.87-1.86 Ga orthogneiss bodies in the Clearwater complex that have been recently dated [*Lewis et al.*, 2011]. These ages are similar to those of dioritic rocks from the 1.86 Ga Little Belt magmatic arc in the Great Falls tectonic zone [*Gifford et al.*, 2009; *Mueller et al.*, 2002]. The range of both negative and positive initial ε_{Hf} isotopic values of intrusive bodies of this age in the Clearwater complex is similar to whole-rock Sm-Nd isotopic data from the Little Belt arc, which displays initial ε_{Nd} values ranging from -1 to +4 [*Mueller et al.*, 2002].

The zircon age of this sample also falls within the range of basement rocks exposed within the proposed Selway Terrane, most of which range in age from 1.63-1.89 Ga [*Foster et al.*, 2006]. Additionally, the bulk crustal zircon Hf model ages from this sample are similar to ~2.45 Ga U-Pb zircon ages from the oldest rocks exposed in the Selway Terrane [*Foster et al.*, 2006; *Mueller et al.*, 2004a]. Rocks of similar age are also exposed to the south in the Farmington zone [*Mueller et al.*, 2011]. The Hf bulk crustal model ages reported in this study

(2.4-2.6 Ga) are slightly older than the 2.2-1.9 Ga range of two-stage zircon Hf model ages reported for granodiorite of the western Pioneer batholith, which is also interpreted to be underlain by Paleoproterozoic juvenile lower crust of the Great Falls tectonic zone [*Foster et al.*, 2012].

Despite the data presented here, the basement architecture of the region remains uncertain. Basement rocks of the Clearwater complex may indeed be part of the proposed Selway Terrane, which has been described as a collage of juvenile Paleoproterozoic to Archean crust west of the Wyoming craton [*Foster et al.*, 2006]. However, the exposures of ~2.67 Ga orthogneiss in the Clearwater complex are older than any rocks described as part of the Selway Terrane, and thus may be part of the Wyoming Craton or Medicine Hat block. The age of these Archean orthogneiss bodies coincides with 2.95-2.55 Ga calc-alkalic magmatism that occurred within the Wyoming Province, and thus may have formed during this event [*Chamberlain et al.*, 2003]. However, there is no geophysical evidence to indicate that the Clearwater complex is underlain by anomalously thick, high-velocity lithosphere that is characteristic of the Wyoming Craton.

Alternatively, the ~2.67 Ga orthogneisses of the Clearwater complex may be part of the Medicine Hat or Priest River blocks, where basement rocks of similar age have been identified [*Doughty et al.*, 1998; *Ross et al.*, 1991; *Whitehouse et al.*, 1992]. The Priest River block lies almost directly to the north of the Clearwater complex, and it is unclear whether the Priest River block is an extension of the Medicine Hat block. There is also no geophysical evidence that indicates that the Clearwater complex is underlain by Medicine Hat crust.

Another possibility is that the Clearwater complex is underlain by a 1.87-1.86 Ga magmatic arc instead of an Archean basement province, similar to the Little Belt Mountains in

west-central Montana. The 2.67 Ga orthogneiss bodies in the complex could be part of either the Medicine Hat/Priest River block or Wyoming Province that has been translated due to Cretaceous-Eocene fault movement within the Lewis and Clark fault zone.

Overall, the results of this study suggest that the Clearwater complex is underlain by early Paleoproterozoic to Archean juvenile crust. This crust was likely reworked during ~1.87-1.86 Ga magmatism in this region. The location of the Clearwater complex within the Lewis and Clark fault zone suggests that this structure delineates a tectonic boundary between two distinct basement terranes along which magmatism occurred at ~1.87-186 Ga. The age and Hf isotopic characteristics of this pulse of magmatism in northern Idaho suggest correlation with the Great Falls tectonic zone, of which the 1.87-1.86 orthogneiss bodies of the Cleawater complex are likely the western extension. The basement terrane north of this tectonic boundary is probably the Medicine Hat block and/or Priest River block. The southern basement terrane is either a hitherto unknown western extension of the Wyoming Province, or the Selway Terrane. If the latter is the case, the period between ~1.87-1.77 Ga represents a time of voluminous crustal growth and cratonic assembly in western Laurentia that is more significant than previously thought, as both the Selway Terrane and Wyoming craton would have been simultaneously converging with the Medicine Hat block in this scenario.

6. Conclusions

The discovery of Paleoproterozoic orthogneiss and overlying pre-Belt quartzite in this study demonstrates that stratigraphic interpretations in the Clearwater complex, and, more broadly, the stratigraphy of metasediments in high-grade metamorphic terranes can be assessed using a combination of geologic mapping and geochronological analyses. The quartzites, which

are feldspar-poor and have dominant detrital zircon populations at ~1.8 Ga, are similar to the pre-Belt Neihart quartzite and thus probably represent a correlative unit of mature quartz arenite that underlies the Belt Supergroup. The quartzites directly overlie schist and paragneiss that is intruded by 1870 Ma orthogneiss, which was previously thought to be Cretaceous in age. The surrounding metasediments are thus interpreted to represent pre-Belt supracrustal rocks.

Hf isotopic analyses of zircon from the orthogneiss reveal information on the basement architecture underlying the Clearwater complex, which is located in an area where basement exposure has been obscured by Belt sedimentation and Cretaceous intrusion of the Idaho Batholith. The zircon initial ε_{Hf} values for the orthogneiss range from ~-5 to ~+5, indicating that magma genesis for the orthogneiss involved two isotopically distinct sources: a mantle source, and a juvenile Paleoproterozoic to Archean (2.35-2.85 Ga) crustal source, as constrained by the bulk crust and lower crust Hf model ages. This suggests that the Clearwater complex is underlain by juvenile Archean to Paleoproterozoic crust of varying ages, which is consistent with previous work on the Selway Terrane. However, it is also possible that the Clearwater complex is underlain by crust of the Wyoming Craton or Medicine Hat block. This juvenile crust was likely reworked during a magmatic event ca. 1.86-1.87 Ga that seems to be localized in the Lewis and Clark fault zone, and correlates with magmatism in the Great Falls tectonic zone, which may extend further to the west than previously thought.

7. References

Boerner, D. E., J. A. Craven, R. D. Kurtz, G. M. Ross, and F. W. Jones (1998), The Great Falls Tectonic Zone: suture or intracontinental shear zone?, *Can. J. Earth Sci.*, *35*(2), 175-183.

Brewer, R. A., J. D. Vervoort, R. S. Lewis, R. M. Gaschnig, and G. Hart (2008), New constraints on the extent of Paleoproterozoic and Archean basement in the northwest U.S, paper presented at AGU Fall Meeting, San Francisco, CA.

Chamberlain, K. R., C. D. Frost, and B. R. Frost (2003), Early Archean to Mesoproterozoic evolution of the Wyoming Province: Archean origins to modern lithospheric architecture, *Can J Earth Sci*, *40*(10), 1357-1374.

Cheney, J. T., et al. (2004), Proterozoic metamorphism of the Tobacco Root Mountains, Montana, *Geological Society of America Special Papers*, *377*, 105-129.

Devlin, W. J. (1989), Stratigraphy and sedimentology of the Hamill Group in the northern Selkirk Mountains, British Columbia: evidence for latest Proterozoic-Early Cambrian extensional tectonism, *Can. J. Earth Sci.*, *26*(3), 515-533.

Doughty, P. T., and K. R. Chamberlain (2007), Age of Paleoproterozoic basement and related rocks in the Clearwater Complex, Northern Idaho, U.S.A., in *Proterozoic Geology of Western North America and Siberia*, edited by P. K. Link and R. S. Lewis, pp. 9-35, SEPM Special Publication, Tulsa, OK.

Doughty, P. T., and K. R. Chamberlain (2008), Protolith age and timing of Precambrian magmatic and metamorphic events in the Priest River complex, northern Rockies, *Can. J. Earth Sci.*, *45*(1), 99-116.

Doughty, P. T., R. A. Price, and R. R. Parrish (1998), Geology and U-Pb geochronology of Archean basement and Proterozoic cover in the Priest River complex, northwestern United States, and their implications for Cordilleran structure and Precambrian continent reconstructions, *Can. J. Earth Sci.*, *35*(1), 39-54.

Doughty, P. T., K. R. Chamberlain, D. A. Foster, and G. S. Sha (2007), Structural, metamorphic, and geochronologic constraints on the origin of the Clearwater core complex, northern Idaho, *Geological Society of America Special Papers*, *433*, 211-241.

Evans, K. V., J. N. Aleinikoff, J. D. Obradovich, and C. M. Fanning (2000), SHRIMP U-Pb geochronology of volcanic rocks, Belt Supergroup, western Montana: evidence for rapid deposition of sedimentary strata, *Can. J. Earth Sci.*, *37*(9), 1287-1300.

Foster, D. A., P. A. Mueller, D. W. Mogk, J. L. Wooden, and J. J. Vogl (2006), Proterozoic evolution of the western margin of the Wyoming craton: implications for the tectonic and magmatic evolution of the northern Rocky Mountains, *Can. J. Earth Sci.*, *43*(10), 1601-1619.

Foster, D. A., P. A. Mueller, A. Heatherington, J. N. Gifford, and T. J. Kalakay (2012), Lu-Hf systematics of magmatic zircons reveal a Proterozoic crustal boundary under the Cretaceous Pioneer batholith, Montana, *Lithos*, *142,Äì143*(0), 216-225.

Foster, D. A., P. T. Doughty, T. J. Kalakay, C. M. Fanning, S. Coyner, W. C. Grice, and J. Vogl (2007), Kinematics and timing of exhumation of metamorphic core complexes along the Lewis and Clark fault zone, northern Rocky Mountains, USA, *Geological Society of America Special Papers*, *434*, 207-232.

Gaschnig, R. M., J. D. Vervoort, R. S. Lewis, and W. C. McClelland (2010), Migrating magmatism in the northern US Cordillera: in situ U-Pb geochronology of the Idaho batholith, *Contributions to Mineralogy and Petrology*, *159*, 863-883.

Gaschnig, R. M., J. D. Vervoort, R. S. Lewis, and B. Tikoff (2011), Isotopic Evolution of the Idaho Batholith and Challis Intrusive Province, Northern US Cordillera, *Journal of Petrology*, *52*(12), 2397-2429.

Gehrels, G. E., and G. M. Ross (1998), Detrital zircon geochronology of Neoproterozoic to Permian miogeoclinal strata in British Columbia and Alberta, *Can. J. Earth Sci.*, *35*(12), 1380-1401.

Gifford, J. N., D. A. Foster, and P. A. Mueller (2009), U-Pb zircon and whole-rock geochemistry of basement samples from bore holes and xenoliths; age and tectonic significance of the Great Falls tectonic zone, paper presented at Geological Society of America Annual Meeting, Portland, OR.

Goodge, J. W., J. D. Vervoort, C. M. Fanning, D. M. Brecke, G. L. Farmer, I. S. Williams, P. M. Myrow, and D. J. DePaolo (2008), A Positive Test of East Antarctica,ÄìLaurentia Juxtaposition Within the Rodinia Supercontinent, *Science*, *321*(5886), 235-240.

Henstock, T., A. Levander, C. Snelson, R. Keller, K. Miller, S. Harder, A. Gorman, R. Clowes, M. Burianyk, and E. Humphreys (1998), Probing the Archean and Proterozoic lithosphere of western North America, *GSA Today*, *8*(7), 1-5.

Hietanen, A. (1968), Belt Series in the region around Snow Peak and Mallard Peak, Idaho, *USGS Professional Paper Rep. 344-E*, 1-34 pp, United States Geological Survey, Washington, D.C.

Hoffman, P. F. (1988), United Plates of America, The Birth of a Craton: Early Proterozoic Assembly and Growth of Laurentia, *Annu. Rev. Earth Planet. Sci.*, *16*(1), 543-603.

Jansen, A. C., J. D. Vervoort, and R. S. Lewis (2011), Precambrian basement rocks of the Clearwater metamorphic core complex: a new piercing point along the Western Laurentian margin, paper presented at Geological Society of America Annual Meeting, Minneapolis, MN.

Lemieux, S., G. M. Ross, and F. A. Cook (2000), Crustal geometry and tectonic evolution of the Archean crystalline basement beneath the southern Alberta Plains, from new seismic reflection and potential-field studies, *Can J Earth Sci*, *37*(11), 1473-1491.

Lewis, R. S., J. D. Vervoort, R. F. Burmester, and P. J. Oswald (2007), Geochronological constraints on Mesoproterozoic and Neoproterozoic high-grade metasedimentary rocks of north-central Idaho, U.S.A, in *Proterozoic Geology of Western North America and Siberia*, edited by P. K. Link and R. S. Lewis, pp. 37-53, SEPM, Tulsa, OK.

Lewis, R. S., J. D. Vervoort, R. F. Burmester, and P. J. Oswald (2010), Detrital zircon analysis of Mesoproterozoic and Neoproterozoic metasedimentary rocks of north-central Idaho: implications for development of the Belt-Purcell basin, *Can. J. Earth Sci.*, *47*(11), 1383-1404.

Lewis, R. S., R. A. Brewer, A. C. Jansen, V. E. Guevara, J. D. Vervoort, and J. A. Baldwin (2011), Below the Belt: A Road Log of Archean and Paleoproterozoic Rocks in the Eastern Clearwater Complex, Idaho, *Northwest Geology*, *40*, 143-158.

Mueller, P. A., D. A. Foster, D. W. Mogk, and J. Wooden (2004a), New insights into the Proterozoic evolution of the western margin of Laurentia and their tectonic implications, paper presented at Geological Society of America Annual Meeting, Denver, CO.

Mueller, P. A., J. L. Wooden, D. W. Mogk, and D. A. Foster (2011), Paleoproterozoic evolution of the Farmington zone: Implications for terrane accretion in southwestern Laurentia, *Lithosphere*, *3*(6), 401-408.

Mueller, P. A., A. L. Heatherington, D. M. Kelly, J. L. Wooden, and D. W. Mogk (2002), Paleoproterozoic crust within the Great Falls tectonic zone: Implications for the assembly of southern Laurentia, *Geology*, *30*(2), 127-130.

Mueller, P. A., H. R. Burger, J. L. Wooden, A. L. Heatherington, D. W. Mogk, and K. D'Arcy (2004b), Age and evolution of the Precambrian crust of the Tobacco Root Mountains, Montana, *Geological Society of America Special Papers*, *377*, 181-202.

Nesheim, T. O., J. D. Vervoort, W. C. McClelland, J. A. Gilotti, and H. M. Lang (2012), Mesoproterozoic syntectonic garnet within Belt Supergroup metamorphic tectonites: Evidence of Grenville-age metamorphism and deformation along northwest Laurentia, *Lithos*, *134*(0), 91-107.

Ross, G. M., and M. Villeneuve (2003), Provenance of the Mesoproterozoic (1.45 Ga) Belt basin (western North America): Another piece in the pre-Rodinia paleogeographic puzzle, *Geological Society of America Bulletin*, *115*(10), 1191-1217.

Ross, G. M., R. R. Parrish, M. E. Villeneuve, and S. A. Bowring (1991), Geophysics and geochronology of the crystalline basement of the Alberta Basin, western Canada, *Can J Earth Sci*, *28*(4), 512-522.

Rudnick, R. L., and S. Gao (2003), Composition of the Continental Crust, in *The Crust*, edited by R. L. Rudnick, pp. 1-64, Elsevier Ltd, Oxford, UK.

Schieber, J. (1989), The origin of the Neihart Quartzite, a basal deposit of the mid-Proterozoic Belt Supergroup, Montana, U.S.A, *Geological Magazine*, *126*, 271-281.

Sears, J. W., and R. A. Price (2003), Tightening the Siberian connection to western Laurentia, *Geological Society of America Bulletin*, *115*(8), 943-953.

Sears, J. W., and M. S. Hendrix (2004), Lewis and Clark line and the rotational origin of the Alberta and Helena salients, North American Cordillera, *Geological Society of America Special Papers*, *383*, 173-186.

Sears, J. W., K. R. Chamberlain, and S. N. Buckley (1998), Structural and U-Pb geochronological evidence for 1.47 Ga rifting in the Belt basin, western Montana, *Can. J. Earth Sci.*, *35*(4), 467-475.

Sims, P. K., K. Lund, and E. Anderson (2004), Precambrian crystalline basement map of Idaho – an interpretation of aeromagnetic anomalies, United States Geological Survey, Denver, CO.

Slama, J., et al. (2008), Plesovice zircon - A new natural reference material for U-Pb and Hf isotopic microanalysis, *Chemical Geology*, *249*(1‚Äì2), 1-35.

Vervoort, J. D., N. A. Zirakparvar, R. S. Lewis, and R. F. Burmester (2007), Evidence for recurrent Paleoproterozoic and Mesoproterozoic magmatism and metamorphism in the Boehls Butte-Clarkia area, north-central Idaho, USA, paper presented at Geological Society of America Annual Meeting, Denver, CO.

Vogl, J. J., D. A. Foster, P. A. Mueller, J. L. Wooden, and D. W. Mogk (2004), Lithology and age of pre-belt Precambrian basement in the Little Belt Mountains, Montana: implications for the role of the Great Falls Tectonic Zone in the Paleoproterozoic assembly of North America, *Northwest Geology*, *33*, 15-34.

Whitehouse, M. J., J. S. Stacey, and F. K. Miller (1992), Age and Nature of the Basement in Northeastern Washington and Northern Idaho: Isotopic Evidence from Mesozoic and Cenozoic Granitoids, *The Journal of Geology*, *100*(6), 691-701.

Whitmeyer, S. J., and K. E. Karlstrom (2007), Tectonic model for the Proterozoic growth of North America, *Geosphere*, *3*(4), 220-259.

Winston, D., and P. K. Link (1993), Middle Proterozoic rocks of Montana, Idaho, and Eastern Washington: The Belt Supergroup, in *Precambrian: Conterminous U.S.*, edited by J. C. Reed, M. E. Bickford, R. S. Houston, P. K. Link, D. W. Rankin, P. K. Sims and W. R. Van Schmus, pp. 487-517, Geological Society of America, Boulder, CO.

Appendices

Appendix 1: Introduction to $^{40}Ar/^{39}Ar$ thermochronology and detailed description of methods

Introduction

$^{40}Ar/^{39}Ar$ thermochronology was used in this study to place new constraints on the thermal and temporal evolution of the Clearwater complex during Eocene exhumation, particularly with respect to the eastern external zone. This isotopic system is superior to others in determining the thermal history of rapidly exhumed rocks, as it allows for the possibility of analysis of several different minerals, each with a different closure temperature, which is the temperature at which parent and daughter isotopes are no longer exchanged between the mineral and its surroundings. Therefore, a certain mineral can be targeted for $^{40}Ar/^{39}Ar$ analysis if there is a specific stage in the thermal history of a rock that needs to be dated.

$^{40}Ar/^{39}Ar$ thermochronology is based on the ^{40}K decay scheme, in which ^{40}K decays to ^{40}Ar. However, instead of measuring the amount of ^{40}K and ^{40}Ar separately, as is done in the original $^{40}K/^{40}Ar$ thermochronological method, the sample is first bombarded with neutrons in a nuclear reactor, which converts a small proportion of ^{39}K atoms to ^{39}Ar atoms. This is done simultaneously with a standard of known age, in order to calibrate the parent/daughter isotope ratios for the sample being analyzed. The ^{39}Ar that is produced in the nuclear reactor thus serves as a proxy for ^{39}K, which maintains a constant ratio with ^{40}K. The $^{40}Ar/^{39}Ar$ ratio as measured in a noble gas mass spectrometer is therefore proportional to the $^{40}K/^{40}Ar$ ratio, and, consequently, the cooling age of the sample.

The $^{40}Ar/^{39}Ar$ method has several advantages over the $^{40}K/^{40}Ar$ method: 1) the ratio of daughter to parent isotopes is measured in a single analysis, allowing for smaller sample volume as well as accounting for sample inhomogeneity, 2) isotope ratios can be measured more

precisely because they are measured in a single analysis, 3) after irradiation, a sample can be heated in steps, starting at temperatures below the fusion temperature, providing insight to the distribution of radiogenic argon in the sample [*McDougall and Harrison*, 1999]. Moreover, $^{40}Ar/^{39}Ar$ thermochronology, in conjunction with detailed geologic mapping and structural analysis, has been successfully employed to constrain the exhumation histories of other Cordilleran core complexes [*Doughty and Price,* 1999; *Doughty et al.*, 2000; *Foster and Fanning,* 1997; *Foster et al.*, 2010]. Thus, performing $^{40}Ar/^{39}Ar$ thermochronological analyses on rocks of the Clearwater complex in this study allows for a simple and direct comparison of exhumation ages determined by previous workers for both the Clearwater complex and other Cordilleran core complexes.

In this study, $^{40}Ar/^{39}Ar$ thermochronological analyses of muscovite and biotite were used to determine when rocks of the Clearwater complex cooled below the closure temperatures of muscovite and biotite, which are generally considered to be ~350°C and ~300°C, respectively, thus providing an approximate minimum age of exhumation to the upper crust, given a geothermal gradient of ~30°C/km, and assuming rapid, isothermal decompression [*McDougall and Harrison*, 1999; *Kearey et al.*, 2009]. Muscovite and biotite were chosen for $^{40}Ar/^{39}Ar$ thermochronological analysis because of their abundance in both metasedimentary and granitic rocks over amphiboles, allowing for consistency of exhumation ages among the different rock types in the Clearwater complex, which is comprised mostly of quartzites, pelites and granitoids. Additionally, muscovite and biotite were chosen for $^{40}Ar/^{39}Ar$ thermochronological analysis over plagioclase and alkali feldspar, as the latter two have lower closure temperatures (150 °C) and relatively low argon retentivity [*McDougall and Harrison*, 1999].

Because footwall rocks of the eastern external zone are dominantly pelitic and presumed to have been rapidly exhumed and likewise cooled, traditional whole-grain step-heating analyses were performed instead of spot-fusion analyses, which are typically used to constrain thermal histories of slowly-cooled rocks in high-temperature, low-pressure metamorphic terranes [*Hodges et al.*, 1994].

Methods

The following is an excerpt from *Foster et al.* [2009], which describes the methods used for $^{40}Ar/^{39}Ar$ thermochronological analyses in this study. The $^{40}Ar/^{39}Ar$ analyses of hand picked mineral separates were undertaken at the University of Florida following standard methods [*McDougall and Harrison*, 1999; *Gray et al.*, 2006]. Samples were irradiated in the core of the Oregon State University research reactor facility along with the flux monitor GA1550 biotite (98.79 ± 0.69 Ma [*Renne et al.*, 1998]). Step heating took place in a Modifications Ltd. double vacuum resistance furnace for the hornblende and with a CO2 laser for the white mica. The extracted gas was expanded into a stainless steel cleanup line and purified with two 50 L/s SAES getters. Argon isotopes were measured using a MAP215-50 mass spectrometer in electron multiplier mode. Data were corrected for system blanks, machine background, and mass discrimination. Correction factors for interfering isotopes were determined from irradiated K glass and optical grade CaF2 salts. Data reduction was done using ArArCALC [*Koppers*, 2002]. Errors on calculated ages are 2-sigma and include internal and external errors.

References

Foster, D. A., B. D. Goscombe, and D. R. Gray (2009), Rapid exhumation of deep crust in an obliquely convergent orogen: The Kaoko Belt of the Damara Orogen, *Tectonics*, *28*(4), TC4002-TC4002.

Hodges, K. V., W. E. Harries, and S. A. Bowring (1994), $^{40}Ar/^{39}Ar$ age gradients in micas from a high-temperature-low-pressure metamorphic terrain: Evidence for very slow cooling and implications for the interpretation of age spectra, *Geology*, *22*(1), 55-58.

Koppers, A. A. P. (2002), ArArCALC—Software for 40Ar/39Ar age calculations, *Comput. Geosci.*, 28, 605–619, doi:10.1016/S0098-3004(01)00095-4.

McDougall, I. & Harrison, T.M. *Geochronology and Thermochronology by the $^{40}Ar/^{39}Ar$ method.* (Oxford University Press: New York, NY, 1999).

Appendix 2: Introduction to Hf in zircon isotopic analysis and detailed description of methods

Introduction

The Lu-Hf isotopic system has long been known as a useful tracer for tracking the chemical differentiation and evolution of the Earth's crust and mantle. This system relies on the radioactive decay of ^{176}Lu to ^{176}Hf. Lu is a compatible element that remains in the parent material and is thus excluded from the melt during fractionation. Hf is more incompatible than Lu and so will stay in the melt. Since ^{176}Lu decays to ^{176}Hf, the mantle becomes more enriched in ^{176}Hf, while the crust becomes more depleted in ^{176}Hf as the Earth continues to chemically differentiate through tectonomagmatic processes. Zircon preferentially incorporates Hf, and thus has an extremely low Lu/Hf value, so any ^{176}Hf in zircon produced by the in situ decay of ^{176}Lu is negligible. Therefore, zircon essentially preserves the initial ^{176}Hf/^{177}Hf ratio (typically symbolized as ε_{Hf}) of its source magma at the time of crystallization, and a Hf model age can reveal the time at which a melt was extracted from its source. When combined with the U-Pb crystallization age, the Lu/Hf isotopic system in zircon can be used as a powerful geochemical tracer to determine the magmatic origin of a host rock, as well as the residence time of a magma from source extraction to crystallization.

Methods

Methods of zircon Hf isotopic analyses employed in this study are outlined in *Foster et al.* [2012]. Lu–Hf isotopic data were acquired from zircon grains that were mounted in epoxy, polished, and then ablated using a New Wave 213 nm laser. The ablated material was analyzed using a Nu Plasma multi-collector plasma source mass spectrometer (MC-ICP-MS) following

methods summarized by *Mueller et al.* [2008]. Laser ablation targeted only euhedral zircon grains showing concentric magmatic zoning in CL images, and was focused on zones or spots previously determined to have crystallized in the Cretaceous magma by U–Pb measurements via SIMS or LA-MC-ICP-MS, whenever possible. A smaller number of xenocrystic grains with known U–Pb age were also ablated for Lu–Hf isotopic analysis. Hf isotopic measurements were performed with on-line Lu and Yb isobaric interference corrections using $^{176}Lu/^{175}Lu = 0.02653$ and $^{176}Yb/^{172}Yb = 0.5870$, which are within the range of published values [*Vervoort et al.*, 2004]. All isotopic ratios, including Lu and Yb, were corrected for mass-bias using $^{178}Hf/^{177}Hf = 1.46718$. Hundreds of analyses of reference zircon FC-1 over several years yield $^{176}Hf/^{177}Hf = 0.282169$ (±0.000032, 2σ). This value is indistinguishable from our analyses of FC-1 zircon dissolved and aspirated into dry plasma ($^{176}Hf/^{177}Hf = 0.282174$; ± 0.000013, 2σ) and from values reported by Woodhead et al. (2004) ($^{176}Hf/^{177}Hf = 0.282172$; ± 0.000042, 2σ). Measured and mass-bias corrected $^{176}Lu/^{177}Hf$ ratios were used to calculate initial $^{176}Hf/^{177}Hf$ ratios [*Griffin et al.*, 2000, 2002]. εHf values are calculated based on the CHUR values of Bouvier et al. (2008). Depleted mantle values are based on a linear model (εHf = 0 at 4.56 Ga and 16 at 0 Ga; Mueller et al., 2008). The ^{176}Lu decay constant ($1.867x10^{-11}yr^{-1}$) is after Söderlund et al. (2004). Typical reproducibility for Hf isotopic compositions is about ±1 εHf (2σ) for measured ratios with b 25% cumulative isobaric corrections for Lu and Yb [*Mueller et al.*, 2008]. Corrections of measured $^{176}Hf/^{177}Hf$ ratios averaged 14% (range 5 to 27%) and are not correlated with initial Hf isotopic ratios. Whole-rock Sm–Nd isotopic data were determined using isotope dilution and ICP-MS methods after *Heatherington and Mueller* [1991].

References

Griffin, W. L., N. J. Pearson, E. Belousova, S. E. Jackson, E. van Achterbergh, S. Y. O'Reilly, and S. R. Shee (2000), The Hf isotope composition of cratonic mantle: LAM-MC-ICPMS analysis of zircon megacrysts in kimberlites, *Geochimica et Cosmochimica Acta*, *64*(1), 133-147.

Griffin, W. L., X. Wang, S. E. Jackson, N. J. Pearson, S. Y. O'Reilly, X. S. Xu, and X. M. Zhou (2002), Zircon chemistry and magma mixing, SE China: In-situ analysis of Hf isotopes, Tonglu and Pingtan igneous complexes, *Lithos*, *61*(3-4), 237-269.

Heatherington, A. L., and P. A. Mueller (1991), Geochemical Evidence for Triassic Rifting in Southwestern Florida, *Tectonophysics*, *188*(3-4), 291-302.

Mueller, P. A., G. D. Kamenov, A. L. Heatherington, and J. Richards (2008), Crustal evolution in the southern Appalachian orogen: Evidence from Hf isotopes in detrital zircons, *J Geol*, *116*(4), 414-422.

Vervoort, J. D., P. J. Patchett, U. Soderlund, and M. Baker (2004), Isotopic composition of Yb and the determination of Lu concentrations and Lu/Hf ratios by isotope dilution using MC-ICPMS, *Geochem Geophy Geosy*, *5*.

Appendix 3: Description of Rock Units in the map area

Introduction

The lithologies in the map area were identified through a combination of the results of U-Pb zircon geochronology in this study, mineralogy, and stratigraphic characterisitics and relationships. The metasedimentary rock units in the map area, in stratigraphically-descending order, are: Wallace schist, Wallace quartzite, Ravalli Group quartzite (undifferentiated), Prichard schist, Fawn Lake quartzite, and basement paragneiss/schist. This section provides detailed descriptions of the rocks of each unit within the map area, both in outcrop and in thin section.

Metasedimentary Rocks

Wallace schist

The Wallace schist occurs in the easternmost part of the map area and consists of fine-grained, crenulated garnet-biotite schist and phyllite. Garnet porphyroblasts are subhedral to euhedral and range in size from 0.1 mm to 2 cm in diameter (Figure 1). Staurolite and/or kyanite are locally abundant, particularly near Pole Mountain and east of Club Point. In many localities, pseudomorphs of muscovite and/or biotite after kyanite and/or staurolite are present (Figure 1). Crenulation folds range in width from 0.5 cm to 2 cm (Figure 1). Original bedding is visible, and has been transposed with respect to the foliation.

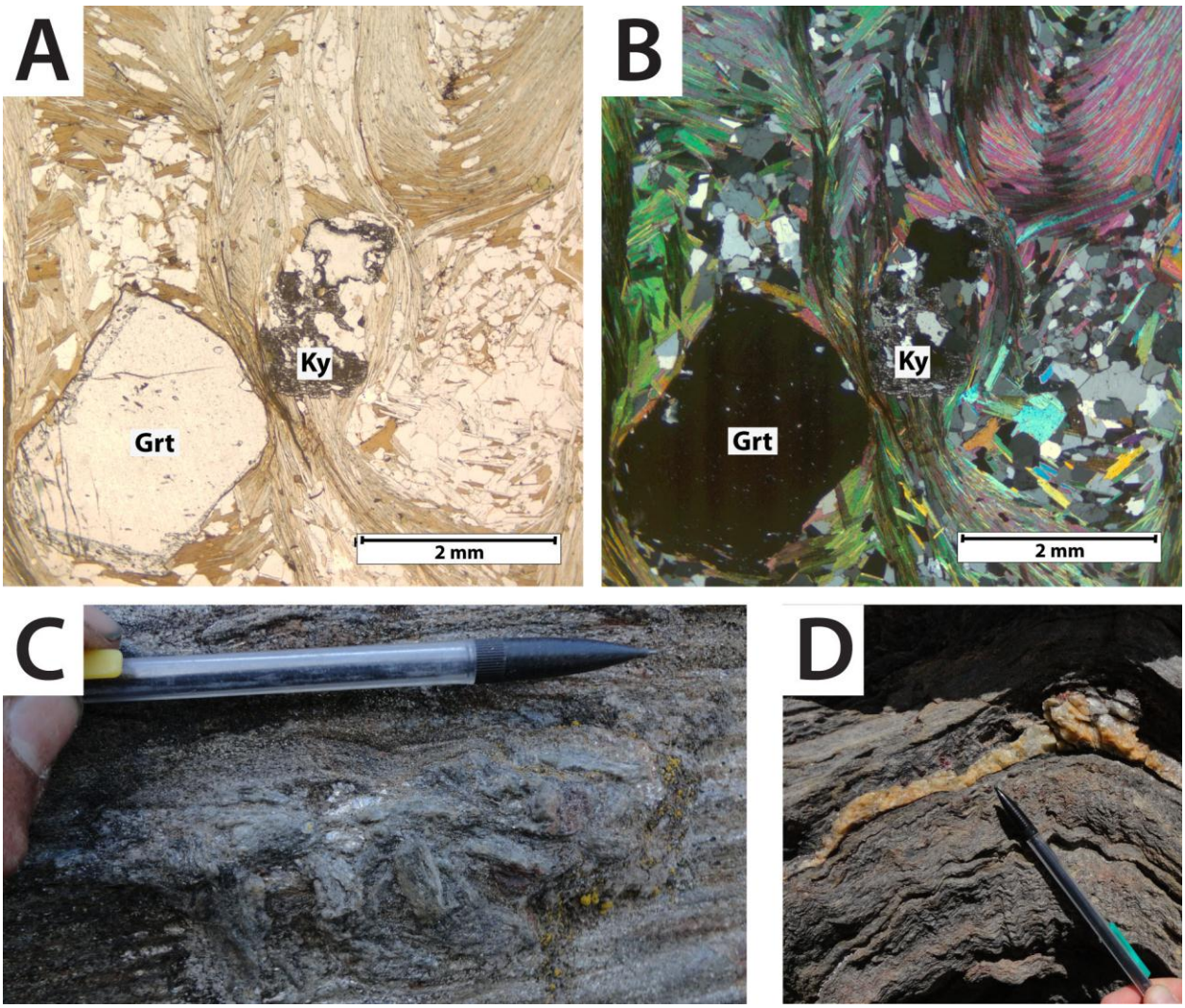

Figure 1: Photomicrgraphs and field photos of the Wallace schist. A): Subhedral zoned garnet porphyroblast, adjacent to resorbed kyanite. Micas define crenulation folds. Plane polarized light. B): Same as A in cross-polarized light. C) Muscovite pseudomorphs after kyanite. D) Cm-scale crenulation folds in garnet schist.

Wallace quartzite

The Wallace quartzite in the map area is dominantly comprised of calc-silicate gneiss and quartzite. The dominant lithology in the map area is fine- to medium-grained actinolite gneiss (Figure 2). Scapolite-bearing layers are present but rare, with scapolite crystals ranging in size from 0.5 cm to 3 cm in diameter. Actinolite-rich layers are present near Elk Prairie, with small,

randomly-oriented prismatic amphibole needles up to 3 mm long. The contact with the overlying Wallace schist is gradational, as this unit becomes increasingly micaceous up-section.

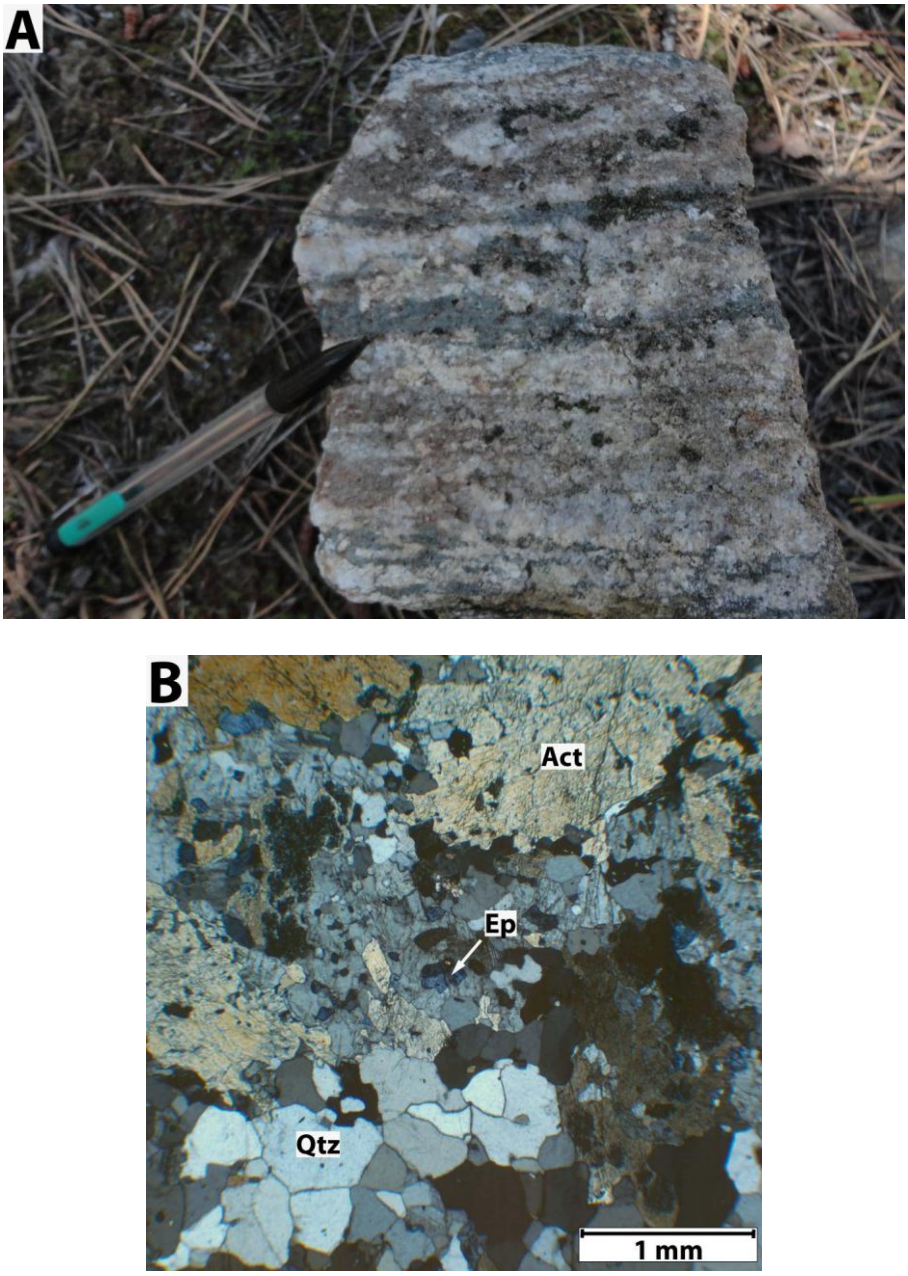

Figure 2: A): Photograph of calc-silicate gneiss of the Wallace Formation. Green layers are rich in actinolite. B) Photomicrograph of calc-silicate gneiss of the Wallace Formation, with epidote and actinolite. Cross-polarized light. Act = actinolite, Ep= epidote, Qtz = quartz.

Ravalli Group quartzite

The quartzite of the Ravalli Group in the map area is a thin-bedded, fine-grained, friable feldspathic quartzite interbedded with layers of fine-grained micaceous quartzite. Quartz-rich layers range in thickness from 3-10 cm, while more micaceous layers range in thickness from 1 mm-5 cm. More massive, competent layers of fine-grained feldspathic white quartzite are interbedded with the friable, more micaceous quartzites described above. The more competent quartzite layers are mica-poor, and bedding ranges in thickness from 2-10 cm.

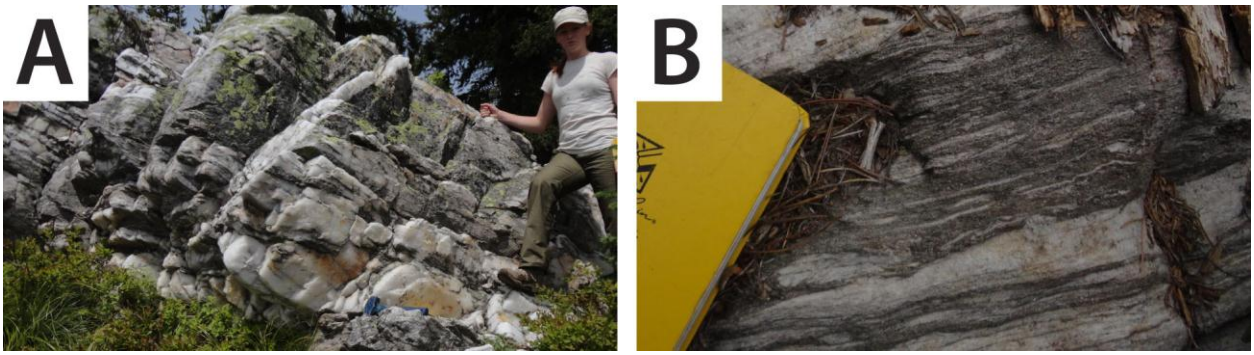

Figure 3: Field photographs of the Ravalli Group quartzite, with layers of quartzite interbedded with micaceous layers.

Prichard schist

Two distinct units interpreted to be schist of the Prichard Formation are identified in the map area. The two units are distinct from each other compositionally and texturally, and likely represent two different lithofacies within the ~6500-m-thick Prichard Formation [*Winston and Link*, 1993]. The characteristics of these two distinct units are described below.

The Prichard schist in the west-central part of the map area, near Surveyors Ridge Lookout, Martin Peak, and Collins Peak, occurs as a coarse-grained garnet biotite schist. Anhedral to subhedral garnet porphyroblasts are abundant, ranging in size from 1 cm to 6 cm in diameter. Small (< 1 mm) porphyroblasts of staurolite are locally present (Figure 4).

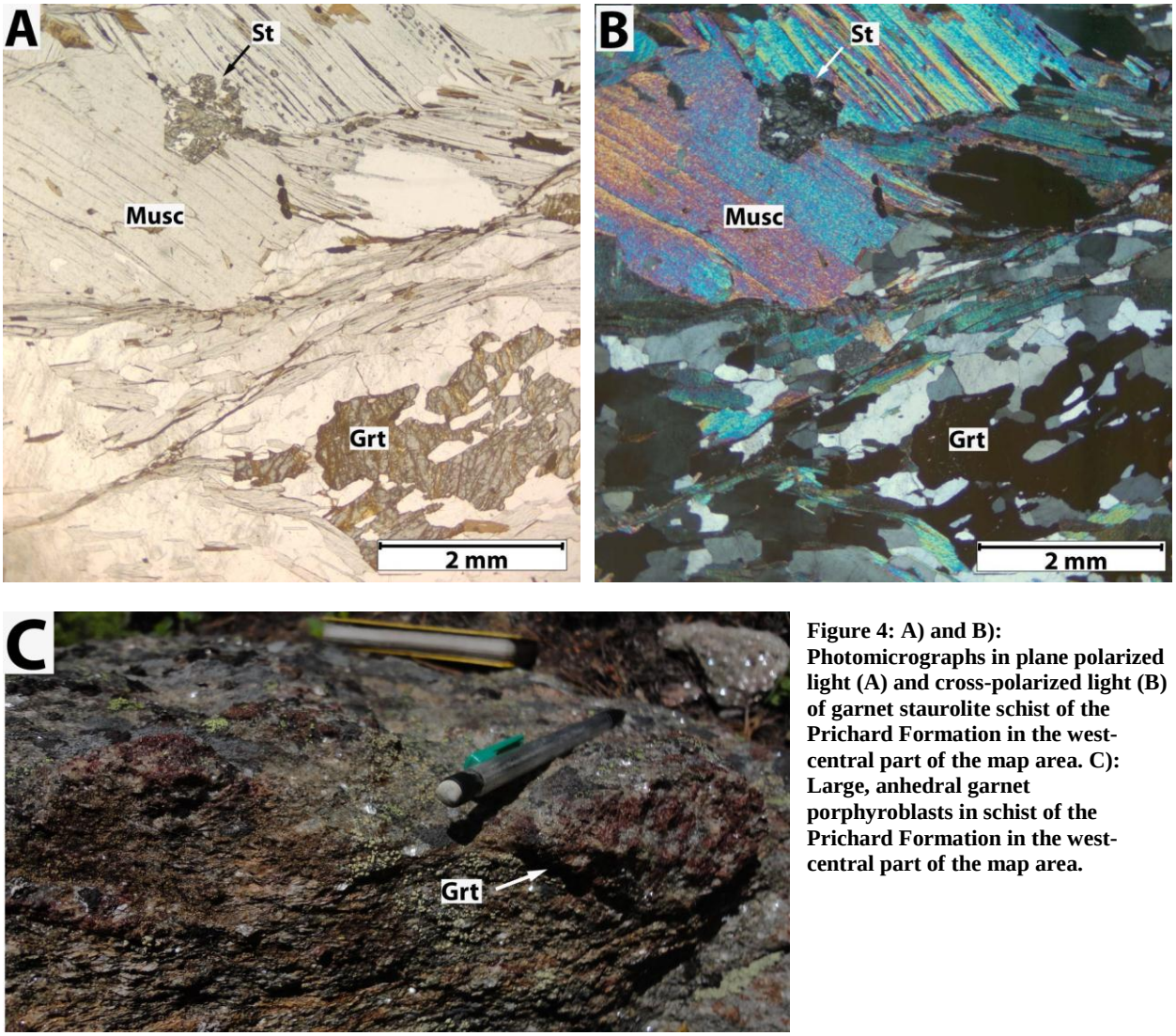

Figure 4: A) and B): Photomicrographs in plane polarized light (A) and cross-polarized light (B) of garnet staurolite schist of the Prichard Formation in the west-central part of the map area. C): Large, anhedral garnet porphyroblasts in schist of the Prichard Formation in the west-central part of the map area.

In the northern part of the map area, near Surveyors Peak, the Prichard schist consists of fine- to medium-grained garnet biotite schist interbedded with layers of gray, fine-grained micaceous quartzite (Figure 5). The quartzite layers of this unit exhibit a friable texture. Bedding thicknesses range from 2-30 cm. Garnet porphyroblasts in this unit are subhedral to euhedral and range in size from 1-2 cm in width. This unit becomes increasingly quartzitic up-section, as garnet-bearing schistose layers dominate the bottom part of the section and become less frequent up-section.

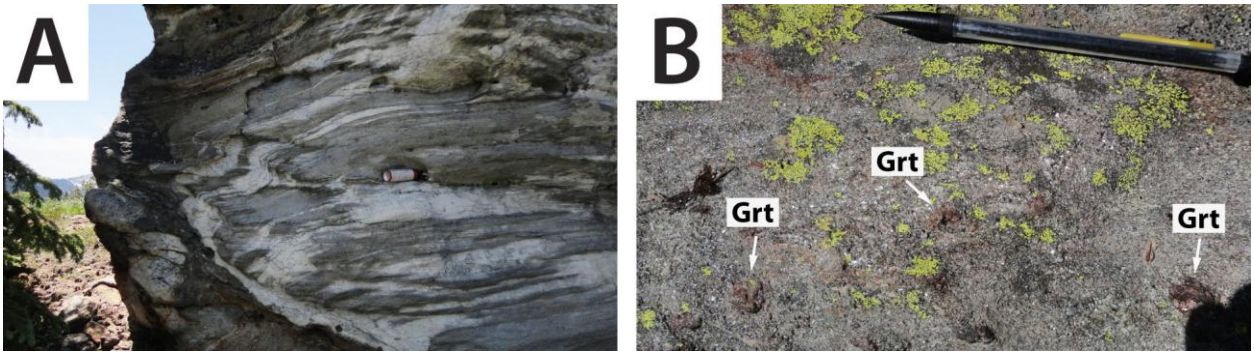

Figure 5: Field photographs of the Prichard schist in the northern part of the map area. A) Recumbent fold, with quartz-rich layers interbedded with layers of garnetiferous schist. B) Garnet porphyroblasts in schistose layer.

Fawn Lake quartzite

The Fawn Lake quartzite is a coarse-grained, foliated, massive-bedded quartzite. Quartz grains range in size from 1 to 12 mm wide, but is reduced to the range of 1-5 mm wide near brittle-ductile detachment faults, probably the result of grain size reduction and dynamic recrystallization during fault movement. Quartz grains exhibit undulose extinction in thin section. Biotite and muscovite flakes are common and range in size from 0.5-3 mm, and form distinct down-dip stretching lineations near normal faults. Subhedral garnet porphyroblasts occur locally and range in size from 2 to 15 mm wide. On a north-south trending ridge west of Skyland Lake, garnet crystals appear to have been stretched and form a distinct down-dip lineation along with mica grains (Figure 6). At this locality, small staurolite porphyroblasts (< 1 mm in width) are evident in thin section and are aligned with the foliation. Quartz makes up 95% of the rock, muscovite and biotite 3%, and garnet, staurolite, and feldspar make up the remaining 2%.

The basal part of this unit is marked by a thin (~30 m thick) layer of garnetiferous schist underlain by an equally thin layer of coarse-grained, feldspar-poor quartzite, which in turn is underlain by feldspathic basement schist (Figure 6). This transition from the Fawn Lake quartzite to underlying basement is well exposed on the southern slope of Mallard Peak.

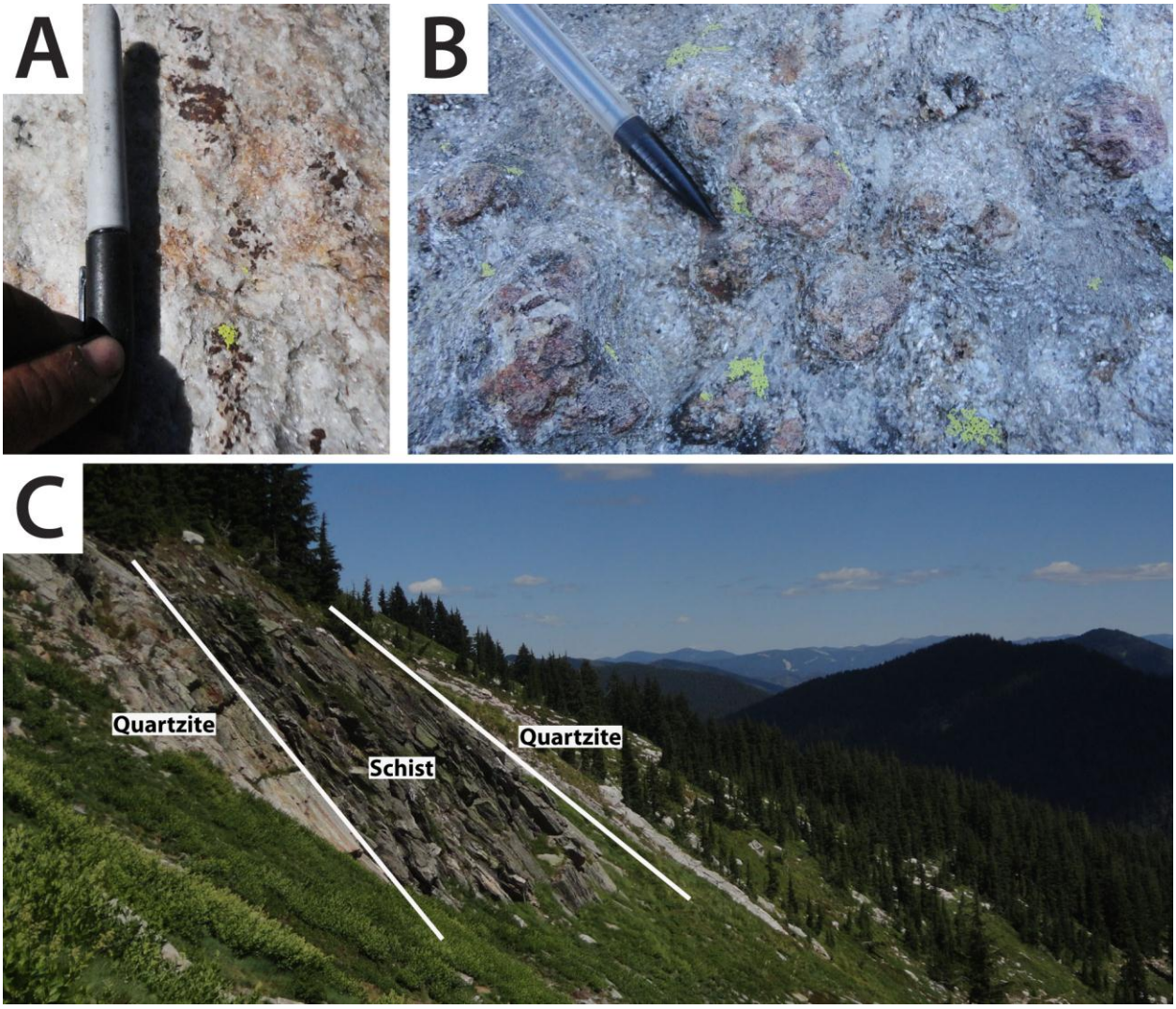

Figure 6: A): Stretched garnet in the Fawn Lake quartzite, on ridge west of Skyland Lake. B): Garnetiferous schist layer in basal part of the Fawn Lake quartzite. C): Southern slope of Mallard Peak, showing outcrop of garnetiferous schist in between layers of quartzite at the basal part of the unit.

Basement gneiss/schist

Basement gneiss and schist of the Mallard Peak basement complex consists of three distinct rock types: 1) coarse-grained feldspathic garnet schist, 2) banded gneiss that is characterized by alternating fine-grained quartzofeldspathic and coarse-grained biotite-rich domains and 3) calc-silicate gneiss (Figure 7).

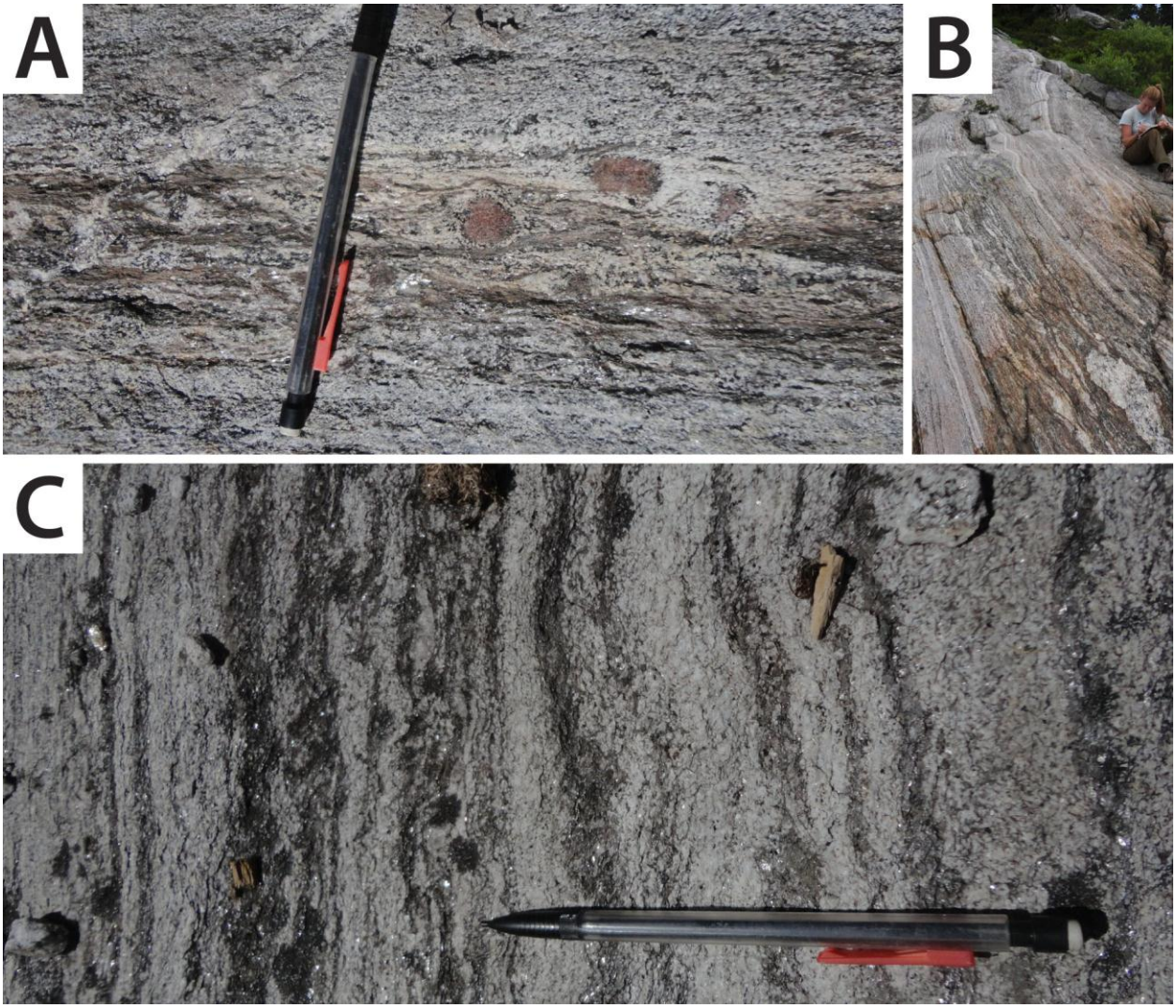

Figure 7: Field photographs of basement metasediments in the map area. A): Feldspathic garnet schist. B): Banded gneiss with quartzofeldspathic layers interbedded with micaceous, biotite-rich layers. C): Calc-silicate gneiss.

The coarse-grained garnet schist is typically more feldspathic than schist of the Prichard formation in the map area. Garnets are anhedral to subhedral, and range in size from 2 mm to 5 cm in diameter. The layers of the banded gneiss range in thickness between 3 cm to 30 cm. The fine-grained quartzofeldspathic layers contain abundant muscovite but almost no biotite. The biotite-rich layers locally contain subhedral to euhedral garnet porphyroblasts, ranging in size from 2 mm to 5 cm in diameter. Kyanite blades 1 to 3 cm long are locally abundant. Calc-silicate gneiss is sparsely interbedded with the garnet schist and banded gneiss, and contains quartz,

plagioclase, biotite, muscovite, epidote, titanite, and ilmenite (Figure 8). Because of a lack of age constraints, the age of the basement schist and gneiss in the Mallard Peak area ranges from Paleoproterozoic to Archean.

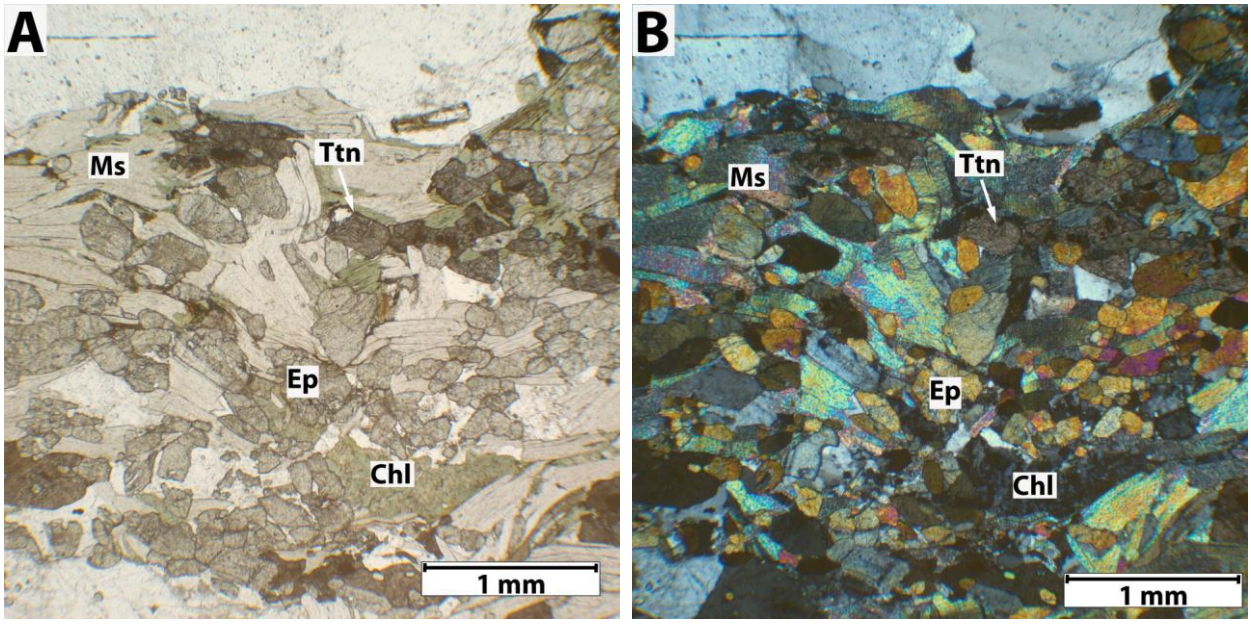

Figure 8: Photomicrographs in plane polarized light (A) and cross-polarized light (B) of calc-silicate gneiss in the map area, with chlorite (Chl), epidote (Ep), muscovite (Ms), and titanite (Ttn).

Intrusive Rocks

Pegmatite and granite (Cretaceous to Tertiary)

Outcrop-scale sills and dikes of unfoliated pegmatitic two-mica granite intrude the metasedimentary rocks in the map area (Figure 9). These bodies contain feldspar phenocrysts as large as 3 cm in diameter. A large, foliated granite granite stock in the Collins Creek drainage in the southern part of the map area was mapped and described by *Hietanen* [1968] and is interpreted to be Cretaceous in age.

Figure 9: Pegmatite dike intruding schist of the Prichard Formation.

Amphibolite (Mesoproterozoic to Cretaceous)

Several bodies of fine-grained, foliated amphibolite intrude metasedimentary rocks in the map area. A small plutonic body approximately 1.5 miles west of Sawtooth Peak was mapped by *Hietanen* [1968] and has been described as consisting of plagioclase and hornblende, with or without augite and biotite. Two sills in the eastern part of the map area contain abundant hornblende, plagioclase, and biotite. Chlorite, epidote, and calcite occur as alteration products. The ages of these bodies is uncertain and can be as young as Cretaceous, but are more likely Proterozoic, as they may correlate to syndepositional mafic sills in the Mesoproterozoic Belt Supergroup or Neoproterozoic Windermere Supergroup.

Garnet Amphibolite (Neoproterozoic to Mesoproterozoic)

Several sills of fine- to medium-grained, foliated sills of garnet amphibolite intrude the metasedimentary rocks of the map area. These bodies are dominantly comprised of hornblende, plagioclase, quartz, and garnet. Ilmenite occurs as an accessory mineral, while epidote and chlorite occur as alteration products (Figure 10). Garnet crystals are 3 to 5 mm in diameter. Sills of this type occur in the map area exclusively in the Fawn Lake and Mallard Peak basement schist and thus may predate the Belt Supergroup, correlating to 1587 Ma garnet amphibolite sills in the Goat Mountain area to the west [*Doughty and Chamberlain*, 2007]. Alternatively, these sills may correlate to syn-depositional mafic sills found in the Mesoproterozoic Belt Supergroup or Neoproterozoic Windermere Supergroup [*Sears et al.*, 1998; R. Lewis, personal communication, 2012].

Amphibolite (Paleoproterozoic)

A small amphibolite body intrudes a Paleoproterozoic biotite granodiorite pluton southwest of Mallard Peak, and contains plagioclase, hornblende, and biotite. The age of this body is assumed to be Paleoproterozoic, as it exhibits the same east-west striking foliation as the surrounding pluton, which differs markedly from the dominant northwest-southeast striking foliation in the map area. This east-west striking foliation most likely developed during magma intrusion.

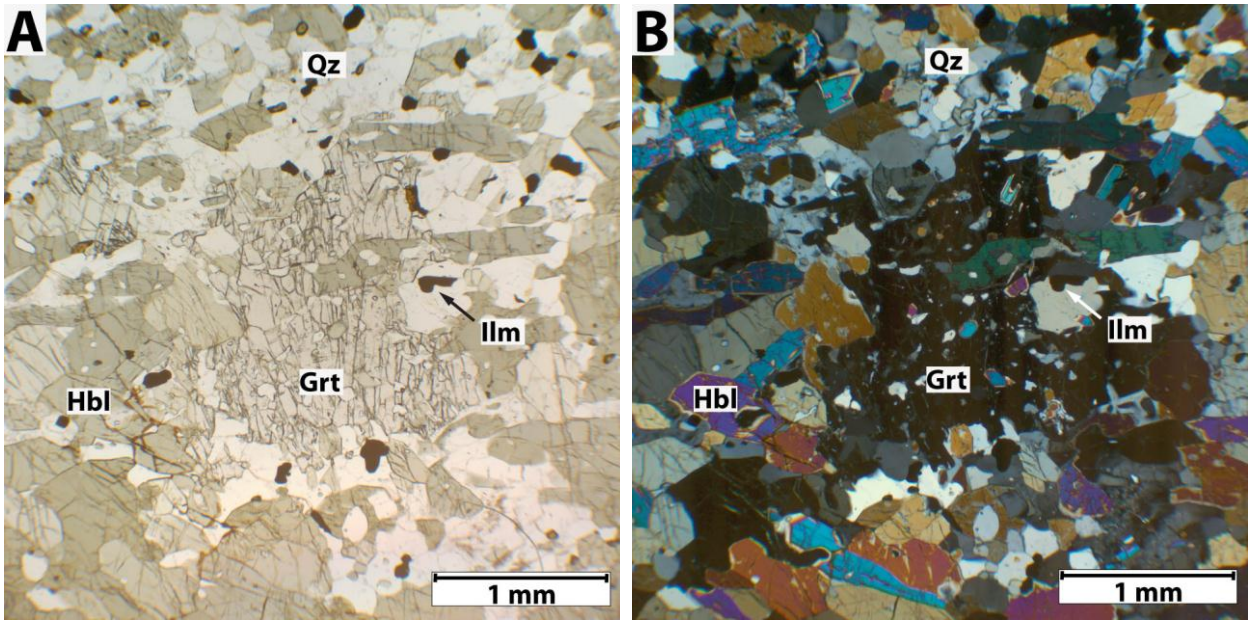

Figure 10: Photomicrograph in PPL (A) and XPL (B) of Mesoproterozoic to Neoproterozoic garnet amphibolite in the map area. Grt = garnet, Hbl = hornblende, Ilm = ilmenite, Qz = quartz.

Biotite granodiorite (Paleoproterozoic)

A large body of Paleoproterozoic orthogneiss in the map area intrudes basement schist and gneiss on a ridge SW of Mallard Peak. The orthogneiss in this body dominantly consists of foliated, coarse-grained biotite granodiorite (Figure 11). The dominant minerals in this rock are plagioclase, quartz, biotite, and microcline. Apatite and tourmaline occur as accessory minerals. The foliation in this pluton strikes to the east and dips to the south.

Figure 11: Foliated Paleoproterozoic biotite granodiorite southwest of Mallard Peak.

References

Doughty, P. T., and K. R. Chamberlain (2007), Age of Paleoproterozoic basement and related rocks in the Clearwater Complex, Northern Idaho, U.S.A., in *Proterozoic Geology of Western North America and Siberia*, edited by P. K. Link and R. S. Lewis, pp. 9-35, SEPM Special Publication, Tulsa, OK.

Hietanen, A. (1968), Belt Series in the region around Snow Peak and Mallard Peak, Idaho, *USGS Professional Paper Rep. 344-E*, 1-34 pp, United States Geological Survey, Washington, D.C.

Sears, J. W., K. R. Chamberlain, and S. N. Buckley (1998), Structural and U-Pb geochronological evidence for 1.47 Ga rifting in the Belt basin, western Montana, *Can. J. Earth Sci.*, *35*(4), 467-475.

Winston, D., and P. K. Link (1993), Middle Proterozoic rocks of Montana, Idaho, and Eastern Washington: The Belt Supergroup, in *Precambrian: Conterminous U.S.*, edited by J. C. Reed, M. E. Bickford, R. S. Houston, P. K. Link, D. W. Rankin, P. K. Sims and W. R. Van Schmus, pp. 487-517, Geological Society of America, Boulder, CO.

Appendix 4: Table of $^{40}Ar/^{39}Ar$ thermochronolgic data

Sample	J-value	Step	^{36}Ar (Ar)	^{37}Ar (Ca)	^{38}Ar (Cl)	^{39}Ar (K)	^{40}Ar (r)	Calculated age (Ma)	Error	^{40}Ar (r) (%)	^{39}Ar (K) (%)
CW10-26 muscovite	0.001232	1	0.00222	0.03007	0.02249	0.15935	3.2001	44.1	3.4	82.9	100.0
CW11-99 biotite	0.001457	1	0.00161	0.00192	0.00103	0.01440	0.2386	43.0	4.3	33.4	100.0
CW10-16 muscovite	0.001316	1	0.00812	0.00198	0.00001	0.04971	1.6718	78.1	4.0	41.1	100.0
CW11-29 muscovite	0.001232	1	0.00238	0.03567	0.02940	0.11278	2.2723	44.2	4.8	76.3	100.0
CW11-53 biotite	0.001457	1	0.00073	0.03398	0.02730	0.11010	1.7915	42.2	4.4	89.1	100.0
CW11-65 muscovite	0.001232	1	0.00226	0.00362	0.00135	0.08489	1.8579	48.0	2.1	73.5	100.0
CW10-4 biotite	0.001189	1	0.00081	0.05280	0.00197	0.04901	1.5150	65.1	4.4	86.3	20.2
		2	0.00226	0.01444	0.00039	0.03453	1.0661	65.0	9.5	61.5	14.2
		3	0.00086	0.01021	0.00049	0.01535	0.4930	67.6	11.5	65.9	6.3
		4	0.00028	4.93900	0.00096	0.02533	1.4033	115.1	13.0	94.4	10.4
		5	0.00065	0.00409	0.00033	0.01290	0.3993	65.2	8.4	67.3	5.3
		6	0.00166	0.00659	0.00024	0.01912	0.5267	58.2	10.8	51.7	7.9
		7	0.00147	0.00781	0.00024	0.01822	0.6207	71.6	11.6	58.8	7.5
		8	0.00101	0.00897	0.00053	0.02584	0.9618	78.1	7.1	76.3	10.6
		9	0.00097	0.00227	0.00029	0.02918	0.9506	68.6	6.4	76.8	12.0
		10	0.00074	0.00312	0.00011	0.01327	0.4418	70.0	9.0	66.9	5.5
CW10-5 biotite	0.001189	1	0.00048	0.00103	0.00059	0.00758	0.6391	172.4	23.9	81.9	14.3
		2	0.00024	0.00043	0.00016	0.01003	0.2991	62.8	1.7	80.9	18.9
		3	0.00115	0.00278	0.00026	0.03541	0.9832	58.6	2.3	74.2	66.8
CW11-61	0.001316	1	0.00031	0.05410	0.03687	0.13030	2.4800	44.6	5.1	96.2	100.0

Appendix 5: Tables of U-Pb geochronological data

CW10-26

Analysis	U (ppm)	Th (ppm)	$^{206}Pb^*$ (ppm)	Th/U	$^{206}Pb/^{204}Pb$	$^{206}Pb^*/^{238}U$	±2σ (%)	$^{206}Pb^*/^{207}Pb^*$	±2σ (%)	$^{206}Pb^*/^{238}U^*$ (Ma)	±2σ (Ma)	$^{207}Pb^*/^{206}Pb^*$ (Ma)	±2σ (Ma)
cw10-26_L_146	484	688	223	1.42	22589.63	0.24	6.04	9.94	6.67	1412	77	1635	124
cw10-26_L_150	107	56	48	0.53	4271.01	0.34	8.34	9.70	5.66	1882	136	1681	105
cw10-26_M_355	151	66	29	0.44	5832.80	0.31	3.06	9.62	2.17	1741	47	1696	40
cw10-26_M_356	253	424	-51	1.68	1690.66	0.28	4.70	9.33	1.57	1598	67	1752	29
cw10-26_M_337	388	220	181	0.57	1459.64	0.30	3.74	9.27	3.59	1716	56	1764	66
cw10-26_M_333	262	104	134	0.40	4033.81	0.30	2.00	9.22	1.63	1705	30	1774	30
cw10-26_L_168	159	86	54	0.54	23342.88	0.31	8.48	9.19	8.00	1744	130	1780	146
cw10-26_M_330	168	77	84	0.46	1431.94	0.31	2.30	9.18	1.46	1754	35	1781	27
cw10-26_L_156	757	63	274	0.08	16562.35	0.31	4.34	9.17	2.45	1754	67	1783	45
cw10-26_M_357	296	158	39	0.53	31721.70	0.31	1.91	9.16	1.68	1756	29	1785	31
cw10-26_M_328	244	244	197	1.00	5497.99	0.31	3.16	9.15	2.43	1727	48	1788	44
cw10-26_L_185	118	68	35	0.58	1791.88	0.32	5.45	9.14	4.10	1774	84	1789	75
cw10-26_M_331	356	122	184	0.34	1418982.79	0.31	5.31	9.12	3.07	1735	81	1793	56
cw10-26_L_161	118	69	43	0.59	1356.33	0.31	3.63	9.12	2.37	1739	55	1794	43
cw10-26_L_166	82	36	29	0.43	4993.31	0.31	5.84	9.11	5.80	1750	90	1795	106
cw10-26_L_160	123	56	47	0.46	2103.95	0.33	3.99	9.11	3.38	1826	63	1797	62
cw10-26_L_151	123	53	51	0.43	1529.06	0.33	7.03	9.10	6.06	1848	113	1797	110
cw10-26_L_144	584	182	226	0.31	108728.74	0.29	6.92	9.10	6.72	1640	100	1797	122
cw10-26_L_187	417	207	134	0.50	4693.02	0.34	4.12	9.09	2.90	1877	67	1799	53
cw10-26_L_178	122	62	38	0.51	6554.30	0.31	6.93	9.09	6.75	1741	106	1799	123
cw10-26_M_342	212	87	88	0.41	3108.30	0.30	2.03	9.07	1.63	1713	31	1803	30
cw10-26_M_326	149	197	131	1.32	723.55	0.31	3.46	9.05	3.85	1741	53	1807	70
cw10-26_L_154	333	172	115	0.52	2807.05	0.28	5.22	9.05	3.81	1572	73	1809	69
cw10-26_L_192	148	112	37	0.76	3549.01	0.31	5.36	9.05	3.20	1746	82	1809	58
cw10-26_M_351	172	163	39	0.95	9705.81	0.34	2.52	9.02	2.28	1890	41	1814	41
cw10-26_M_363	106	55	2	0.52	9168.01	0.32	3.15	9.00	2.14	1796	49	1818	39
cw10-26_L_174	193	81	61	0.42	1099.20	0.30	6.78	8.99	4.85	1701	101	1819	88
cw10-26_L_175	213	234	63	1.10	24678.16	0.32	6.95	8.98	6.74	1799	109	1822	122
cw10-26_M_320	69	87	76	1.25	13808.12	0.31	2.06	8.98	2.38	1749	32	1822	43
cw10-26_L_184	824	186	233	0.23	1996.22	0.27	6.10	8.97	5.84	1543	84	1825	106
cw10-26_M_314	254	111	164	0.44	5077.32	0.32	2.60	8.96	2.04	1782	41	1825	37
cw10-26_L_157	136	102	61	0.75	10618.18	0.35	4.56	8.96	2.65	1915	76	1826	48
cw10-26_L_172	239	131	83	0.55	4842.56	0.33	9.06	8.95	7.14	1816	143	1827	129
cw10-26_L_153	106	92	43	0.86	615.44	0.31	5.15	8.95	3.26	1753	79	1828	59
cw10-26_M_332	71	106	59	1.50	440.24	0.32	2.70	8.94	2.65	1780	42	1829	48

cw10-26_L_177	143	43	49	0.30	2677.46	0.32	8.51	8.94	6.61	1793	133	1829	120
cw10-26_M_362	122	67	11	0.55	1781.00	0.34	2.84	8.94	2.09	1874	46	1830	38
cw10-26_L_167	407	14	153	0.03	52895.30	0.33	6.16	8.94	5.27	1834	98	1830	96
cw10-26_M_359	515	371	-2	0.72	14073.95	0.33	3.28	8.93	2.47	1859	53	1831	45
cw10-26_M_360	395	177	64	0.45	4940.21	0.32	4.93	8.92	3.41	1784	77	1833	62
cw10-26_L_197	67	83	11	1.24	898.14	0.30	6.03	8.92	5.65	1709	90	1833	102
cw10-26_L_182	191	56	58	0.29	3381.81	0.29	6.20	8.92	4.30	1646	90	1834	78
cw10-26_L_194	430	121	126	0.28	16840.68	0.29	6.42	8.92	4.83	1642	93	1835	88
cw10-26_M_318	239	104	149	0.44	7539.64	0.32	2.51	8.90	1.73	1791	39	1838	31
cw10-26_L_191	120	71	34	0.59	1353.85	0.32	3.71	8.90	4.42	1774	58	1838	80
cw10-26_L_170	130	73	45	0.56	13653.58	0.32	7.53	8.87	6.36	1781	117	1844	115
cw10-26_M_338	276	233	167	0.84	282410.78	0.32	2.93	8.87	2.86	1812	46	1844	52
cw10-26_L_173	225	270	58	1.20	1105.91	0.27	7.67	8.85	6.92	1525	104	1848	125
cw10-26_L_163	92	32	34	0.35	10565.55	0.32	5.90	8.83	3.82	1778	92	1851	69
cw10-26_L_159	221	87	82	0.39	6917.95	0.31	4.08	8.83	2.98	1740	62	1853	54
cw10-26_L_190	194	94	52	0.48	7972.23	0.29	6.32	8.82	3.78	1633	91	1853	68
cw10-26_M_322	438	314	339	0.72	7639.19	0.32	2.82	8.81	1.35	1774	44	1857	24
cw10-26_M_329	434	96	203	0.22	6931.00	0.32	3.47	8.80	1.95	1791	54	1859	35
cw10-26_L_155	413	174	166	0.42	5608.08	0.32	4.59	8.79	3.34	1808	72	1860	60
cw10-26_M_335	102	53	56	0.52	4308.67	0.33	3.57	8.78	2.23	1826	57	1862	40
cw10-26_L_199	523	224	139	0.43	43633.25	0.29	6.79	8.78	4.54	1639	98	1862	82
cw10-26_L_169	235	141	83	0.60	6436.72	0.32	7.79	8.77	6.64	1808	123	1864	120
cw10-26_M_350	193	128	61	0.66	7446.85	0.35	3.73	8.76	2.30	1949	63	1866	41
cw10-26_M_339	138	105	81	0.76	2817.27	0.35	3.51	8.76	2.96	1920	58	1867	53
cw10-26_M_321	100	56	68	0.56	2560.02	0.33	2.35	8.75	2.01	1851	38	1869	36
cw10-26_M_311	76	46	54	0.60	796.18	0.33	2.86	8.75	3.02	1815	45	1869	55
cw10-26_M_352	256	156	70	0.61	27243.92	0.34	2.52	8.74	1.46	1886	41	1870	26
cw10-26_M_312	181	72	122	0.40	20775.49	0.33	2.92	8.74	2.20	1859	47	1871	40
cw10-26_M_345	376	221	147	0.59	5222.01	0.32	1.85	8.73	1.70	1781	29	1873	31
cw10-26_M_343	36	16	14	0.45	511.09	0.33	3.66	8.67	2.95	1829	58	1886	53
cw10-26_M_317	260	140	172	0.54	2802.30	0.31	2.63	8.66	1.44	1753	40	1887	26
cw10-26_L_152	72	30	29	0.41	11614.39	0.31	6.53	8.64	6.30	1728	99	1892	113
cw10-26_L_195	236	101	72	0.43	125873.91	0.32	5.81	8.60	3.97	1806	91	1899	71
cw10-26_L_181	24	8	9	0.33	963.46	0.35	8.53	8.60	6.85	1916	141	1899	123
cw10-26_L_183	158	78	46	0.50	4394.34	0.30	5.55	8.59	5.97	1706	83	1901	107
cw10-26_M_313	78	65	76	0.83	1541.04	0.36	3.31	8.58	2.81	1968	56	1904	50
cw10-26_M_336	135	172	100	1.28	713.41	0.35	2.40	8.52	2.41	1918	40	1917	43
cw10-26_M_341	74	62	43	0.84	48358.21	0.33	3.20	8.40	2.29	1839	51	1942	41
cw10-26_L_180	171	81	62	0.48	8686.34	0.35	7.82	8.09	6.54	1956	132	2009	116
cw10-26_L_198	79	77	23	0.97	619.81	0.39	8.51	7.42	6.20	2113	153	2161	108
cw10-26_L_188	136	84	50	0.62	1393.65	0.39	3.60	7.16	3.31	2145	66	2223	57
cw10-26_M_327	575	176	376	0.31	424600.02	0.37	6.51	7.15	3.81	2031	113	2225	66

cw10-26_M_364	327	174	10	0.53	12666.48	0.42	1.85	6.62	2.06	2240	35	2359	35
cw10-26_M_319	103	98	120	0.95	1349.05	0.42	3.33	6.56	2.04	2241	63	2374	35
cw10-26_L_145	179	87	120	0.49	28936.54	0.46	8.12	6.46	8.27	2450	166	2400	141
cw10-26_L_196	161	73	71	0.45	5316.74	0.45	6.49	6.43	6.00	2385	129	2407	102
cw10-26_M_347	344	81	198	0.23	3687980.45	0.48	5.13	6.42	1.21	2545	108	2409	21
cw10-26_M_340	78	38	48	0.49	2067.05	0.41	1.91	6.42	1.55	2228	36	2410	26
cw10-26_L_193	207	90	102	0.43	18290.90	0.48	4.50	6.36	3.48	2547	95	2425	59
cw10-26_M_323	263	248	328	0.94	600144.38	0.44	2.51	6.36	1.21	2369	50	2427	21
cw10-26_L_179	168	81	83	0.48	3338.19	0.46	7.38	6.27	7.89	2438	150	2450	133
cw10-26_M_353	171	93	68	0.55	6384.77	0.47	2.43	6.25	1.81	2490	50	2456	31
cw10-26_L_176	239	228	92	0.95	2525.53	0.39	8.82	6.09	6.77	2113	159	2499	114
cw10-26_L_149	158	67	121	0.42	4564.58	0.53	7.57	6.06	7.15	2735	169	2507	120
cw10-26_M_316	180	147	229	0.82	5175.14	0.42	4.30	6.04	2.07	2274	82	2513	35
cw10-26_L_164	158	47	86	0.30	13286.19	0.45	4.51	6.03	3.57	2407	91	2517	60
cw10-26_M_358	185	137	19	0.74	3483.25	0.48	2.17	5.87	1.49	2515	45	2561	25
cw10-26_L_148	82	33	53	0.40	2420.85	0.47	8.71	5.84	6.17	2492	180	2571	103
cw10-26_M_348	334	142	189	0.42	2767.83	0.49	2.58	5.81	1.38	2564	55	2579	23
cw10-26_M_334	70	65	79	0.93	5930.67	0.48	2.84	5.70	1.71	2539	60	2609	28
cw10-26_L_147	92	51	73	0.56	3632.38	0.55	9.03	5.69	7.74	2810	206	2613	129
cw10-26_M_315	241	164	305	0.68	4164.77	0.49	2.59	5.65	1.84	2559	55	2624	31
cw10-26_M_344	221	230	169	1.04	4886.40	0.46	4.89	5.59	1.62	2451	100	2642	27
cw10-26_L_171	348	383	181	1.10	3918.53	0.48	6.51	5.54	6.42	2506	135	2657	106
cw10-26_L_158	42	35	26	0.82	509.19	0.49	4.98	5.49	3.31	2589	106	2671	55
cw10-26_M_349	107	69	59	0.65	11745.68	0.52	3.33	5.48	2.26	2694	73	2675	37
cw10-26_M_324	98	74	118	0.75	10775.21	0.49	2.68	5.45	2.03	2588	57	2685	34
cw10-26_L_189	50	78	16	1.57	1319.13	0.50	3.91	5.45	2.60	2609	84	2685	43
cw10-26_L_186	60	31	30	0.51	1325.88	0.47	4.17	5.45	3.53	2494	86	2686	58
cw10-26_M_310	64	119	173	1.84	4676.76	0.53	3.67	5.31	2.45	2733	82	2729	40
cw10-26_M_346	82	139	58	1.69	7406.15	0.52	4.53	5.22	2.21	2694	100	2755	36
cw10-26_M_354	364	151	182	0.41	12338.97	0.54	3.05	5.21	1.29	2764	69	2758	21
cw10-26_M_361	74	111	-45	1.49	1314.69	0.53	3.46	5.10	3.35	2741	77	2795	55
cw10-26_M_325	261	189	370	0.72	9364.59	0.60	4.43	4.28	2.63	3013	107	3079	42
cw10-26_L_162	40	28	38	0.70	1287.58	0.67	4.17	3.33	2.85	3316	108	3473	44

CW11-90

Analysis	U (ppm)	Th (ppm)	$^{206}Pb^*$ (ppm)	Th/U	$^{206}Pb/^{204}Pb$	$^{206}Pb^*/^{238}U$	±2σ (%)	$^{206}Pb^*/^{207}Pb^*$	±2σ (%)	$^{206}Pb^*/^{238}U^*$ (Ma)	±2σ (Ma)	$^{207}Pb^*/^{206}Pb^*$ (Ma)	±2σ (Ma)
cw11-90_L_215	484	168	134	0.35	60014.52	0.28	4.99	9.58	2.62	1586	70	1703	48
cw11-90_L_254	813	710	256	0.87	11639.46	0.29	6.47	9.54	4.06	1620	93	1711	75
cw11-90_L_252	114	47	38	0.41	1609.84	0.31	6.48	9.45	4.93	1740	99	1728	91
cw11-90_L_249	189	68	68	0.36	2317.65	0.33	7.95	9.44	5.89	1835	127	1732	108
cw11-90_L_242	375	151	113	0.40	8413.24	0.29	4.89	9.41	4.01	1657	71	1737	73
cw11-90_L_219	148	89	44	0.60	2260.83	0.34	3.87	9.33	2.10	1899	64	1751	38
cw11-90_L_214	159	94	43	0.59	6131.05	0.32	4.81	9.27	2.44	1778	75	1765	45
cw11-90_L_246	189	101	61	0.53	2321.45	0.31	7.58	9.26	5.50	1754	116	1765	100
cw11-90_L_223	101	106	22	1.05	1037.69	0.31	6.81	9.24	3.97	1733	104	1769	73
cw11-90_xl_73	110	73	40	0.66	762.19	0.26	4.94	9.19	2.27	1471	65	1779	41
cw11-90_L_251	207	62	69	0.30	2918.71	0.30	8.29	9.16	6.85	1705	124	1785	125
cw11-90_xl_75	54	26	22	0.48	960.39	0.31	2.84	9.15	2.89	1748	44	1787	53
cw11-90_L_228	82	38	26	0.46	4595.51	0.33	4.53	9.13	2.70	1821	72	1791	49
cw11-90_xl_59	82	119	48	1.45	18369.82	0.31	2.78	9.13	2.20	1740	42	1791	40
cw11-90_xl_60	296	286	142	0.97	5319.26	0.30	2.34	9.13	1.12	1677	35	1792	20
cw11-90_xl_55	84	38	35	0.45	1114.83	0.31	2.75	9.13	1.80	1723	42	1793	33
cw11-90_L_227	30	19	9	0.61	767.15	0.31	3.50	9.12	4.62	1748	54	1794	84
cw11-90_xl_69	137	42	53	0.31	1059.34	0.31	2.45	9.10	1.58	1737	37	1797	29
cw11-90_xl_34	258	147	98	0.57	43258.06	0.29	2.89	9.05	1.94	1655	42	1809	35
cw11-90_xl_77	71	61	32	0.87	673.62	0.32	2.88	9.04	1.89	1787	45	1810	34
cw11-90_L_245	92	52	30	0.57	1830.20	0.32	8.34	9.03	5.24	1767	129	1811	95
cw11-90_L_210	158	44	50	0.28	3823.98	0.31	5.51	9.00	3.54	1762	85	1817	64
cw11-90_xl_62	249	100	103	0.40	1870.11	0.31	3.25	9.00	1.72	1753	50	1817	31
cw11-90_xl_83	67	24	25	0.35	1090.75	0.31	2.62	8.99	1.97	1729	40	1819	36
cw11-90_L_204	45	19	16	0.41	268.28	0.34	6.71	8.98	6.26	1864	109	1821	114
cw11-90_xl_86	221	127	88	0.58	5926.32	0.31	2.88	8.98	1.47	1762	44	1823	27
cw11-90_xl_61	178	93	79	0.52	79916.27	0.31	2.76	8.96	1.83	1729	42	1826	33
cw11-90_L_240	170	62	59	0.36	11904.01	0.33	5.04	8.96	4.29	1859	81	1827	78
cw11-90_xl_80	1086	89	403	0.08	85807.75	0.30	2.49	8.94	0.76	1711	37	1830	14
cw11-90_xl_41	302	38	111	0.13	3066.04	0.31	2.87	8.94	1.15	1724	43	1830	21
cw11-90_L_253	481	166	168	0.35	16916.51	0.31	6.33	8.92	6.32	1750	97	1833	115
cw11-90_L_239	74	60	20	0.81	578.19	0.30	5.28	8.91	3.73	1681	78	1836	68
cw11-90_xl_71	54	18	21	0.33	762.24	0.31	2.39	8.91	2.33	1747	37	1836	42
cw11-90_L_209	399	484	67	1.21	24800.33	0.33	4.54	8.90	4.60	1831	72	1837	83
cw11-90_xl_68	147	102	71	0.69	3530.39	0.31	2.94	8.90	1.43	1751	45	1839	26
cw11-90_L_248	166	100	55	0.60	2050.58	0.31	6.70	8.88	4.91	1757	103	1843	89
cw11-90_xl_64	245	317	141	1.30	3607.36	0.31	3.11	8.87	1.92	1760	48	1843	35
cw11-90_xl_52	83	41	33	0.49	506.57	0.31	2.88	8.87	1.80	1763	44	1844	33
cw11-90_L_218	79	94	15	1.19	1320.49	0.32	3.99	8.86	2.52	1801	63	1845	46
cw11-90_xl_82	318	52	116	0.16	2248.07	0.30	2.43	8.85	1.23	1712	37	1847	22
cw11-90_L_205	275	68	73	0.25	2036.12	0.27	6.13	8.85	4.79	1541	84	1848	87

cw11-90_L_212	105	181	9	1.73	2861.06	0.31	5.58	8.83	3.22	1764	86	1853	58
cw11-90_L_213	118	121	23	1.02	20604.06	0.31	4.65	8.82	3.03	1759	72	1853	55
cw11-90_xl_48	995	711	485	0.71	63563.07	0.31	1.77	8.80	0.83	1741	27	1857	15
cw11-90_xl_51	151	67	68	0.45	7636.75	0.31	2.79	8.80	1.58	1753	43	1859	29
cw11-90_xl_58	98	59	46	0.60	6368.14	0.32	3.20	8.79	2.42	1784	50	1860	44
cw11-90_xl_56	183	154	90	0.84	1014.77	0.32	2.12	8.78	1.61	1772	33	1862	29
cw11-90_L_243	43	46	12	1.08	306.56	0.32	4.56	8.78	3.99	1796	71	1862	72
cw11-90_L_235	62	20	19	0.32	5622.75	0.30	3.41	8.78	2.73	1705	51	1863	49
cw11-90_L_247	110	42	37	0.38	2820.07	0.31	7.49	8.77	6.11	1750	115	1864	110
cw11-90_xl_81	278	102	111	0.37	11472.88	0.31	2.41	8.77	1.19	1733	37	1865	21
cw11-90_xl_46	31	18	14	0.59	2022.36	0.31	2.87	8.76	2.72	1738	44	1867	49
cw11-90_xl_50	176	107	86	0.60	44327.95	0.32	2.35	8.74	1.52	1795	37	1870	27
cw11-90_xl_33	197	137	79	0.69	1509.96	0.32	2.25	8.68	1.44	1769	35	1883	26
cw11-90_L_250	133	150	42	1.13	6901.58	0.31	8.42	8.67	5.28	1756	129	1885	95
cw11-90_xl_87	383	257	158	0.67	37550.95	0.32	2.71	8.64	1.45	1797	42	1890	26
cw11-90_xl_72	47	5	17	0.11	1125.57	0.32	1.33	8.63	2.67	1809	21	1893	48
cw11-90_L_233	41	13	14	0.31	3422.91	0.33	3.86	8.62	3.37	1832	62	1895	61
cw11-90_L_231	207	106	65	0.51	24156.44	0.33	3.74	8.62	2.71	1839	60	1896	49
cw11-90_xl_49	22	34	13	1.50	497.72	0.33	2.85	8.57	3.25	1816	45	1905	58
cw11-90_xl_78	149	62	61	0.42	1305.11	0.31	1.90	8.53	1.49	1757	29	1914	27
cw11-90_L_221	231	49	65	0.21	14103.91	0.28	4.58	8.39	3.13	1580	64	1943	56
cw11-90_xl_57	147	160	85	1.09	852.76	0.35	2.89	8.21	1.67	1922	48	1983	30
cw11-90_xl_35	20	138	21	6.81	2469.37	0.35	3.46	7.70	3.11	1950	58	2095	55
cw11-90_L_237	423	110	132	0.26	7360.43	0.30	5.66	7.54	3.31	1699	85	2133	58
cw11-90_xl_38	110	167	67	1.52	948.57	0.38	3.12	6.88	1.97	2090	56	2292	34
cw11-90_xl_67	8	4	1	0.47	101.84	0.43	3.14	6.51	3.80	2307	61	2387	65
cw11-90_xl_74	22	12	20	0.53	407.15	0.64	15.60	6.43	6.73	3199	393	2408	114
cw11-90_xl_37	1012	159	556	0.16	14131.68	0.43	3.33	6.34	1.24	2308	65	2433	21
cw11-90_L_220	73	149	11	2.05	617.24	0.44	3.32	6.28	2.53	2342	65	2447	43
cw11-90_L_208	69	37	27	0.53	10142.33	0.43	7.29	6.28	5.50	2296	141	2449	93
cw11-90_xl_76	623	132	364	0.21	14959.08	0.44	2.10	6.17	0.83	2335	41	2478	14
cw11-90_L_236	125	109	52	0.87	3731.30	0.45	4.01	6.13	3.34	2382	80	2488	56
cw11-90_L_216	98	70	35	0.72	1648.67	0.41	3.68	6.07	3.29	2198	68	2506	55
cw11-90_xl_39	37	30	22	0.82	398.11	0.44	3.06	6.01	1.87	2359	60	2522	31
cw11-90_L_206	236	84	113	0.35	5657.71	0.47	7.66	5.97	6.88	2493	158	2533	115
cw11-90_L_229	74	155	16	2.09	9970.98	0.49	3.48	5.96	2.57	2565	74	2534	43
cw11-90_xl_54	52	40	38	0.78	1723.23	0.44	2.31	5.95	1.82	2372	46	2539	31
cw11-90_xl_45	29	5	14	0.16	356.20	0.47	2.06	5.90	2.23	2476	42	2553	37
cw11-90_xl_84	35	48	23	1.36	401.82	0.46	2.47	5.85	1.31	2444	50	2567	22
cw11-90_xl_40	124	163	97	1.32	1270.98	0.46	3.35	5.81	1.14	2447	68	2580	19
cw11-90_xl_85	108	157	79	1.45	8550.97	0.48	3.69	5.80	1.49	2516	77	2582	25
cw11-90_L_230	151	117	70	0.78	1350.51	0.49	3.63	5.76	2.73	2573	77	2593	45
cw11-90_L_238	222	262	99	1.18	4090.74	0.51	4.36	5.76	3.31	2663	95	2593	55
cw11-90_L_224	565	114	298	0.20	10967.20	0.47	3.30	5.72	2.34	2465	68	2604	39
cw11-90_xl_43	143	110	95	0.77	1331.57	0.42	2.31	5.71	0.85	2241	44	2606	14
cw11-90_L_234	310	254	149	0.82	7052.21	0.51	3.92	5.65	2.02	2668	86	2625	34

cw11-90_xl_53	33	8	22	0.25	17295.94	0.47	2.76	5.63	1.99	2463	56	2632	33
cw11-90_L_217	180	120	84	0.67	2898.54	0.52	3.87	5.58	2.47	2681	85	2645	41
cw11-90_L_211	718	950	225	1.32	85269.31	0.51	4.10	5.57	2.37	2677	90	2647	39
cw11-90_L_241	115	76	59	0.66	17777.46	0.49	5.45	5.56	3.58	2570	115	2652	59
cw11-90_L_222	112	150	36	1.34	2036.27	0.50	3.03	5.53	2.95	2598	65	2660	49
cw11-90_xl_70	485	271	355	0.56	8600.82	0.47	2.77	5.53	0.78	2479	57	2661	13
cw11-90_xl_42	129	133	104	1.03	2479.03	0.48	2.54	5.52	1.35	2507	53	2664	22
cw11-90_xl_65	94	63	74	0.66	26115.67	0.48	2.57	5.49	1.40	2516	54	2672	23
cw11-90_xl_44	170	340	178	2.00	2678.21	0.48	2.19	5.49	1.06	2509	45	2672	18
cw11-90_xl_36	119	79	79	0.66	1523.20	0.47	2.41	5.49	1.09	2505	50	2672	18
cw11-90_xl_47	122	88	93	0.72	2661.65	0.47	1.98	5.48	0.90	2503	41	2675	15
cw11-90_L_226	196	80	101	0.41	3159.80	0.50	1.96	5.48	1.42	2614	42	2676	24
cw11-90_xl_79	62	53	45	0.85	490.94	0.50	2.59	5.47	1.77	2608	56	2678	29
cw11-90_L_225	155	141	68	0.91	3184.90	0.49	1.88	5.45	1.38	2587	40	2684	23
cw11-90_L_232	92	53	47	0.58	1361.33	0.50	3.46	5.45	2.53	2619	75	2685	42
cw11-90_L_207	115	71	52	0.62	3742.03	0.49	6.32	5.40	5.23	2586	135	2699	86
cw11-90_xl_66	7	5	6	0.76	234.92	0.66	3.66	3.53	3.27	3257	94	3383	51
cw11-90_xl_63	217	97	243	0.45	3769.59	0.68	2.79	3.24	1.41	3339	73	3513	22

CW11-102

Analysis	U (ppm)	Th (ppm)	$^{206}Pb^*$ (ppm)	Th/U	$^{206}Pb/^{204}Pb$	$^{206}Pb^*/^{238}U$	±2σ (%)	$^{206}Pb^*/^{207}Pb^*$	±2σ (%)	$^{206}Pb^*/^{238}U^*$ (Ma)	±2σ (Ma)	$^{207}Pb^*/^{206}Pb^*$ (Ma)	±2σ (Ma)
cw11-102_xl_118	724	65	180	0.09	5764.63	0.25	2.16	10.38	1.22	1421	28	1554	23
cw11-102_L_278	285	293	109	1.03	3682.70	0.33	5.18	9.46	3.42	1842	83	1727	63
cw11-102_L_258	250	52	45	0.21	1684.64	0.28	11.99	9.39	6.73	1606	170	1741	123
cw11-102_L_27	121	65	42	0.54	1956.32	0.32	4.03	9.38	4.10	1777	63	1741	75
cw11-102_L_255	276	114	-9	0.41	1289.97	0.30	7.29	9.35	7.61	1705	109	1748	139
cw11-102_L_259	245	108	-29	0.44	21637.04	0.32	8.48	9.32	6.62	1780	132	1753	121
cw11-102_L_273	93	40	27	0.43	421.08	0.31	4.59	9.21	3.56	1729	70	1775	65
cw11-102_xl_99	128	56	42	0.43	1587.67	0.31	2.93	9.19	2.10	1760	45	1780	38
cw11-102_L_274	290	69	90	0.24	9163.14	0.32	4.12	9.16	3.31	1776	64	1786	60
cw11-102_L_286	148	108	84	0.73	7441.88	0.31	3.69	9.15	2.86	1720	56	1787	52
cw11-102_L_261	353	133	11	0.38	4705.11	0.32	10.57	9.15	5.27	1768	163	1787	96
cw11-102_xl_136	52	27	11	0.51	328.85	0.32	2.69	9.14	2.71	1787	42	1789	49
cw11-102_xl_121	666	110	185	0.17	22346.19	0.30	2.68	9.13	0.88	1688	40	1791	16
cw11-102_L_262	193	144	-48	0.75	2728.52	0.32	8.03	9.12	6.43	1810	127	1793	117
cw11-102_L_282	102	43	43	0.42	1424.35	0.33	3.03	9.05	2.36	1852	49	1807	43
cw11-102_xl_125	155	117	4	0.75	1157.26	0.29	2.17	9.05	1.77	1666	32	1808	32
cw11-102_L_279	243	135	94	0.56	2224.69	0.32	4.33	9.03	3.51	1799	68	1811	64
cw11-102_L_309	199	294	297	1.48	6336.72	0.33	8.26	9.03	5.87	1832	132	1811	107
cw11-102_L_301	151	91	112	0.60	10439.94	0.30	3.30	9.03	2.18	1715	50	1812	40
cw11-102_xl_120	180	102	24	0.57	3447.74	0.31	3.25	9.02	1.51	1738	50	1814	27
cw11-102_L_275	39	24	13	0.62	330.93	0.35	6.05	9.01	4.70	1928	101	1815	85
cw11-102_xl_131	131	51	18	0.39	1243.71	0.31	3.15	9.00	1.73	1718	48	1818	31
cw11-102_xl_133	125	54	10	0.43	1256.79	0.31	3.21	8.98	1.43	1728	49	1823	26
cw11-102_xl_140	85	30	17	0.35	604.53	0.30	2.74	8.98	2.08	1712	41	1823	38
cw11-102_xl_95	136	63	46	0.47	1181.66	0.31	2.77	8.96	1.49	1727	42	1826	27
cw11-102_xl_100	621	127	214	0.20	6561.38	0.31	2.58	8.94	1.31	1740	39	1830	24
cw11-102_xl_96	184	72	64	0.39	5412.08	0.31	2.73	8.91	1.52	1764	42	1835	28
cw11-102_xl_112	207	89	46	0.43	9831.86	0.31	5.98	8.89	5.30	1732	91	1840	96
cw11-102_L_306	264	138	190	0.52	2026.23	0.32	7.76	8.89	6.09	1798	122	1840	110
cw11-102_xl_91	504	254	182	0.50	3362.51	0.31	2.43	8.89	1.25	1732	37	1841	23
cw11-102_L_287	134	100	81	0.75	991.57	0.34	3.99	8.88	3.04	1888	65	1843	55
cw11-102_xl_137	470	181	-3	0.38	20044.67	0.31	4.79	8.88	3.06	1726	73	1843	55
cw11-102_xl_128	249	183	-24	0.74	4304.48	0.31	2.55	8.86	1.42	1752	39	1847	26
cw11-102_L_296	170	64	106	0.38	8995.10	0.34	4.25	8.85	3.12	1902	70	1847	56
cw11-102_L_290	78	27	41	0.35	2144.52	0.34	4.19	8.84	2.66	1898	69	1851	48
cw11-102_xl_142	73	53	-26	0.72	1463.08	0.32	2.21	8.83	2.58	1797	35	1851	47
cw11-102_L_280	281	127	108	0.45	3107.60	0.31	4.55	8.83	3.80	1741	69	1852	69
cw11-102_xl_110	165	72	41	0.43	8028.02	0.31	2.59	8.83	1.95	1734	39	1853	35
cw11-102_xl_127	282	186	4	0.66	2580.87	0.32	2.64	8.82	1.07	1770	41	1854	19
cw11-102_L_303	60	76	68	1.27	1372.62	0.31	3.91	8.82	3.07	1758	60	1854	55

cw11-102_L_265	152	114	-15	0.75	1962.76	0.32	5.95	8.82	4.50	1813	94	1855	81
cw11-102_xl_113	93	27	28	0.30	1250.11	0.32	3.63	8.80	2.25	1779	56	1858	41
cw11-102_L_256	81	43	6	0.53	457.66	0.32	6.45	8.79	6.51	1779	100	1861	117
cw11-102_xl_106	585	90	207	0.15	5732.62	0.33	1.68	8.79	1.25	1815	27	1861	23
cw11-102_xl_97	235	81	83	0.35	2600.50	0.32	2.73	8.79	1.13	1793	43	1861	20
cw11-102_L_289	93	71	55	0.76	1035.09	0.30	3.72	8.78	3.62	1686	55	1863	65
cw11-102_xl_89	304	147	120	0.48	3355.73	0.32	2.64	8.77	1.11	1813	42	1865	20
cw11-102_L_295	394	211	273	0.54	6177.56	0.32	4.40	8.76	3.03	1814	70	1866	55
cw11-102_xl_109	104	61	25	0.58	3951.96	0.33	2.64	8.76	2.31	1839	42	1867	42
cw11-102_xl_124	77	101	-16	1.32	1274.83	0.31	3.34	8.75	1.99	1741	51	1869	36
cw11-102_xl_114	319	109	78	0.34	3745.42	0.30	3.31	8.75	1.68	1693	49	1869	30
cw11-102_L_272	129	104	15	0.80	12598.46	0.32	6.55	8.73	3.94	1786	102	1872	71
cw11-102_xl_104	135	30	47	0.22	2520.83	0.32	1.76	8.72	1.49	1796	28	1875	27
cw11-102_xl_119	257	130	47	0.50	1927.07	0.32	2.06	8.71	0.97	1785	32	1877	17
cw11-102_xl_117	29	17	5	0.58	1111.48	0.32	3.17	8.69	2.46	1780	49	1882	44
cw11-102_L_308	316	110	199	0.35	39628.35	0.31	10.92	8.68	8.60	1723	165	1882	155
cw11-102_L_285	65	119	45	1.84	242.35	0.33	3.28	8.68	3.03	1845	53	1883	55
cw11-102_xl_101	227	83	76	0.36	1920.07	0.32	3.04	8.68	1.56	1809	48	1884	28
cw11-102_L_298	189	93	115	0.49	1155.88	0.33	4.13	8.67	3.44	1820	66	1885	62
cw11-102_L_266	246	155	1	0.63	3928.38	0.33	3.60	8.67	3.11	1851	58	1885	56
cw11-102_xl_92	268	158	96	0.59	3747.13	0.31	2.94	8.66	1.76	1743	45	1887	32
cw11-102_xl_139	457	286	-106	0.63	4737.26	0.33	2.54	8.65	1.20	1815	40	1888	22
cw11-102_xl_134	278	314	-160	1.13	13984.89	0.31	2.96	8.65	1.67	1759	46	1889	30
cw11-102_xl_108	93	76	20	0.82	618.58	0.33	3.75	8.63	2.15	1830	60	1893	39
cw11-102_xl_132	761	158	162	0.21	90557.93	0.32	2.75	8.62	1.10	1786	43	1896	20
cw11-102_xl_135	382	158	-3	0.42	6095.64	0.29	2.58	8.62	1.92	1662	38	1896	34
cw11-102_xl_123	187	77	32	0.41	18974.17	0.31	3.11	8.62	1.75	1746	48	1896	31
cw11-102_xl_122	167	84	29	0.50	1286.24	0.32	3.00	8.55	1.64	1786	47	1910	29
cw11-102_xl_126	120	37	27	0.31	4120.29	0.32	2.74	8.50	1.90	1781	43	1920	34
cw11-102_L_291	86	36	40	0.42	726.56	0.32	3.74	8.48	3.65	1769	58	1925	65
cw11-102_L_271	327	137	89	0.42	11222.84	0.39	5.58	7.80	3.44	2119	101	2073	61
cw11-102_L_304	160	79	121	0.49	1711.14	0.37	5.26	7.66	3.86	2022	91	2105	68
cw11-102_L_307	354	115	247	0.32	31620.10	0.35	7.72	7.46	5.16	1955	130	2151	90
cw11-102_L_305	555	339	635	0.61	12657.19	0.45	8.70	6.46	5.48	2402	175	2400	93
cw11-102_xl_111	356	62	152	0.18	9043.62	0.41	2.45	6.38	1.19	2203	46	2422	20
cw11-102_L_269	136	96	15	0.71	3779.46	0.44	4.03	6.37	2.72	2337	79	2422	46
cw11-102_xl_143	152	81	-20	0.53	1872.08	0.44	4.25	6.23	2.24	2370	84	2462	38
cw11-102_L_293	637	220	524	0.35	11068.83	0.48	5.47	6.22	4.02	2519	114	2465	68
cw11-102_xl_93	365	148	194	0.41	2988.80	0.44	2.12	6.21	0.88	2335	42	2467	15
cw11-102_xl_107	163	76	71	0.47	4926.71	0.46	2.28	6.20	1.86	2445	46	2469	31
cw11-102_L_264	128	69	1	0.54	6588.74	0.47	6.31	6.20	3.38	2466	129	2469	57
cw11-102_L_263	150	76	5	0.50	2150.00	0.42	5.43	6.19	3.20	2241	103	2472	54
cw11-102_L_276	99	53	53	0.53	1754.58	0.48	4.45	6.18	3.28	2518	93	2474	55
cw11-102_L_300	111	52	105	0.47	3137.40	0.45	2.80	6.17	2.36	2413	56	2479	40
cw11-102_L_268	108	68	13	0.63	24833.72	0.45	2.98	6.16	3.17	2387	60	2481	54
cw11-102_L_281	105	51	66	0.49	2177.23	0.47	3.36	6.12	2.83	2465	69	2490	48

cw11-102_xl_103	161	60	77	0.38	4253.38	0.45	2.45	6.09	1.34	2373	49	2500	23
cw11-102_L_294	130	75	117	0.58	1267.83	0.45	3.90	6.08	2.96	2377	78	2502	50
cw11-102_L_302	114	60	113	0.53	4478.19	0.45	4.86	6.05	2.53	2384	97	2510	43
cw11-102_L_270	161	75	47	0.46	2233.30	0.44	3.79	6.02	2.72	2350	75	2520	46
cw11-102_xl_90	166	88	99	0.53	20311.91	0.46	2.69	5.86	1.80	2434	55	2564	30
cw11-102_xl_116	359	129	140	0.36	17271.68	0.46	3.62	5.63	0.89	2452	74	2630	15
cw11-102_L_260	64	35	-16	0.54	3652.94	0.48	7.00	5.57	6.40	2514	146	2650	106
cw11-102_L_297	202	91	200	0.45	3699.81	0.49	5.84	5.50	2.81	2556	123	2671	46
cw11-102_xl_105	44	23	22	0.54	1233.21	0.50	2.29	5.39	2.26	2601	49	2702	37
cw11-102_xl_138	108	88	-46	0.81	1424.37	0.50	2.89	5.34	1.85	2593	62	2717	31
cw11-102_L_284	317	236	280	0.74	174064.69	0.53	2.79	5.25	1.96	2728	62	2746	32
cw11-102_L_299	415	237	540	0.57	49958.21	0.54	3.44	5.21	2.16	2786	78	2759	35
cw11-102_xl_94	339	155	225	0.46	4869.29	0.53	2.99	5.07	0.80	2733	67	2804	13
cw11-102_xl_98	404	96	263	0.24	5601.60	0.52	2.65	4.89	0.87	2692	58	2862	14
cw11-102_xl_141	160	86	-25	0.54	4628.00	0.56	2.53	4.77	2.04	2846	58	2903	33
cw11-102_L_267	93	108	-31	1.16	4328.38	0.61	3.28	4.16	2.32	3074	80	3123	37
cw11-102_L_283	45	42	51	0.95	1851.09	0.65	3.14	3.86	2.35	3219	80	3243	37
cw11-102_xl_129	359	135	149	0.38	15953.74	0.59	2.31	3.66	0.87	2978	55	3325	14
cw11-102_xl_130	152	51	69	0.34	8254.22	0.61	3.00	3.65	0.99	3088	74	3327	15
cw11-102_L_292	300	78	354	0.26	14787.32	0.69	4.74	3.42	3.20	3364	124	3432	50
cw11-102_xl_102	47	30	40	0.64	802.92	0.71	2.56	3.23	1.26	3449	68	3520	19

CW11-94

Analysis	U (ppm)	Th (ppm)	$^{206}Pb^*$ (ppm)	Th/ U	$^{206}Pb/^{204}Pb$	$^{206}Pb^*/^{238}U$	±2σ (%)	$^{206}Pb^*/^{207}Pb^*$	±2σ (%)	$^{206}Pb^*/^{238}U^*$ (Ma)	±2σ (Ma)	$^{207}Pb^*/^{206}Pb^*$ (Ma)	±2σ (Ma)	Used in weighted mean age calculation?
CW11-94_m_11	257	152	77	0.59	3867.70	0.33	3.48	8.85	2.67	1846	56	1848	48	Yes
CW11-94_m_26	282	177	112	0.63	5603.74	0.34	3.54	8.75	3.76	1879	58	1868	68	Yes
CW11-94_m_28	249	125	99	0.50	2455.65	0.33	1.95	8.64	1.55	1861	32	1892	28	Yes
CW11-94_m_3	961	154	347	0.16	5472.57	0.35	4.41	8.56	2.68	1942	74	1908	48	Yes
CW11-94_m_21	1199	365	465	0.30	5112.77	0.34	2.50	8.77	1.81	1901	41	1865	33	Yes
CW11-94_m_32	1186	247	489	0.21	19525.90	0.34	3.64	8.81	2.36	1893	60	1856	43	Yes
CW11-94_m_1	437	223	88	0.51	5548.11	0.34	3.89	8.76	1.94	1906	64	1866	35	Yes
CW11-94_m_17	141	69	49	0.49	1091.72	0.34	3.59	8.76	2.38	1910	59	1866	43	Yes
CW11-94_m_2	851	213	255	0.25	18129.42	0.33	4.18	8.67	2.34	1832	67	1885	42	Yes
CW11-94_m_24	298	147	112	0.49	57520.22	0.33	2.78	8.69	1.58	1825	44	1881	28	Yes
CW11-94_m_19	288	136	92	0.47	2958.86	0.31	4.74	9.00	2.82	1752	73	1818	51	Yes
CW11-94_m_18	238	114	85	0.48	72357.56	0.35	3.97	8.72	3.43	1947	67	1874	62	Yes
CW11-94_m_14	1947	115	698	0.06	74581.29	0.32	2.78	8.88	1.28	1767	43	1842	23	Yes
CW11-94_m_5	636	201	205	0.32	39887.19	0.36	3.52	8.68	1.46	1960	60	1883	26	Yes
CW11-94_m_31	579	643	254	1.11	5349.42	0.32	4.36	8.76	2.89	1786	68	1867	52	Yes
CW11-94_m_30	326	131	126	0.40	4045.60	0.32	3.73	8.71	3.20	1786	58	1876	58	Yes
CW11-94_m_16	401	351	109	0.87	4550.42	0.31	3.40	8.73	2.25	1765	52	1873	41	Yes
CW11-94_m_8	305	125	86	0.41	5692.75	0.31	1.72	8.71	1.40	1751	26	1876	25	Yes
CW11-94_m_6	560	246	145	0.44	6988.76	0.31	1.95	8.63	1.09	1746	30	1893	20	Yes
CW11-94_m_12	1283	445	387	0.35	35661.72	0.29	2.00	8.90	1.85	1663	29	1838	33	Yes
CW11-94_m_7	1906	220	587	0.12	13149.89	0.29	2.32	8.85	1.04	1627	33	1849	19	Yes
CW11-94_m_9	303	217	66	0.71	1957.01	0.30	2.81	8.58	2.34	1675	41	1905	42	Yes
CW11-94_m_22	543	296	175	0.54	6821.40	0.29	2.21	8.71	1.81	1634	32	1877	33	Yes
CW11-94_m_13	2768	182	967	0.07	44078.86	0.31	2.92	8.96	1.30	1736	44	1825	24	No
CW11-94_m_29	2178	195	784	0.09	24591.36	0.31	4.07	8.96	1.23	1727	62	1825	22	No
CW11-94_m_27	967	246	313	0.25	7318.10	0.28	3.78	9.04	1.67	1577	53	1810	30	No
CW11-94_m_20	910	279	360	0.31	41095.73	0.36	5.57	8.94	1.63	1972	95	1829	30	No
CW11-94_m_4	221	185	32	0.84	212817.84	0.39	4.36	8.76	2.47	2123	79	1866	45	No
CW11-94_m_15	187	119	83	0.64	7004.15	0.45	2.59	6.43	1.47	2374	51	2409	25	No
CW11-94_m_23	236	91	111	0.39	6036.23	0.40	5.72	6.71	4.02	2151	105	2336	69	No
CW11-94_m_10	330	197	104	0.60	3632.48	0.38	4.46	8.69	2.42	2069	79	1881	44	No
CW11-94_m_10	330	197	104	0.60	3632.48	0.38	4.46	8.69	2.42	2069	79	1881	44	No

Appendix 6: Table of zircon Hf isotopic data

CW11-94

Analysis	$^{176}Lu/^{177}Hf$	1σ error	$^{176}Hf/^{177}Hf$	1σ error	ε(0)	2 σ error	Tchur (Ga)	Tdm (Ga)	t (Ga)	$^{176}Hf/^{177}Hf(t)$	ε(t)	Error	Tcr bulk crust (Ga)	Tcr mafic lower crust (Ga)
CW11-94 3_2	0.0007592	0.0000240	0.2814710	0.0000110	-46.5	0.8	2.10	2.44	1.87	0.28144	-5.23	0.9	2.59	2.85
CW11-94 23_2	0.0006263	0.0000059	0.2814960	0.0000280	-45.6	2.0	2.05	2.40	1.87	0.28147	-4.17	2.0	2.54	2.78
CW11-94 31_2	0.0012842	0.0001000	0.2815740	0.0000140	-42.8	1.0	1.97	2.34	1.87	0.28153	-2.23	1.3	2.44	2.64
CW11-94 8_2	0.0010616	0.0000510	0.2815840	0.0000140	-42.5	1.0	1.94	2.31	1.87	0.28155	-1.60	1.1	2.40	2.59
CW11-94 15_2	0.0006982	0.0000041	0.2812280	0.0000130	-55.1	0.9	2.48	2.77	2.4	0.28120	-1.75	1.0	2.84	2.99
CW11-94 22_2	0.0008841	0.0000230	0.2815820	0.0000170	-42.5	1.2	1.93	2.30	1.87	0.28155	-1.44	1.3	2.39	2.58
CW11-94 18_2	0.0012549	0.0000410	0.2815960	0.0000160	-42.0	1.1	1.93	2.30	1.87	0.28155	-1.41	1.3	2.39	2.58
CW11-94 28_2	0.0005733	0.0000240	0.2815850	0.0000120	-42.4	0.8	1.91	2.28	1.87	0.28156	-0.94	0.9	2.37	2.55
CW11-94 1_2	0.0009239	0.0000230	0.2815980	0.0000160	-42.0	1.1	1.91	2.28	1.87	0.28157	-0.92	1.2	2.37	2.54
CW11-94 6_2	0.0009293	0.0000190	0.2815990	0.0000160	-41.9	1.1	1.91	2.28	1.87	0.28157	-0.90	1.2	2.36	2.54
CW11-94 12_2	0.0015683	0.0000100	0.2816220	0.0000170	-41.1	1.2	1.91	2.29	1.87	0.28157	-0.89	1.3	2.36	2.54
CW11-94 14_2	0.0007400	0.0000140	0.2816010	0.0000130	-41.9	0.9	1.90	2.27	1.87	0.28157	-0.59	1.0	2.35	2.52
CW11-94 21_2	0.0007586	0.0000058	0.2816040	0.0000110	-41.8	0.8	1.89	2.26	1.87	0.28158	-0.50	0.8	2.34	2.51
CW11-94 11_2	0.0006155	0.0000160	0.2815990	0.0000120	-41.9	0.8	1.89	2.26	1.87	0.28158	-0.50	0.9	2.34	2.51
CW11-94 2_2	0.0007399	0.0000140	0.2816050	0.0000120	-41.7	0.8	1.89	2.26	1.87	0.28158	-0.44	0.9	2.34	2.51
CW11-94 10_2	0.0005293	0.0000110	0.2816110	0.0000140	-41.5	1.0	1.87	2.24	1.87	0.28159	0.04	1.0	2.31	2.47
CW11-94 32_2	0.0007078	0.0000037	0.2816200	0.0000110	-41.2	0.8	1.86	2.24	1.87	0.28159	0.13	0.8	2.31	2.47
CW11-94 19_2	0.0008497	0.0000210	0.2816260	0.0000120	-41.0	0.8	1.86	2.24	1.87	0.28160	0.16	0.9	2.31	2.47
CW11-94 9_2	0.0005945	0.0000095	0.2816210	0.0000200	-41.2	1.4	1.86	2.23	1.87	0.28160	0.31	1.5	2.30	2.46
CW11-94 24_2	0.0008462	0.0000160	0.2816300	0.0000110	-40.8	0.8	1.86	2.23	1.87	0.28160	0.31	0.8	2.30	2.45
CW11-94 16_2	0.0010964	0.0000540	0.2816440	0.0000130	-40.3	0.9	1.85	2.23	1.87	0.28161	0.49	1.1	2.29	2.44
CW11-94 13_2	0.0013885	0.0000340	0.2816570	0.0000180	-39.9	1.3	1.84	2.23	1.87	0.28161	0.58	1.4	2.29	2.44
CW11-94 26_2	0.0008527	0.0000440	0.2816390	0.0000210	-40.5	1.5	1.84	2.22	1.87	0.28161	0.62	1.6	2.28	2.43
CW11-94 30_2	0.0005831	0.0000016	0.2816340	0.0000120	-40.7	0.8	1.84	2.21	1.87	0.28161	0.78	0.9	2.28	2.42
CW11-94 25_2	0.0012193	0.0000550	0.2816570	0.0000120	-39.9	0.8	1.83	2.22	1.87	0.28161	0.80	1.0	2.27	2.42
CW11-94 5_2	0.0013539	0.0000170	0.2816620	0.0000140	-39.7	1.0	1.83	2.22	1.87	0.28161	0.81	1.1	2.27	2.42
CW11-94 4_2	0.0007398	0.0000037	0.2816510	0.0000094	-40.1	0.7	1.82	2.20	1.87	0.28162	1.19	0.7	2.25	2.39
CW11-94 29_2	0.0008206	0.0000041	0.2816570	0.0000130	-39.9	0.9	1.81	2.19	1.87	0.28163	1.30	1.0	2.25	2.38
CW11-94 20_2	0.0008215	0.0000092	0.2816690	0.0000130	-39.5	0.9	1.79	2.18	1.87	0.28164	1.73	1.0	2.23	2.35
CW11-94 7_2	0.0012509	0.0000100	0.2816870	0.0000150	-38.8	1.1	1.79	2.18	1.87	0.28164	1.82	1.1	2.22	2.35
CW11-94 27_2	0.0010554	0.0000130	0.2817010	0.0000120	-38.3	0.8	1.75	2.15	1.87	0.28166	2.57	0.9	2.18	2.29
CW11-94 17_2	0.0010754	0.0000240	0.2817830	0.0000150	-35.4	1.1	1.63	2.04	1.87	0.28174	5.45	1.1	2.03	2.08